USED FUEL DISPOSITION CAMPAIGN

Review of NDE Methods for Detection and Monitoring of Atmospheric SCC in Welded Canisters for the Storage of Used Nuclear Fuel

Fuel Cycle Research & Development

Prepared for
U.S. Department of Energy
Used Fuel Disposition Campaign

RM Meyer
AF Pardini
BD Hanson
KB Sorenson

January 14, 2013

FCRD-UFD-2013-000085
PNNL-22158

Abstract

Dry cask storage systems (DCSSs) for used nuclear fuel were originally envisioned for storage periods of short duration (approximately a few decades). However, uncertainty challenges the opening of a permanent repository for used nuclear fuel, implying that used nuclear fuel will need to remain in dry storage for much longer durations than originally envisioned. Thus, aging degradation of DCSSs becomes an issue that may not have been sufficiently considered in the design phase and that can challenge the efficacy of very long-term storage of used nuclear fuel. A particular aging degradation concern is atmospheric stress corrosion cracking (SCC) of DCSSs located in marine environments. In this report, several nondestructive examination methods are evaluated with respect to their potential for effective monitoring of atmospheric SCC in welded canisters of DCSSs. The technologies considered include bulk ultrasonic techniques, acoustic emission, visual techniques, eddy current, and guided ultrasonic waves. Many of the nondestructive examination methods considered are screening technologies and are suitable for the detection of atmospheric SCC, but not for sizing of detected cracks. Eddy current techniques are considered to have good potential for detecting atmospheric SCC flaws in welded canisters, and the conditions for which eddy current techniques may be used to depth size atmospheric SCC flaws should be enumerated. Bulk ultrasonic techniques may have the best potential for depth sizing detected atmospheric SCC flaws. The only other technology considered to have potential for depth sizing of detected flaws is guided ultrasonic waves, although considerable development is required for the application to DCSS canisters and to understand the sensitivity and accuracy of the techniques. Visual techniques can be used to detect cracks, but not to determine their depth. Further, the reliability of visual techniques for detecting atmospheric SCC flaws is a potential concern. Finally, acoustic emission may be used to continuously monitor for atmospheric SCC and may be especially desirable for monitoring regions of the canister that are difficult to access. However, the sensitivity of AE to atmospheric SCC is unclear. In addition to a summary assessment for each technology, cross-cutting needs that would benefit several of the technologies assessed, and several monitoring strategies are identified.

Summary

Dry cask storage systems (DCSSs) for used nuclear fuel are intended for temporary storage. Uncertainty regarding the feasibility of opening a repository for eventual disposal implies that DCSSs will need to store used nuclear fuel for periods much longer than originally envisioned. Meanwhile, the structural and leak-tight integrity of DCSSs must not be compromised by their extended period of use. Validating the integrity of DCSSs through monitoring or inspection enables management of the effects of degradation or aging that may occur over the extended storage period and which may threaten the integrity of the DCSS. The *Code of Federal Regulations* requires that storage confinement systems have the capability for continuous monitoring to enable maintenance of safe storage conditions. A gap analysis was recently performed under the U.S. Department of Energy's Used Fuel Disposition Campaign to support extended storage of used nuclear fuel (Hanson et al. 2012). This report highlighted monitoring of DCSSs as a high-priority gap area to ensure the safe long-term storage of used nuclear fuel.

Many different monitoring needs were highlighted in the previous gap analysis and potential needs included technologies to monitor the environmental and structural integrity of DCSS systems, structures, and components, both internal and external to the confinement barrier. High priority was given to monitoring needs associated with detecting degradation of the confinement barrier. A specific concern is the potential for degradation of DCSSs located in coastal areas as a result of atmospheric stress corrosion cracking (SCC). SCC has been a persistent form of degradation in the nuclear power industry, particularly in operating nuclear power plants. Although atmospheric SCC in DCSSs and SCC in light-water reactors is a consequence of different environmental factors, many of the nondestructive examination methods used for detection and characterization of SCC occurrences in nuclear power plants should have relevance to the detection and characterization of atmospheric SCC in DCSSs. The methods evaluated in this report include bulk ultrasonics, acoustic emission, visual techniques, eddy current, and guided ultrasonic waves. A summary of the evaluation is given later in Table 5.1.

A few cross-cutting needs that are applicable to improving examinations are identified as follows:

- Development of a robotic crawler or scanner is needed to encode the location of nondestructive examination data on the canister surface, maintain a consistent scan rate, maintain a consistent probe-to-canister surface distance, and minimize the impact of human factors. This need is associated with bulk ultrasonic, visual, eddy current, and circumferentially guided wave methods. Robotic mechanisms are also needed for the placement of acoustic emission and axially guided wave transducers even though the sensors are not scanned over the surface.
- A compilation of atmospheric SCC flaw morphology parameters (width, orientation, etc.) that affect nondestructive examination performance would enable a more complete assessment of the capability of most nondestructive examination methods to detect atmospheric SCC.
- Detailed and specific design information related to welded canisters for DCSSs is needed to understand specific access constraints and examination geometries. In turn, this information is relevant to choosing the most appropriate strategy for examination. It is anticipated that the bottom plate-to-shell welds could be the most difficult to access and may pose the most significant examination challenge. The difficulty of the examination will depend on the specific weld configuration.

- Environmental factors such as temperature and radiation in general can affect both the physics of an examination and the performance of equipment exposed to the environmental conditions. Future efforts should seek to enumerate these effects and identify any gaps in knowledge with regards to the behavior of certain types of sensors in anticipated environments.

The technologies have been classified according to their potential application for screening (crack detection), characterizing (sizing), or both. Eddy current techniques are potentially well suited for the detection of atmospheric stress corrosion cracks in welded canisters and may be able to depth size certain flaws. Previous compilations of SCC flaw characteristics indicate the mean crack opening displacement for SCC flaws is 16–30 μm. Parametric studies performed with remote visual testing equipment typically used within the nuclear power industry indicate these techniques can reliably detect flaws with a crack opening displacement greater than 100 μm, raising concerns about the potential reliability of visual techniques for detecting atmospheric SCC. Better performance and equipment specifications may be able to improve this reliability. The lack of coolant flow noise and manageable size of welded canisters enable global monitoring with acoustic emission sensors. However, the sensitivity and reliability of acoustic emission for detecting and monitoring atmospheric SCC are presently unclear. Bulk ultrasonic techniques have the best potential for depth sizing detected atmospheric SCC flaws, while circumferentially guided waves could potentially be implemented for performing both screening and characterization functions, but require significant development. Potential strategies for inspecting and monitoring atmospheric SCC in welded canisters are identified below:

- Eddy current techniques are considered to have good potential for detection of atmospheric SCC flaws and may be used for screening followed by a bulk ultrasonic examination for characterization of detected flaws.
- Visual methods may be used for screening, followed by a bulk ultrasonic examination for characterization of detected flaws. The reliability of remote visual techniques for detection of atmospheric SCC is a concern. These concerns could potentially be alleviated with the use of equipment with improved performance specifications.
- Acoustic emission may be used for global canister monitoring, followed by a bulk ultrasonic examination for characterization of detected flaws. Presently, the sensitivity of acoustic emission to atmospheric SCC degradation is unclear and laboratory testing would be needed to establish its capability. Further, an understanding of background noise sources and their potential to interfere with atmospheric SCC detection and monitoring is needed to facilitate acoustic emission monitoring.
- Acoustic emission may be used for localized monitoring of existing flaws to monitor their growth and serve as the basis for scheduling follow-up examinations in lieu of periodic, regularly scheduled examinations. Limiting the zone of acoustic emission monitoring limits the interference by background noise sources. Acoustic emission monitoring may be especially desirable for locations of the canister that are difficult or impossible to access by other methods.
- Circumferential guided wave systems could potentially be implemented to perform both screening and characterization functions, although significant work is needed to develop a system for application to welded canisters for DCSSs.

Acknowledgments

Kay Hass is acknowledged for her excellence and patience in the formatting and editing versions of this report. Gratitude is also extended to Mike Larche for creating many of the figures included in this report.

Acronyms and Abbreviations

AE	acoustic emission
ASME	American Society for Mechanical Engineers
ASNT	American Society for Nondestructive Testing
B&PV	Boiler and Pressure Vessel (Code)
BMI	bottom-mounted instrumentation
BOP	balance of plant
BWR	boiling water reactor
CFR	*Code of Federal Regulations*
COD	crack opening displacement
COTS	commercial off-the-shelf
DCSS	dry cask storage system
DSC	dry storage canister
EMAT	electromagnetic acoustic transducer
EPRI	Electric Power Research Institute
ESCC	external stress corrosion cracking
ET	eddy current
f•d	frequency × thickness
FEM	finite element method
GUL	Guided Ultrasonics Ltd.
GUW	guided ultrasonic waves
HAZ	heat-affected zone
ID	inner diameter
IGSCC	intergranular stress corrosion cracking
L	longitudinal (wave)
LWR	light-water reactor
MPC	multi-purpose canister
MsS	magnetostrictive sensor
MTR	material test reactors
NDE	nondestructive examination
NPP	nuclear power plant
NRC	U.S. Nuclear Regulatory Commission
OD	outer diameter
OLM	on-line monitoring
PHWR	pressurized heavy water reactor
PNNL	Pacific Northwest National Laboratory
POD	probability of detection

PTZ	pan/tilt/zoom
PWSCC	primary water stress corrosion cracking
SCC	stress corrosion cracking
S	shear (wave)
SH	shear horizontal (wave)
SKI	Swedish Nuclear Power Inspectorate
SS	stainless steel
SSM	Swedish Radiation Safety Authority
TGSCC	transgranular stress corrosion cracking
TOA	time-of-arrival
TOFD	time-of-flight diffraction
UNF	used nuclear fuel
UT	ultrasonic testing
Vg	group velocity
Vp	phase velocity
VT	visual testing

Contents

Figures

Tables

1.0 Introduction

Dry cask storage systems (DCSSs) are intended for temporary storage of used nuclear fuel (UNF). Uncertainty regarding the feasibility of opening a repository for eventual disposal implies that DCSSs will need to store UNF for periods much longer than originally envisioned. Meanwhile, the structural and leak-tight integrity of DCSSs must not be compromised by their extended period of usage. Validating the integrity of DCSSs through monitoring or inspection enables management of the effects of degradation or aging that may occur over the extended storage period and that may threaten the integrity of the DCSS. The *Code of Federal Regulations* (CFR) requires that storage confinement systems have the capability for continuous monitoring to enable maintenance of safe storage conditions (10 CFR 72.122). A gap analysis, recently performed under the U.S. Department of Energy's Used Fuel Disposition Campaign to support extended storage of UNF (Hanson et al. 2012), highlighted monitoring of DCSSs as a high-priority gap in the safe long-term storage of UNF.

Many different monitoring needs were highlighted in this gap analysis, and potential needs included technologies to monitor the environmental and structural integrity of DCSS systems, structures, and components, both internal and external to the confinement barrier. High priority was given to monitoring needs associated with detecting degradation of the confinement barrier (Hanson et al. 2012). Of specific concern is the potential for atmospheric stress corrosion cracking (SCC) to cause degradation of DCSSs located in coastal areas. SCC has been a persistent form of degradation in the nuclear power industry, particularly in operating nuclear power plants. Although atmospheric SCC in DCSSs and SCC in light-water reactors (LWRs) are a consequence of different environmental factors, many of the nondestructive examination (NDE) methods used for detection and characterization of SCC occurrences in nuclear power plants should have relevance to the detection and characterization of atmospheric SCC in DCSSs.

This report evaluates several NDE methods for managing atmospheric SCC occurrences in welded canisters that act as the main confinement barrier for several dry storage systems. The methods evaluated include bulk ultrasonic methods, acoustic emission (AE), visual techniques, eddy current, and guided ultrasonic wave techniques. These methods are selected based on technology maturity, applicability, and the experience that the nuclear power industry has accumulated in implementing many of these technologies for the examination of nuclear power plant components. Some preliminary experimental assessments of eddy current, phased array ultrasonic, and visual methods are reported in Kunerth et al. (2012). Additionally, TenCate et al. (2012) propose mitigation strategies for several potential degradation mechanisms in DCSS canisters and describe some less conventional monitoring techniques including vibro-infrared imaging and nonlinear acoustic techniques.

Section 2 of this report includes a brief description of welded canisters including their components, their geometry, and materials of construction. In Section 3, a brief discussion of SCC is provided with an emphasis on atmospheric SCC. Section 4 includes the assessment of several structural surveillance technologies including assessments of bulk ultrasonic techniques, acoustic emission, visual, eddy current, and guided ultrasonic wave techniques. A discussion of the evaluations is included in Section 5, which summarizes the findings, identifies cross-cutting needs, and considers strategies for detecting and monitoring atmospheric SCC in welded canisters of DCSSs. Important conclusions of the assessment are summarized in Section 6.

2.0 Description of Welded Canisters

Dry cask storage systems must fulfill several functional requirements such as preventing the release of radioactive material to the environment, providing radiation shielding, maintaining subcriticality of loaded fuel assemblies, and providing an inert environment for loaded UNF. Canister-based DCSSs for UNF are one of the two main types of designs for DCSSs of UNF. In these types of systems, UNF assemblies are loaded into a basket that is integrated into a relatively thin-walled cylinder (canister) that is then placed into a metal or concrete overpack.

Most (1,224 total) of the DCSSs in service in the United States use designs based on a separate welded canister placed in an overpack (Hanson et al. 2012). Of these, most of the vendors supply vertically oriented systems. The exception to this is the NUHOMS system by Transnuclear, in which welded canisters are loaded horizontally into concrete overpack modules. As of May 2011, just under half (43 percent) of all welded canister DCSSs in service were NUHOMS systems.

A description of several DCSSs that have been approved by the U.S. Nuclear Regulatory Commission (NRC) for handling UNF is included in the Industry Spent Fuel Storage Handbook (EPRI 2010). Welded canister-based systems from Holtec International, Transnuclear, NAC International, and BNG Fuel Solutions are described; and some overall geometry and material specifications for the canisters these vendors use are tabulated in Table 2.1. Although the canisters have slight variations, typical components include a cylindrical shell, fuel basket, top and bottom closure or cover plates, top and bottom shield plugs, closure rings, and covers for drain and vent ports. Most of the canisters and canister components are fabricated from stainless steel (SS). The cylindrical shells can have diameters ranging from 1.58 m to 1.83 m and the length of the canister can range from 3.11 m to 5.04 m. Shell wall thicknesses can range from approximately 1.27 cm (0.5 in.) to 2.54 cm (1 in.). A cut-away illustration of a Holtec multi-purpose canister (MPC) and photograph are provided in Figure 2.1.

To provide an inert environment for the fuel, and prevent the in-leaking of air, canisters are backfilled with helium to pressures moderately above atmosphere. For instance, the NUHOMS-61BT canister is designed to withstand 1.68, 2.36, and 5.42 atm (10, 20, and 65 psig) for normal, off-normal, and accident scenarios, respectively (Transnuclear 2004).

Table 2.1. Summary of Canister Geometry and Material Specifications for Canister-Based DCSSs

Vendor	Model	Length	Diameter	Wall Thickness	Material
Holtec	HI-STORM 100U HI-STORM 100	4.93 m	1.74 m	---	Stainless steel
NAC International	MPC	3.11 m	1.79 m	---	Stainless steel
	UMS	4.45–4.84 m	1.70 m	---	Stainless steel
	MAGNASTOR	4.69–4.87 m	1.83 m	1.27 cm (0.5 in.)[(a)]	Stainless steel
Transnuclear	NUHOMS	4.7–5.04 m	1.58–1.77 m	(0.5–0.625 in.)[(b)]	Stainless steel
BNG Fuel Solutions	W150	---	---	---	High strength carbon or stainless steel
	VSC	4.2–4.6 m	1.6165 m	2.54 cm (1 in.)	Stainless steel

(a) Obtained from NAC International 2012.
(b) Transnuclear (2004).

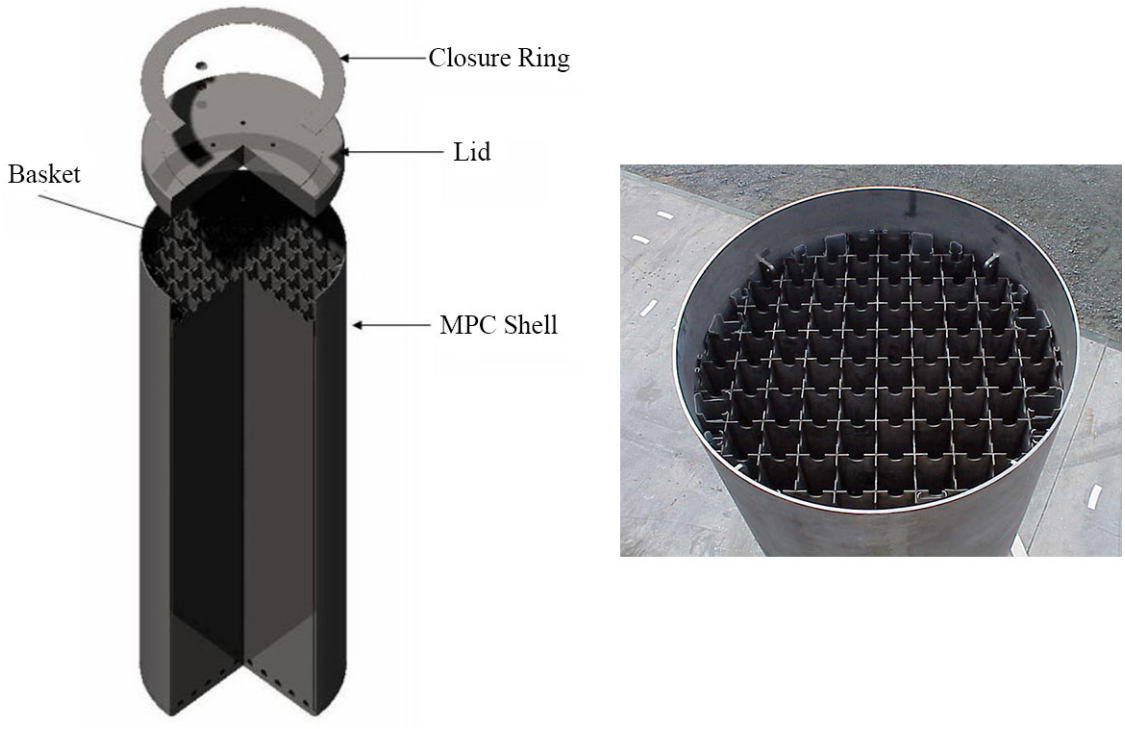

Figure 2.1. Cut-Away Illustration of a Typical Holtec Multi-Purpose Canister (MPC) for Used Fuel Storage (left) and Photograph of a Holtec MPC (right). Used with permission from Holtec International.

3.0 Stress Corrosion Cracking

This section begins with a brief discussion of atmospheric SCC in Section 3.1, which is followed by a definition in Section 3.2 of essential flaw parameters that can affect NDE performance and that enable descriptions of SCC flaws. The Swedish Nuclear Power Inspectorate (or SKI, now part of the Swedish Radiation Safety Authority [SSM]) has compiled essential flaw parameters for cracks observed in nuclear and non-nuclear industries and part of this information relevant to SCC is extracted and presented in Section 3.3 for convenience.

3.1 Atmospheric Stress Corrosion Cracking

Stress corrosion cracking can occur when three necessary preconditions are simultaneously present (see Figure 3.1):

- the presence of a susceptible material
- the presence of tensile stress
- the presence of a corrosive environment.

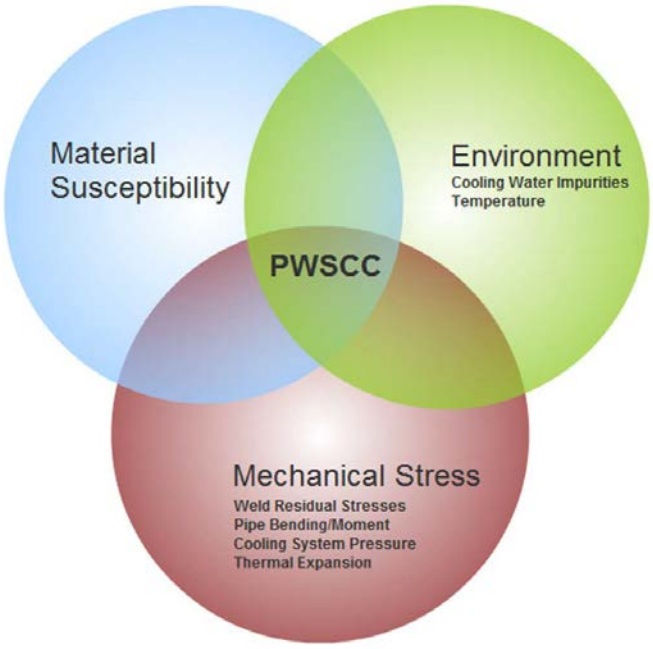

Figure 3.1. Schematic Illustrating the Necessary Preconditions for the Occurrence of SCC (Primary Water Stress Corrosion Cracking [PWSCC])

Generally, SCC can propagate in intergranular (following grain boundaries – known as IGSCC) or transgranular (through grains – known as TGSCC) modes. Propagation can occur through a combination of both modes or may involve switching between modes as the crack progresses. In addition to the three preconditions mentioned above, SCC initiation is highly dependent on surface conditions. Areas of

unusual stress concentration on a material surface resulting from surface imperfections caused by cold work or localized corrosion can trigger the initiation of SCC. Examples of SCC can be found for a range of materials in boiling water reactor (BWR) and pressurized water reactor environments, including carbon steels, stainless steels, and nickel-based alloys. Two major factors contributing to SCC susceptibility of austenitic stainless steels in BWRs include thermal sensitization and cold work. Factors that are considered to most strongly influence primary water stress corrosion cracking (PWSCC) susceptibility in nickel-based alloys include carbide morphology and cold work (IAEA 2011).

SCC induced by sea salt particles and chlorides has been observed on various structures of chemical plants built in coastal regions. This type of SCC is often referred to as external SCC (ESCC) or atmospheric SCC because the cracking starts from the outside surface of components or equipment exposed to the environment. Operating experience near coastal regions in the United States, Japan, and South Africa provide examples of the occurrence of atmospheric SCC in components under ambient conditions in the nuclear power industry. Atmospheric SCC has been observed in several components including refueling water storage tanks, boric acid storage tanks (Mintz et al. 2012), spent fuel pools, safety injection system piping, and containment spray system piping (Alexander et al. 2010). Field occurrences indicate that high residual stresses and marine-like environmental conditions contribute to atmospheric SCC susceptibility.

Limited information exists to assess the susceptibility of dry storage cask containers located near coastal regions to atmospheric SCC. The susceptibility of several materials commonly used for dry cask storage containers (304, 304L, and 316L austenitic stainless steels) to atmospheric SCC was recently explored for both welded and unwelded specimens (Caseres and Mintz 2010). Accelerated tests were conducted to study SCC susceptibility as a function of alloy composition and specimen temperature using both salt sprays and salt fogs to simulate a humid, chloride-rich marine environment. For salt fog tests conducted at 43°C, 85°C, and 120°C, only U-bend specimens at 43°C exhibited SCC. At 43°C, the extent of cracking increased with time from 4 to 52 weeks exposure for specimens of 304 and 304L materials, while cracking was detected at 32 weeks for specimens of 316L (DePaula and Oberson 2012). SCC susceptibility maps were created for each material tested as a function of temperature and time to the initiation of SCC cracks. As an example, the SCC susceptibility map for 304 stainless steel specimens is included in Figure 3.2.

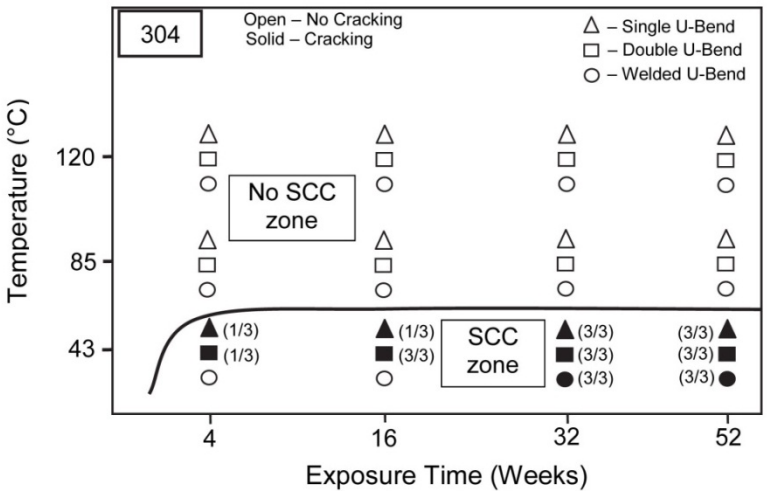

Figure 3.2. Example SCC Susceptibility Map for the Type 304 Stainless Steel (Caseres and Mintz 2010)

The susceptibility of components to atmospheric SCC is also dependent on the deliquescence of salt deposits on the surface of the component. Absolute humidity contours can be plotted versus relative humidity and temperature to aide in the determination of conditions conducive to the deliquescence of chloride salts. Figure 3.3 illustrates several contours with deliquescence zones for several salts superimposed. Figure 3.3 indicates that a threshold relative humidity exists for the deliquescence of chloride salts and that the absolute humidity needed to reach this threshold increases with temperature. It has been noted that the absolute humidity should not exceed 30 g/cm^3 for coastal environments relevant to dry cask storage containers (Mintz et al. 2012).

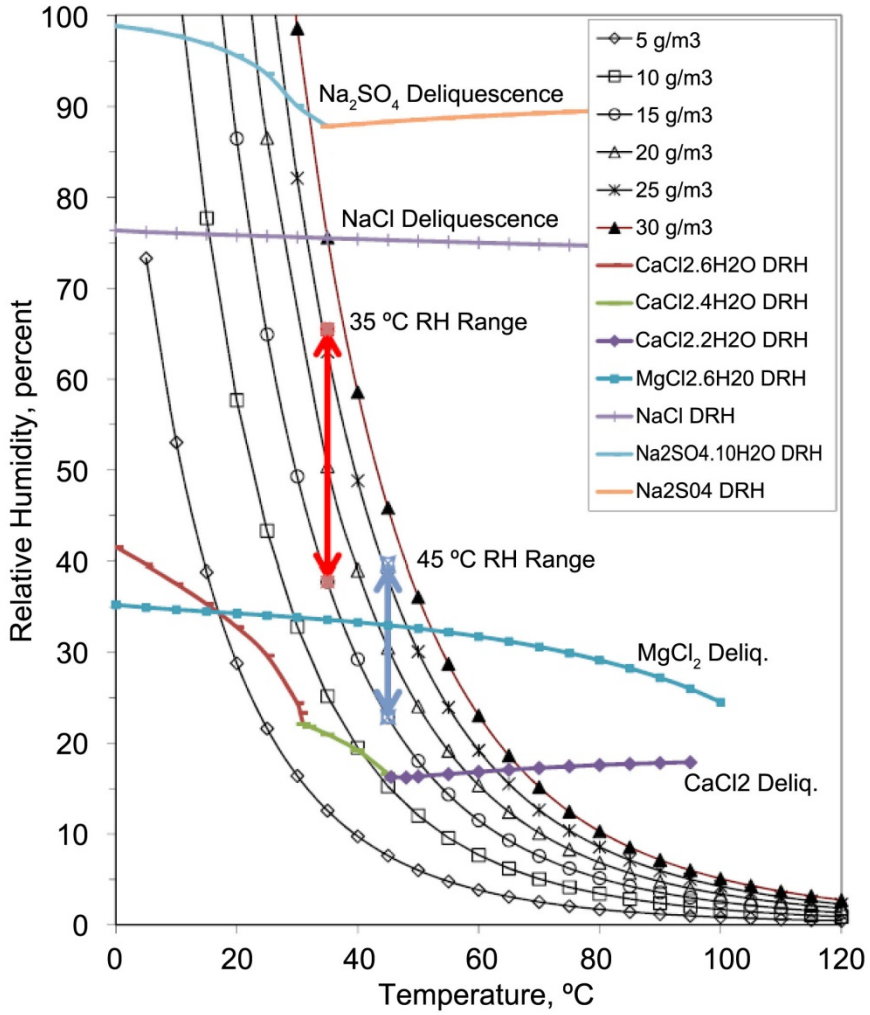

Figure 3.3. Plot of Absolute Humidity Contours versus Relative Humidity and Temperature. Deliquescence thresholds for several salts are superimposed (Mintz et al. 2012). © NACE International 2012.

3.2 Flaw Parameters Affecting Nondestructive Examination Performance

Dimensions: Common dimensional parameters associated with cracks include width, depth, and length; these are defined in Figure 3.4. The width can refer to measurements made at any point along the depth of a crack. The width of a crack at the point where it intersects the surface of a material is referred to as the crack opening displacement (COD). At the crack tip, the "crack tip radius" is the metric often used to quantify separation of fracture surfaces and is approximately half of the crack width. In the flaw morphology compilation efforts of Ekstrom and Wåle (1995) and Wåle (2006), crack width measurements were recorded at the surface, at half the distance between the surface and the crack tip, and at the crack tip.

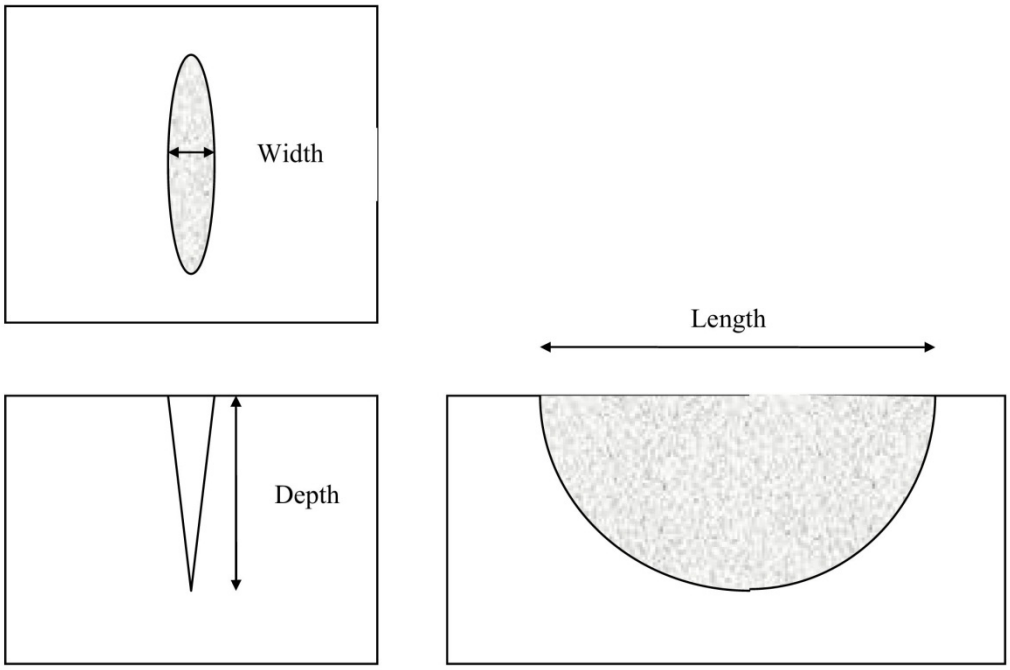

Figure 3.4. Definitions of Crack Length, Depth, and Width (Wåle 2006); reprinted with permission

Orientation: Flaw orientation refers to the through thickness and surface direction of a flaw. Both directions are described using a separate set of angular definitions for flaws located near and far away from a weld. Figure 3.5 provides the definition of through-thickness flaw orientation near a weld according to Wåle (2006). As indicated in Figure 3.5, angles less than 90° are assigned to describe flaws tilted toward the weld, while angles greater than 90° are assigned to describe flaws tilted away from the weld. For cracks located far from welds, the direction of tilt is ambiguous and is always defined as less than 90°. The surface orientation of flaws is similarly defined using angular definitions. Flaws located far from a weld are defined as being oriented at 0° when parallel to the longitudinal direction of a pipe and at 90° when oriented in the circumferential direction. Near a weld, the surface orientation is defined as 0° when the flaw is parallel to the weld and 90° when the orientation is perpendicular to the weld.

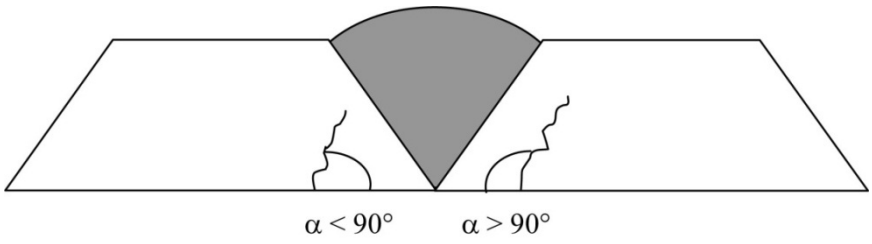

Figure 3.5. Definition of Angles when the Crack is Located Close to a Weld (Wåle 2006); reprinted with permission

Shape: The expressions used to describe the shape of cracks are straight, winding, bend, bilinear, and branched. These expressions, which are defined in Figure 3.6, are qualitative and are used to describe the shape of cracks in the through thickness and surface directions (Wåle 2006).

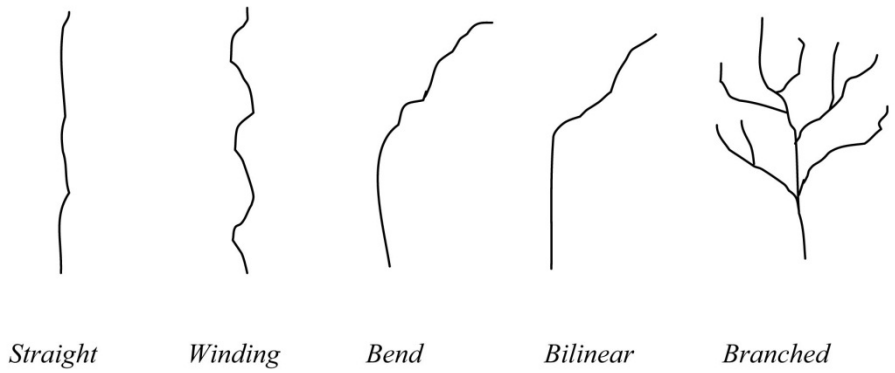

Figure 3.6. Schematic Illustration of Typical Crack Features Used to Categorize Crack Shape in Surface and Through-Thickness Direction (Wåle 2006); reprinted with permission

Fracture Surface Roughness: The roughness of the fracture surface can be quantified using several parameters that may be computed from images or photographs of the fracture surface. A relatively simple parameter is the "ten point height of irregularities," R_z, which is calculated from the five highest peaks and five lowest valleys of the crack profile over some length of the crack (see Figure 3.7),

$$Rz = \left\{ \left(R1 + R2 + R3 + R4 + R5 \right) - \left(R6 + R7 + R8 + R9 + R10 \right) \right\} / 5 \tag{3.1}$$

The correlation length, λ_0, is a parameter to quantify rate of change of fracture surface height along the length of the surface. A definition for λ_0 is provided in Figure 3.8. A simplified formula for computing λ_0 is

$$\lambda_0 = L/2X, \tag{3.2}$$

where X is the number of times the crack intersects a straight line drawn through the fracture surface profile over a certain length, L.

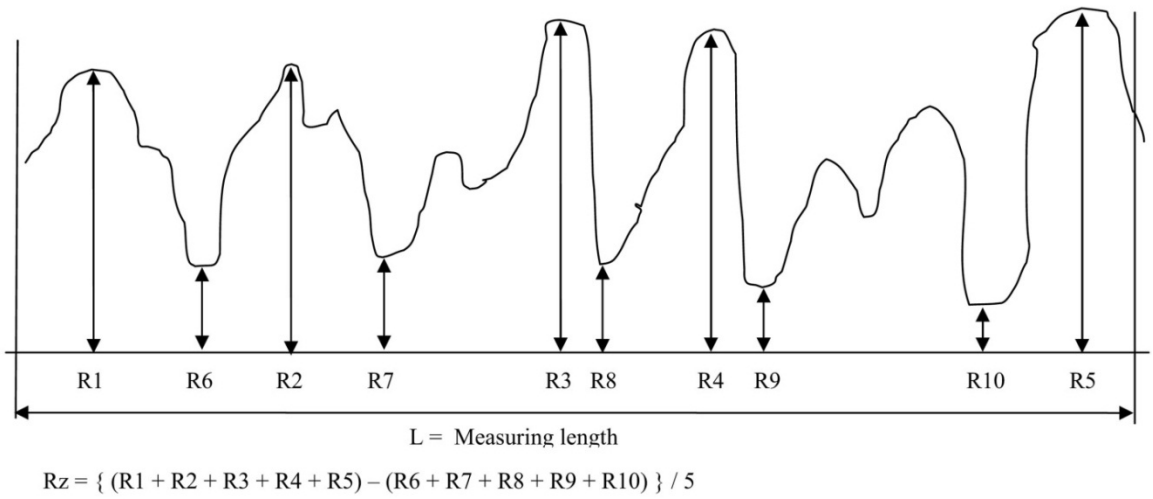

Figure 3.7. Definition of the Crack Surface Roughness Parameter, R_z (Wåle 2006); reprinted with permission

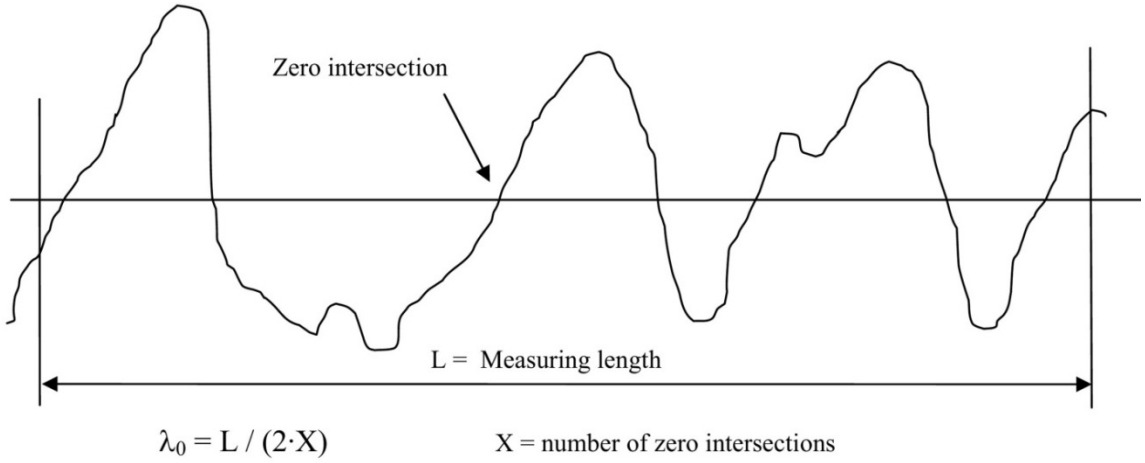

Figure 3.8. Definition of Correlation Length, λ_0 (Wåle 2006); reprinted with permission

3.3 Compilation of Stress Corrosion Cracking Features by the Swedish Radiation Safety Authority

SSM has performed a systematic evaluation of service-induced crack characteristics. This evaluation was initially performed using information from failure analysis reports from the nuclear and non-nuclear industries through 1994 (Ekstrom and Wåle 1995; Wåle 2006). Cracks are assessed according to crack type and material with several different crack types considered in the analysis. The results are compiled in Table 3.1. The mean COD for SCC cracks analyzed ranged from 16 to 30 μm. In many instances, the crack tip radius could not be measured; however, given the data available, the mean crack tip radius appears to be approximately 1 μm or less for SCC cracks. Several other flaw parameters were catalogued

including the flaw orientation, flaw size, fracture surface roughness, flaw tortuosity, and flaw branching characteristics.

Table 3.1. Compilation of SCC Flaw Characteristics in LWR Environments (from Wåle 2006)

		TGSCC SS	IGSCC SS	IGSCC Ni	IDSCC Ni
Angle on Surface	Points	6	26		12
	Minimum	0	0		0
	Maximum	90	20		90
	Mean	45	1.65		78.8
	Median	45	0		90
	RMS	58.1	5.37		82.4
	Std Deviation	40.2	5.21		25.6
	Variance	1620	27.1		655
Shape on Surface	Straight	9	25	3	11
	Winding	2	10	1	4
	Bend	2	4		
	Branched	2			
	Cobble Stone				
Angle Through Thickness	Points	27	71	14	19
	Minimum	45	40	60	45
	Maximum	90	100	90.6	90
	Mean	82.6	85.6	85.0	78.4
	Median	90	90	90	80
	RMS	83.5	86.0	85.7	79.3
	Std Deviation	12.7	8.39	10.9	12.1
	Variance	162	70.5	120	147
Crack Surface Roughness	Points	29	69	19	24
	Minimum	10	8	8	5
	Maximum	90	200	142	288
	Mean	37.1	70.7	42.8	106
	Median	36	68	27	79.5
	RMS	42.7	80.9	55.3	135
	Std Deviation	21.6	39.6	36.0	85.2
	Variance	465	1568	1299	7267
Correlation Length	Points	12	72	17	26
	Minimum	15	5	3.1	17
	Maximum	160	310	150	500
	Mean	50.6	79.5	34.9	150
	Median	31	71	14	113
	RMS	67.2	97.5	53.1	193
	Std Deviation	46.2	56.9	41.3	124
	Variance	2140	3240	1710	15500
Number of Intersections / mm	Points	5	38	3	5
	Minimum	3	1.6	7	1
	Maximum	10	18	72	5
	Mean	6.88	7.01	37.3	2.74
	Median	8.1	6	33	2
	RMS	7.44	8.15	45.9	3.13
	Std Deviation	3.18	4.21	32.7	1.68
	Variance	0.086	17.8	1070	2.84

4.0 Surveillance and Inspection Methods

This section discusses several potential NDE methods for performing examinations of DCSS canister surfaces for detection and characterization of atmospheric SCC flaws. The methods considered in this section include bulk ultrasonic techniques, acoustic emission (AE), visual (VT), eddy current (ET), and guided ultrasonic waves (GUW).

4.1 Bulk Ultrasonics

Ultrasonic testing (UT) refers to the techniques of injecting high-frequency (wavelength much less than component dimensions) ultrasonic waves into specimens for the detection of flaws or other imperfections by sensing the ultrasonic energy scattered by the flaws or imperfections. The scattered ultrasonic energy is converted to electrical signals, which can be immediately viewed or recorded for later analysis. Bulk ultrasonic waves may propagate in solid materials in either longitudinal or shear wave modes. Longitudinal waves are polarized such that the direction of displacement or pressure fluctuations are oriented along the direction of wave propagation, while shear waves are polarized such that pressure fluctuations are perpendicular to the direction of wave propagation. Two different shear wave polarizations are possible and defined in Figure 4.1. Figure 4.1 provides a schematic illustration of possible transmission and reflection scenarios when longitudinal or shear waves are incident on a solid-solid or solid-vacuum (or gas) interface.

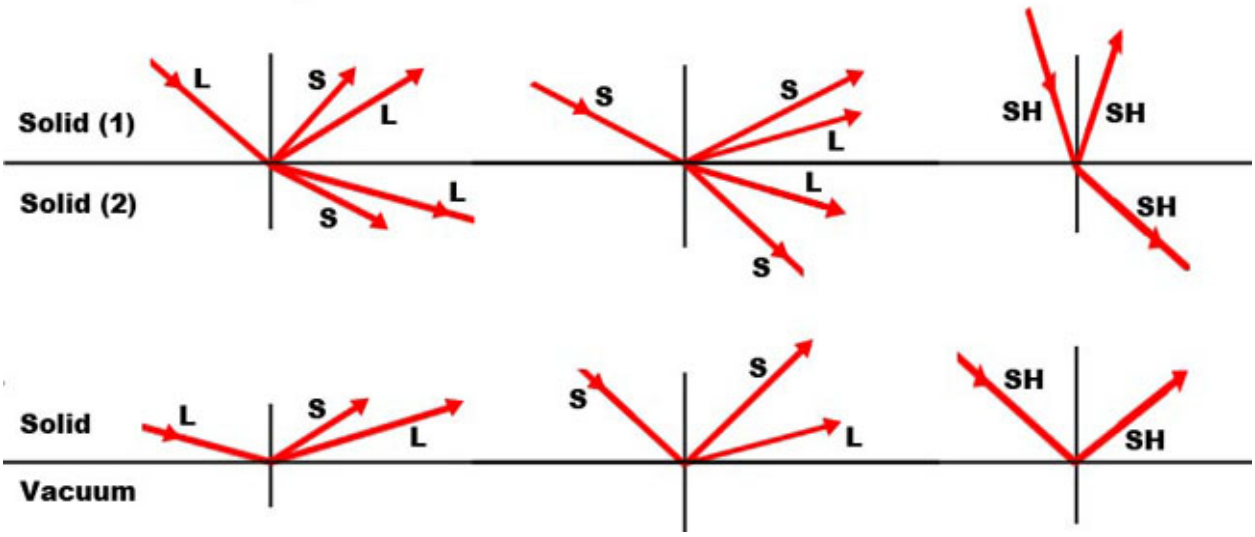

Figure 4.1. Schematic Illustration of the Multiple Types of Mode Conversions that Occur when Longitudinal (L), Shear (S), or Shear Horizontal (SH) Waves are Reflected from an Interface

Bulk waves interact with an interface between two mediums according to Snell's law and as a consequence, because the longitudinal wave velocity is greater than the shear wave velocity, the longitudinal wave is refracted at a larger angle. Several shear wave angles have been calculated (see

Table 4.1) to correlate with several longitudinal wave angles of interest over 0°–90° in steel, assuming the L-wave velocity is 5900 m/s and the S-wave is 3200 m/s.

Table 4.1. Summary of Several L-wave Examination Angles of Interest and Corresponding S-wave Angles

Θ_L (L-wave angle in degrees)	Θ_S (S-wave angle in degrees)
30	16
45	22
60	28
70	30
90	33

4.1.1 Ultrasonics for Weld Inspection

Fundamental science and physics aspects related to ultrasonic wave sources, propagation, and scattering are covered in several textbooks including those by Ensminger and Bond (2011), Cheeke (2002), and Rose (1999). Several practical considerations related to ultrasonic examinations for materials characterization and nondestructive examination applications are provided in the American Society for Nondestructive Testing (ASNT) *Nondestructive Testing Handbook*, Volume 7 (ASNT 2007). An overview of several nondestructive examinations of welds using UT techniques is provided by Moran et al. (2010). Several ultrasonic crack sizing techniques for inner diameter (ID) surface-connected flaws are described in Davis (1998).

A typical UT system consists of transducers, a pulse generator, an amplifier, a receiver, couplant, and a device to record/display the signal. Typical frequencies used to inspect stainless steel and nickel-base alloy materials commonly used in nuclear vessel welds are generally between 0.2 and 2.25 MHz. UT is typically performed by through-transmission (transducer on opposite sides of a component) or pulse-echo mode (a single transducer located on only one side). Pitch-catch mode (also referred to as dual mode) employs two separate transducers located on a single side of a component for signal transmission and receiving. All three of these techniques are illustrated in Figure 4.2. The pitch-catch mode is commonly used for inspecting materials that are naturally noisy (cladding, stainless steels) and is more commonly used for nuclear power plant (NPP) inspections than through-transmission mode. The pulse-echo and pitch-catch modes are able to measure both the transit time and attenuation of signals; whereas the through-transmission mode only allows measurement of signal attenuation. As a consequence, pulse-echo and pitch-catch modes can provide more information about flaws including flaw location, length, and flaw depth. A further disadvantage of through-transmission techniques relative to pulse-echo and pitch-catch is that they require access to both the inside and outside component surfaces.

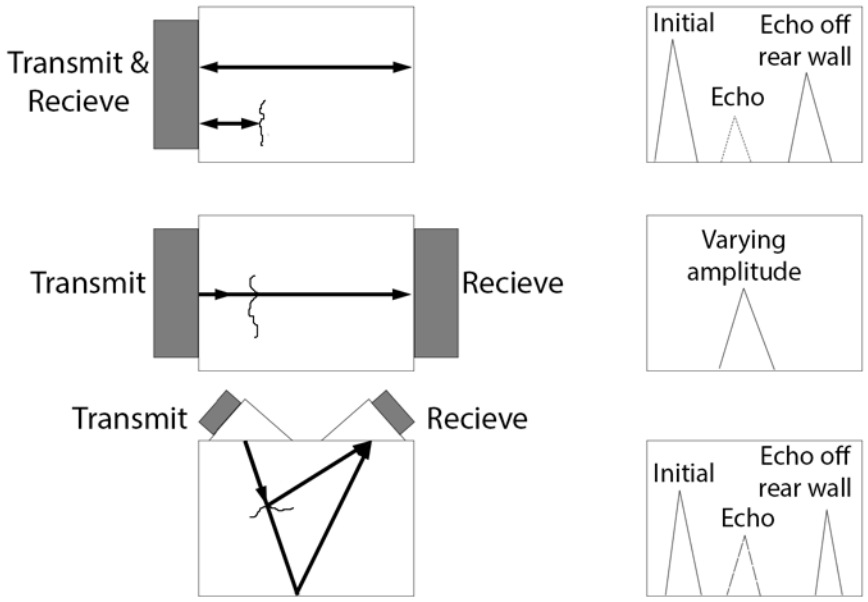

Figure 4.2. Typical Ultrasonic Testing Techniques: a) pulse-echo, b) through-transmission, and c) pitch-catch

4.1.1.1 Angle Beam Examinations

Ultrasonic inspections may be performed using transducers oriented normal to the surface of a component or at an angle. The latter scenario is typical for weld inspections aimed at detecting and characterizing cracks that form in the heat-affected zones (HAZ) because cracks are usually oriented so that the crack face is parallel to the beam direction of normal incidence probes. Introduction of ultrasonic energy at an angle is necessary to ensure significant interaction of the beam with a crack. Angle beam transducers are commonly fabricated to generate longitudinal or shear waves at 30°, 45°, and 60° in stainless steel material (ASNT 1991).

4.1.1.1.1 V-Path Examinations

In the nuclear power industry, service-induced flaws in Class 1 safety piping and vessels typically manifest as ID surface-connected cracks. Pulse-echo mode inspections can be employed using angle beam transducers to detect and characterize back-surface-connected flaws using a half-V beam path as illustrated in Figure 4.3. For front-surface-connected flaws, pulse-echo mode inspections may be conducted using a full-V beam as illustrated in Figure 4.4. A corner trap reflection is indicated in both figures, although the beam can return to the transducer upon reflection from the crack face. Detection of corner trap signals is often used to identify the base of a crack and aid in sizing. Full V-path examinations may be affected by the contact of the fuel basket with the inner surface of the canister.

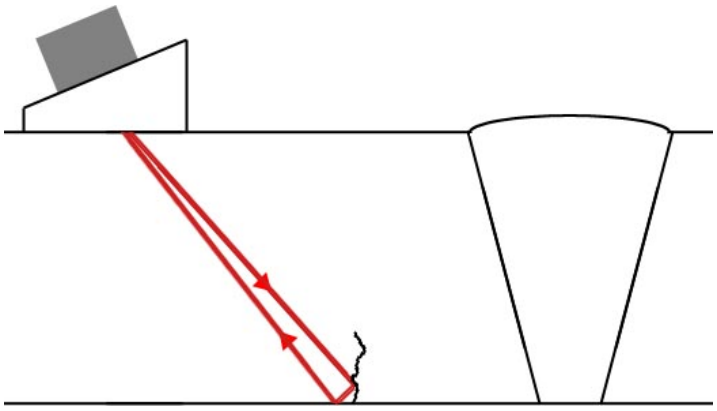

Figure 4.3. Illustration of Half-V Path Technique for Examination of Back Surfaces and Detection of Back-Surface-Connected Flaws

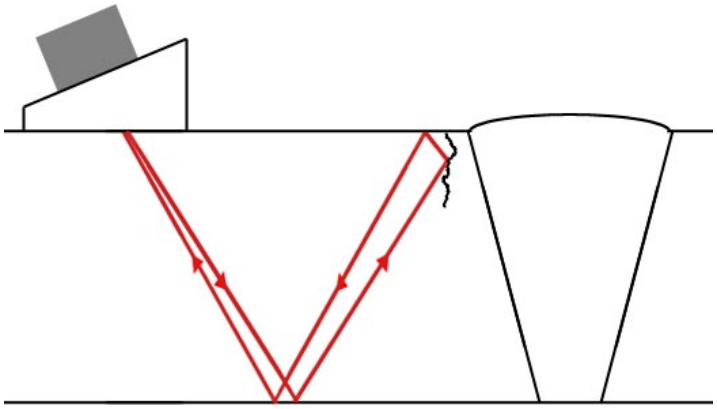

Figure 4.4. Illustration of Full-V Path Technique for Examination of Front Surfaces and Detection of Front-Surface-Connected Flaws

4.1.1.1.2 High-Angle L-Mode Examinations

High-angle longitudinal mode (L-mode) examinations can be performed to detect and help characterize large back-surface-connected cracks (greater than 50 percent through wall) by sampling material located in the region near the front surface of the component under test (ASNT 1991). In practice, the technique is commonly employed using an L-wave refracted at 70° as illustrated in Figures 4.5 and 4.6. This technique may be more effective at detecting and sizing front-surface-connected flaws because material near the front surface is preferentially sampled.

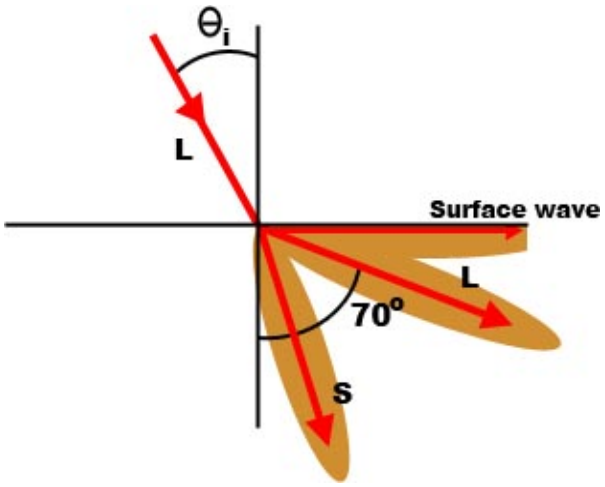

Figure 4.5. Vector Depiction of High-Angle (70 degrees) Longitudinal (L-mode) Refraction and Accompanying Side Lobe Surface Wave

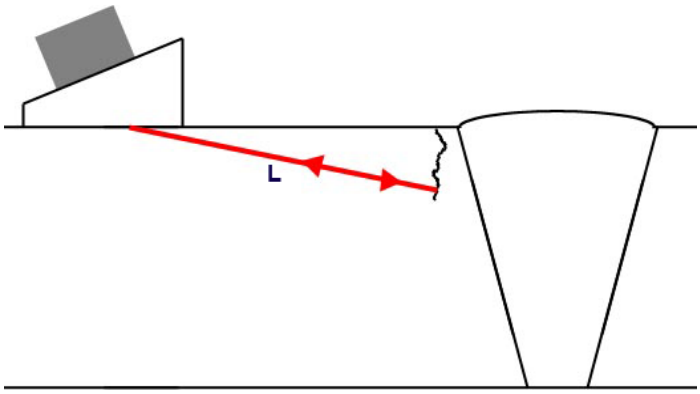

Figure 4.6. Illustration of High-Angle L-mode Examination Technique for Detection of Front-Surface-Connected Flaws

4.1.1.1.3 Tip-Diffracted Signals

Interaction of the incident beam on the face of a crack will induce an oscillation along the face of the crack alternately opening and closing the crack. This signal can propagate along the face of the crack until it reaches the tip where the energy is re-emitted into the bulk material with a spherical wave-front (see Figure 4.7). The re-emitted signal is referred to as the tip-diffracted signal and a portion of the signal travels back to the transducer and may be detected. An accurate technique for depth sizing of flaws involves measuring the relative time-of-arrival (TOA) of the corner-reflected signal from the base of a flaw and the tip-diffracted signal. The tip-diffracted signal is normally very weak compared to the corner-reflected signal and can be difficult to detect in practice. Crack branching can degrade sizing accuracy as multiple crack tips can result in the emission of several tip-diffracted signals making it difficult to resolve the crack tip of interest (typically the deepest tip for use in structural integrity assessment) (see Figure 4.8).

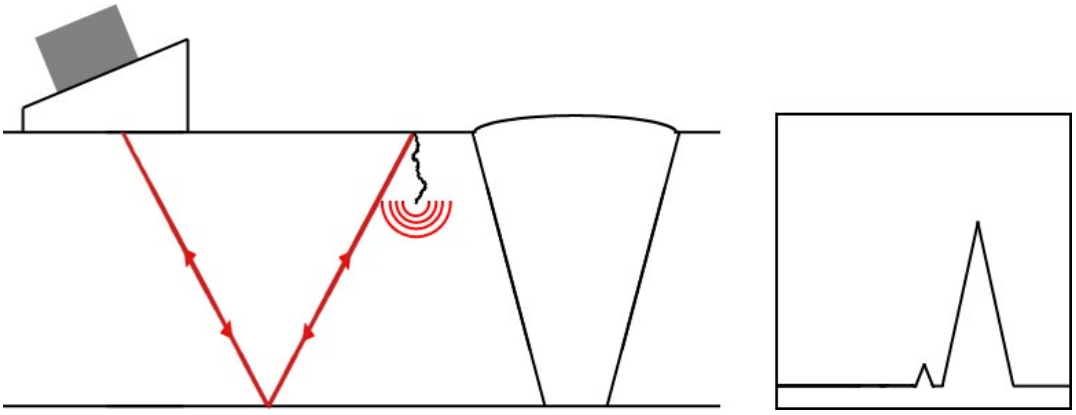

Figure 4.7. Illustration of the Excitation of a Tip-Diffracted Signal Because of Interaction of Incident Beam with Base of Crack

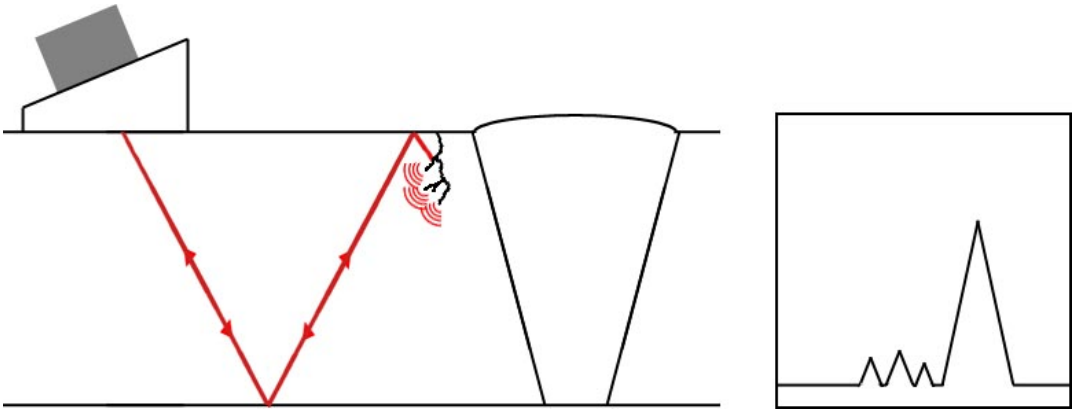

Figure 4.8. Illustration of How Multiple Tip-Diffracted Signals from Branching Cracks May Make It Increasingly Difficult to Resolve Crack Tip Signals of Interest

4.1.1.1.4 Surface Waves

The angle of the incident beam can be increased until a critical angle, θ_{CR1}, is reached at which an L-wave is refracted at 90° in the component of interest; thus, traveling along the surface of the component is indicated by Figure 4.9. Surface waves can also be generated from side lobes of high-angle beams as illustrated in Figure 4.5. Surface waves are very sensitive to surface conditions of the component and attenuation can limit the range of sampling. Surface waves can be useful for detection of front surface cracks and length sizing of such cracks, but they cannot be used to determine crack depth. Depth sizing may be achieved by combining surface wave signals with tip-diffracted signals or high-angle beam reflections.

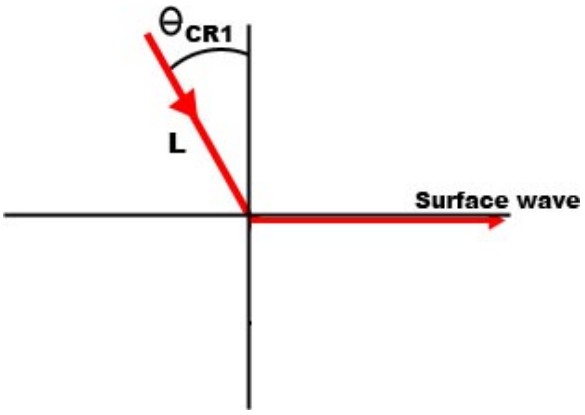

Figure 4.9. Vector Depiction of Surface Wave Generation at the Critical Angle, θ_{CR1}

4.1.1.1.5 Time-of-Flight Diffraction Technique

The time-of-flight diffraction (TOFD) technique is a dual-probe method using one probe for transmitting and the other probe for receiving (Figure 4.10). The transmitter introduces an L-mode beam at an angle and a so-called "lateral wave" that propagates along the component surface. With no flaws present, the receiver will pick up a back-wall echo and the transmitted lateral wave. The transit time information for the back-wall signal and lateral wave can enable crack detection and location. In the case of front-surface cracks, crack detection and location will be based on the lateral wave echo. Depth sizing may be accomplished by detection and transit time analysis of a tip-diffracted signal. TOFD examinations may be affected by the contact of the fuel basket with the inner surface of the canister.

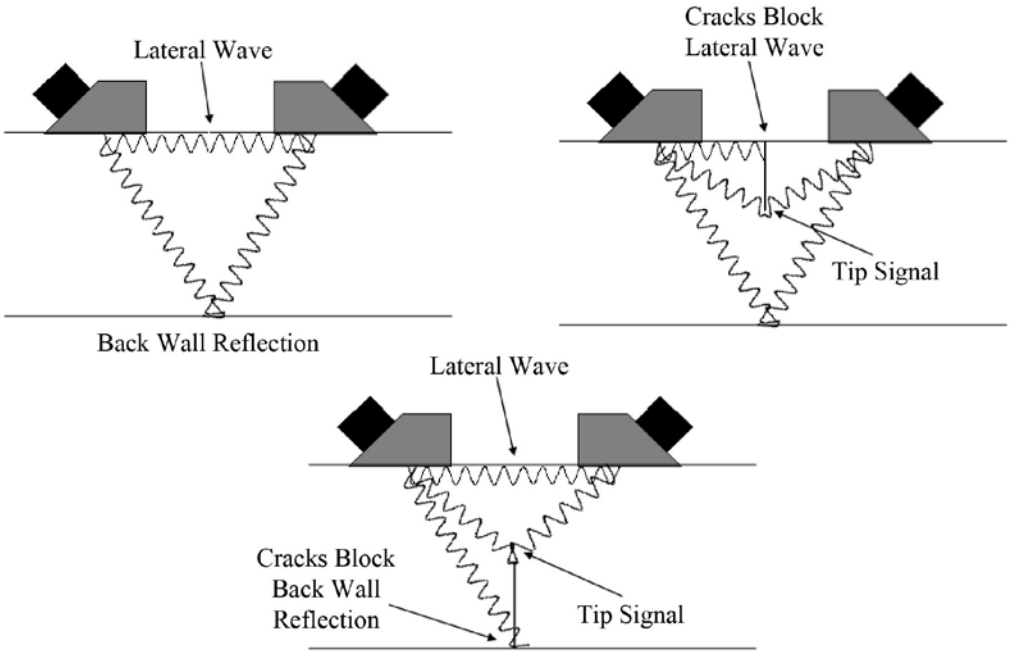

Figure 4.10. Diagram of Time-of-flight Diffraction Technique (Moran et al. 2010)

4.1.1.1.6 Phased Ultrasonic Array Technique

Phased ultrasonic arrays rely on phase shifting of multiple piezoelectric elements to electronically focus and steer a beam as illustrated in the diagram of Figure 4.11. This can help minimize the impact of relative probe-flaw orientation as phased-array probes can rapidly sample a flaw from multiple angles. The multi-view scans can be combined with signal processing electronics to build up images of the flaw as depicted in Figure 4.12. Array probes can have multiple configurations including linear, matrix, or annular element configurations. Phased-array probes are less compact than single-element transducers because they incorporate multiple piezoelectric elements.

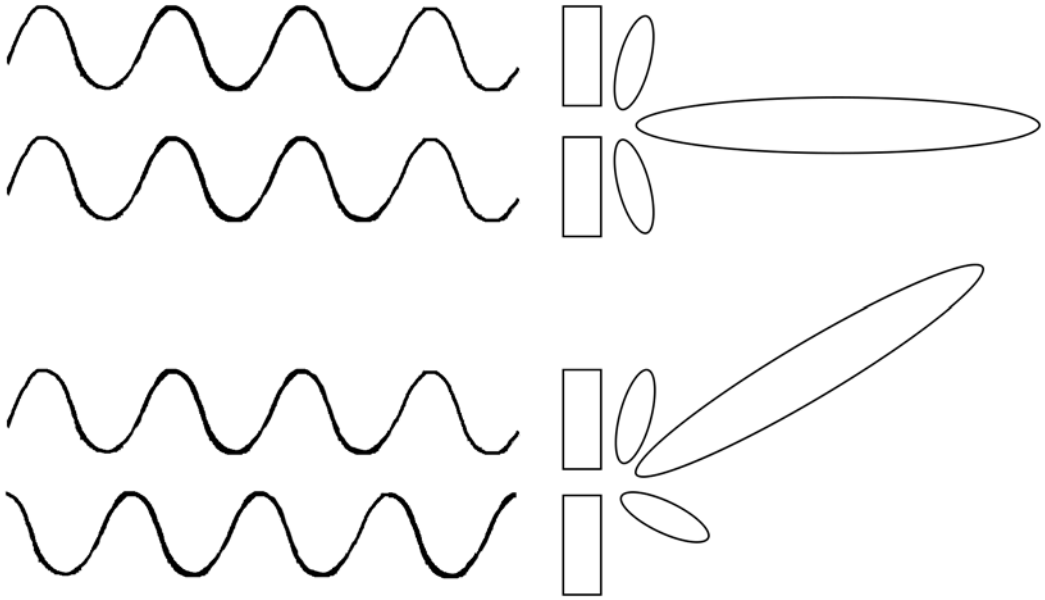

Figure 4.11. Diagram of Phased-Array Principle for Electronic Control of Ultrasonic Beam Formation

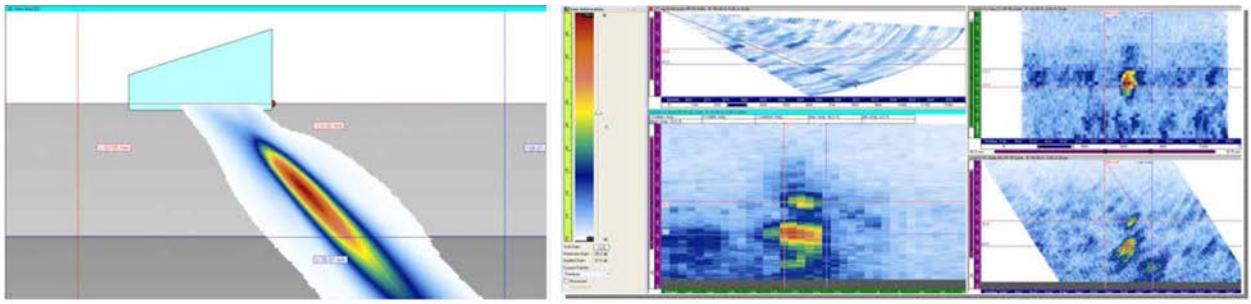

Figure 4.12. Diagram of Phased-Array Beam Formation and Image Display (Moran et al. 2010)

4.1.1.2 Normal Beam Inspections

Normal beam ultrasonic probes are generally not very useful for weld examinations because inspection access is normally limited to component surfaces that are perpendicular to the direction of

crack growth. In the case of the circumferential weld attaching a top lid plate to the cylindrical shell of a dry cask canister, the top lid surface may be parallel to the direction of anticipated crack growth. Therefore, it may be feasible to inspect these circumferential welds from the surface of the top lid plate using a normal beam probe (see Figure 4.13). Lack of access will prevent the application to inspection of circumferential welds attaching the bottom plate to the cylindrical shell. Alternatively, the weld configuration may be as indicated in Figure 4.14. In this case, a normal beam examination of the weld may be conducted with the transducer mounted to the surface of the canister shell. This technique relies on normal reflections from the crack face and therefore sizing may be performed based on amplitude techniques. The feasibility of this technique will depend on the distance from the transducer to the flaw and on details of the lid design.

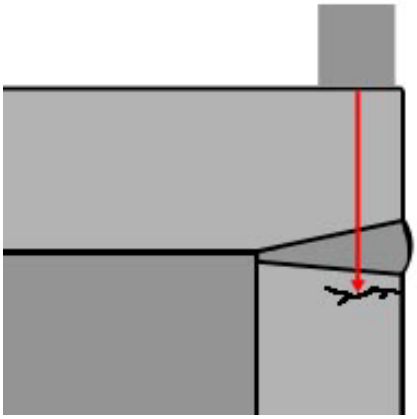

Figure 4.13. Depiction of Examination of Top Lid Plate Circumferential Weld Using a Normal Beam Probe Mounted to the Surface of the Top Lid Plate

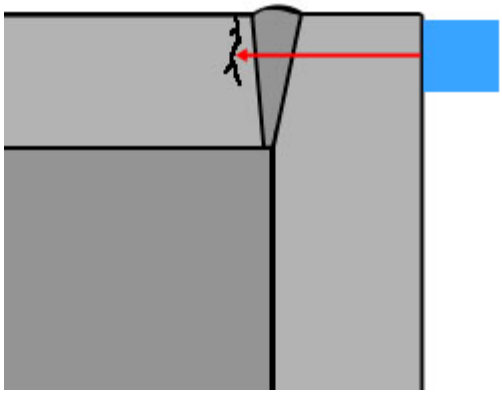

Figure 4.14. Depiction of Examination of Top Lid Plate Weld Using a Normal Beam Probe Mounted to the Canister Shell

4.1.2 Ultrasonic Testing Performance and Reliability

Ultrasonic testing is the dominant NDE method employed for performing in-service examinations of safety-related components in the nuclear power industry. An overview of the history of in-service inspection in the nuclear power industry is provided by Doctor (2008). A series of parametric studies and round-robin studies were initiated in the 1970s to understand the effectiveness and reliability of UT examinations as they are performed in the field. A significant conclusion of these studies was that human factors are a significant source of variability and that UT is very skill-dependent. The results of several of these studies on crack detection in austenitic stainless steel have shown that the average probability of detection (POD) for flaws of 5-mm (0.20-in.) depth has been around 70 percent (Heasler and Doctor 2003).

Moran et al. (2010) have reviewed literature related to the parametric and round-robin studies of UT. Some conclusions that can be drawn from these studies are that the performance of UT inspections are affected by different flaw sizes and shapes, grain structure of materials, frequency and beam angles, interference by detected and refracted signals, couplant variations, human factors in acquiring and analyzing data, curvature of the component and surface interferences, weldment design, and orientation and location of the flaw relative to the angle of the signal beam. Several studies comparing manual UT and automated UT found that automated UT has on average a higher detection rate than manual UT (Heasler et al. 1993; Kim et al. 2004; Rudlin et al. 2004; Rebello et al. 2006).

An in-depth review of the influence of essential flaw parameters on UT examinations is provided by Kemppainen and Virkkunen (2011). This review is performed considering the compilations of crack characteristics by SSM (Ekstrom and Wåle 1995; Wåle 2006) and from the perspective of validating or confirming the representativeness of flaw specimens for NDE qualification. They considered the effects of crack size, crack morphology, fracture surface roughness, fracture surface separation (crack width), crack orientation, and the effects of a crack filled with water or debris. It is noted that a rough fracture surface results in significant diffuse scattering of the incident beam; whereas, a smooth fracture surface results in mostly specular reflection (Ogilvy 1989). Thus, rough fracture surfaces may be advantageous for the detection of cracks oriented at glancing angles with respect to the probe. On the other hand, rough fracture surfaces make sizing more difficult. The COD can affect detection as tightly closed cracks may enable transmission of elastic waves through the crack faces. Observations of this effect have been reported for fatigue cracks with CODs below 10 μm (0.393 mil) (Iida et al. 1988).

4.1.3 Ultrasonic Testing Transducers

A diagram of a typical piezoelectric-based ultrasonic transducer is shown in Figure 4.15. A typical ultrasonic transducer consists of piezoelectric element coupled to a front plate or surface and housed within a metal casing. Transducers also typically incorporate a backing layer for damping that determines the Q and bandwidth of the sensor (Ensminger and Bond 2011).

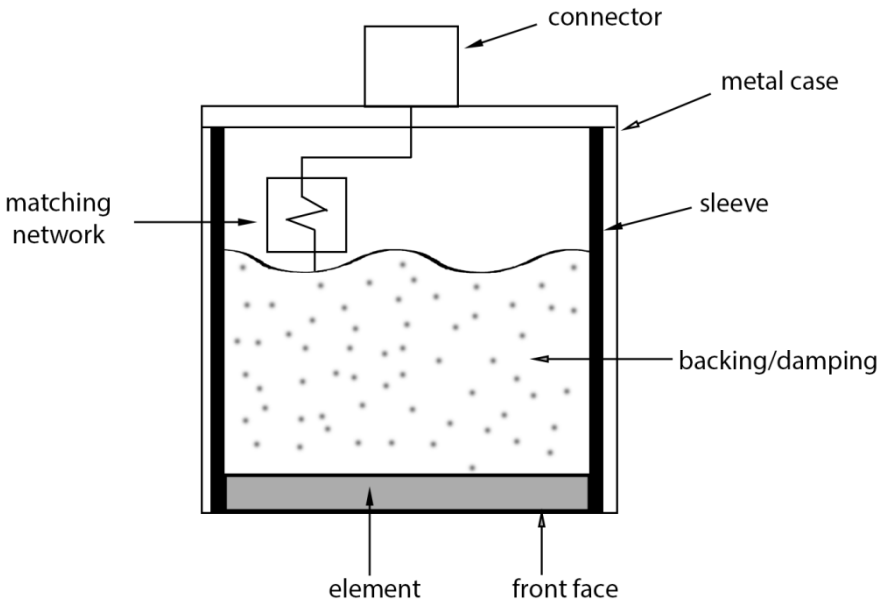

Figure 4.15. Diagram of a Typical Single Element Ultrasonic Transducer with Piezoelectric Element

Several contact transducers (2.25–5.0 MHz) are shown in the photograph of Figure 4.16. This photograph provides a reference for typical transducer dimensions in metric units. A phased-array probe transducer is shown in Figure 4.17. This particular probe is designed to operate at 1.0 MHz and consists of a transmitter and receiver unit. Each unit contains its own matrix array (5×10) of 50 total elements. The ruler in Figure 4.17 provides a reference to the scale of the dimensions of a typical phased-array transducer in metric units. The size of the probe typically scales inversely with the frequency of operation. It may be feasible to work with vendors on customized probe designs to suit particular applications.

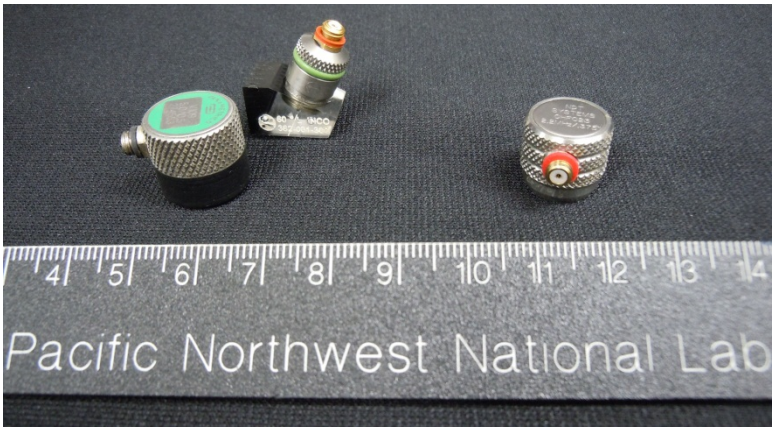

Figure 4.16. Several 2.25-MHz and 5.0-MHz Contact Ultrasonic Transducers Including a Transducer Mounted to a Wedge for Angle-Beam Inspections

Figure 4.17. A 1.0-MHz Phased-Array Probe Consisting of a Transmitter and Receiver Unit

4.2 Acoustic Emission

Acoustic emission refers to the generation of elastic energy in a material resulting from stress accumulation and relaxation. The shedding of stress by a material because of crack extension or corrosion can result in detectable acoustic emissions facilitating the monitoring of materials for damage through coupling of AE transducers to the surface of the test material (see Figure 4.18). AE is unique compared to other NDE technologies in that it is sensitive to the dynamic processes of damage progression.

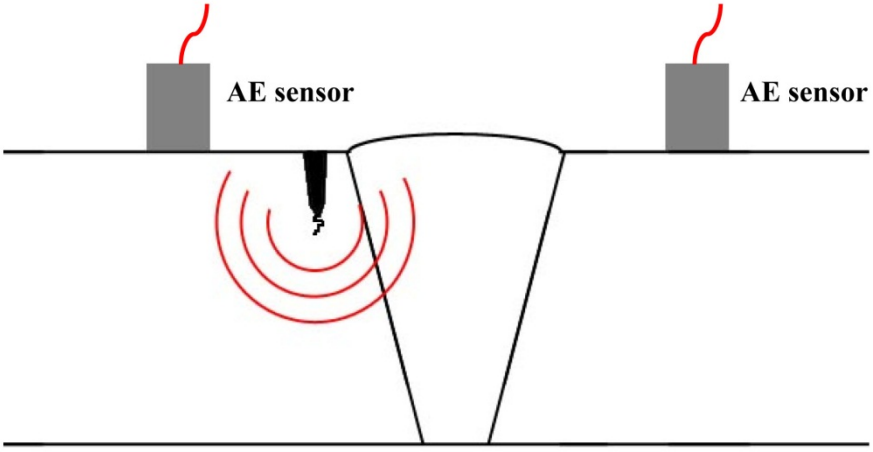

Figure 4.18. Depiction of Acoustic Emission Generation by Crack Extension and Detection by Acoustic Emission Sensors Coupled to the Surface of a Component

4.2.1 Nuclear Power Industry Experience

AE has been intensively studied as an NDE technology since the 1960s. Several documents emphasize that initial enthusiasm for the technique was quenched when it failed to meet initial expectations for performance (Borst 1977; Pollock et al. 1988; Hutton 1989). From the perspective of the

nuclear power industry, several developments that tempered initial enthusiasm included (Bentley 1981; Runow 1985; Scruby 1987; Macleod et al. 1991):

- the realization that originating AE signals are masked by the response functions of typical resonant piezoelectric transducers, diluting the information content of the signals and increasing the difficulty of signal discrimination
- the discovery that ductile material of reactor pressure vessels results in weak acoustic emissions and that, in general, emission characteristics are significantly influenced by material and stress conditions
- knowledge that reactor coolant noise is severe enough at low frequencies (≤ 0.2 MHz) that AE from degradation is "drowned-out." Defect detection should be possible at higher frequencies for which noise is significantly reduced. However, attenuation of AE signals is usually severe at higher frequencies and only localized AE monitoring of damage is feasible.

Despite these drawbacks, AE possesses several positive attributes (Jax and Ruthrof 1989), including the ability to monitor structural components during operation and the ability to monitor in regions that are difficult to access by other NDE means. Consequently, AE is a valuable tool for several niche applications. Within the nuclear industry, applications of AE include pre-service and periodic in-service hydrotesting of pressure vessels (Bentley 1981; Runow 1985; Jax and Ruthrof 1989; Lucia and Tonolini 1989; Benz 1998), continuous monitoring of flaws in pressure boundary components (Bentley 1981; Pollock et al. 1988; Jax and Ruthrof 1989; Benz 1998; Kupperman et al. 2004), continuous monitoring of leaks in pressure boundary components (Bentley 1981; Runow 1985; Pollock et al. 1988; Hutton 1989; Jax and Ruthrof 1989; Lucia and Tonolini 1989; Macleod et al. 1991; Benz 1998; Kupperman et al. 2004), leakage monitoring in valves (Pollock et al. 1988; Hutton 1989; Benz 1998), loose parts monitoring (Lucia and Tonolini 1989; Macleod et al. 1991), and the monitoring of the fabrication welding process (Bentley 1981).

Experience applicable to continuous flaw monitoring implies that 1) the severity of flaws in large, complex structures cannot be easily quantified using AE; and 2) only flaws growing at macroscopic rates can be detected reliably (Bentley 1981; Runow 1985; Jax and Ruthrof 1989).

The viability of implementing AE to continuously monitor IGSCC flaws in pressure boundary components during the operation of nuclear power plants has been demonstrated at the Limerick Unit 1 reactor (Hutton et al. 1993). In this field demonstration, the AE sensors were coupled to the component of interest through metal waveguides to isolate the sensitive piezoelectric materials from the environment at the surface of the component.

The accumulated experience with AE helped form the basis for American Society for Mechanical Engineers (ASME) Boiler and Pressure Vessel (B&PV) Code (ASME Code) rules developed for continuous on-line monitoring (OLM) with AE sensors, which is addressed in Article 13 of Section V of the ASME Code and Section XI. Currently, the ASME Code supports OLM with AE to supplement traditional periodic inspection methods. Despite the ASME Code development effort, continuous AE monitoring has not been widely adopted within the U.S. nuclear power industry. Presumably, this is because of concerns about reliability and because of the lack of regulatory relief or credit awarded to utilities for implementing this technology (Hutton 1989).

4.2.2 ASME Boiler and Pressure Vessel Code Requirements

Section XI of the ASME Code, "Rules for In-service Inspection of Nuclear Power Plant Components," Division I, governs the use of acoustic emission as part of in-service examinations of nuclear power plant components. The use of acoustic emission for volumetric examinations is discussed in paragraph IWA-2234 (ASME 2007). Paragraph IWA-2234 restricts flaw monitoring with AE to monitoring the growth of existing flaws that have been characterized using other NDE technologies (e.g., via ultrasonic examinations). A bounding equation is provided for the purpose of evaluating flaw growth rate from AE activity. This evaluation must be performed every two months and extrapolated to the next outage to determine if mitigating or repair activities are necessary or if operation may continue. The equation used to evaluate flaw growth rate is

$$da/dt = \left(C/\left(A^{n-m}\right)\right)\left(dN/dt\right)^{n-m} \tag{4.1}$$

Section V, Article 13 of the ASME Code specifies $n-m = 0.53$ and $(C/(A^{n-m})) = 290$ where N refers to the number of events and da/dt has units of microinches/second. This equation provides a conservative estimate of flaw growth rate. Requirements for the methodology of continuous AE monitoring are provided in Section V of the ASME Code, Article 13. Article 13 provides guidelines for sensor installation and calibration as well as requirements associated with other components of the AE monitoring system including cables, waveguides, preamplifiers, signal processor, and data monitors.

4.2.3 Emissivity of Stress Corrosion Cracking and Electrochemical Corrosion

The capability of AE for monitoring stress corrosion cracking degradation in nuclear reactor components is assessed by reviewing the emissivity of SCC processes and the relevant field experience with regard to the deployment of AE for monitoring of NPP structures. Several source mechanisms are possible for the generation of AE during SCC degradation, the origins of which are related to mechanical fracture or corrosion processes (Yuyama 1986). Sources associated with mechanical fracture include brittle crack jumps, plastic deformation, decohesion of inclusions or precipitates, martensitic transformation, twinning, microcracking, and slip deformation. Corrosion-related sources include dissolution of metal, evolution of hydrogen gas bubbles, and cracking or breakdown of oxide films (see Figure 4.19). The emissivity of these sources depends significantly on the material and exact crack growth or corrosion process taking place.

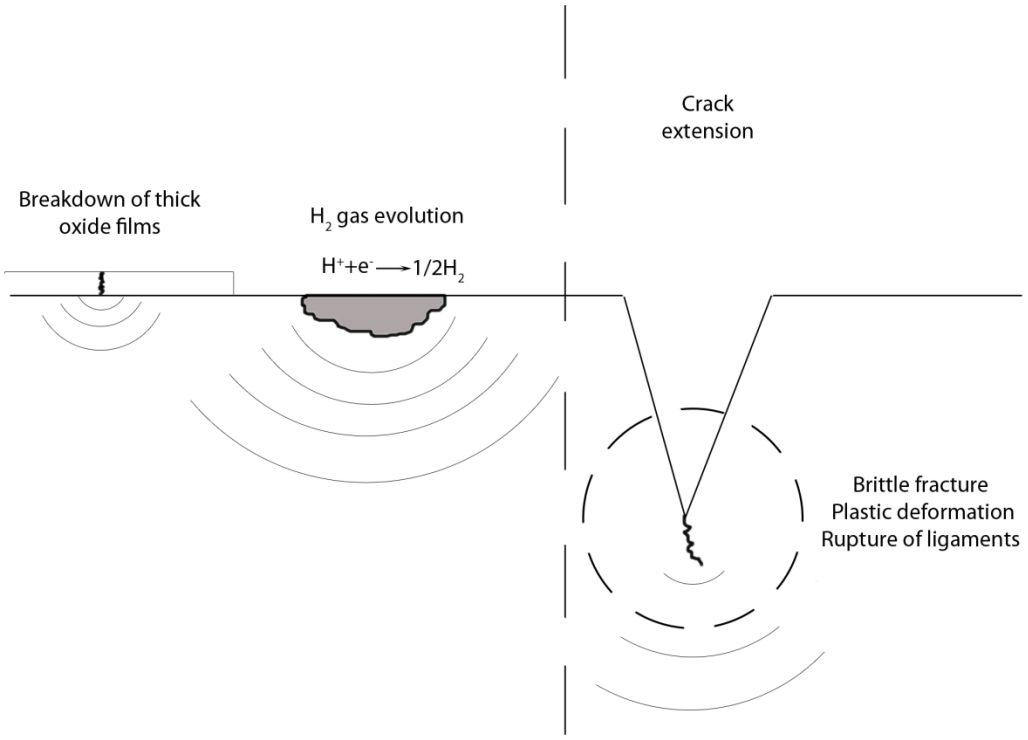

Figure 4.19. Depiction of Possible Acoustic Emission Sources Associated with Corrosion and Stress Corrosion Cracking Phenomena in Metals

4.2.3.1 Emissivity of Brittle Fracture and Hydrogen-Assisted Cracking

In high-strength aluminum and steel alloys, discontinuous brittle fracture is a significant component of the crack growth process. As a result, AE activity is directly linked to the crack growth process and the corresponding AE signals have large amplitudes (Pollock et al. 1988). Similar AE responses are observed for materials undergoing hydrogen-assisted cracking in which material at the crack tip undergoes hydrogen embrittlement. Several investigators (Yuyama 1986; Jones et al. 1991; Shaikh et al. 2007) provide an overview of the early work that characterized the excellent emissivity of high-strength materials and materials suffering from hydrogen embrittlement. Several of these studies are summarized in Table 4.2.

Table 4.2. Summary of Experimental Studies of the Emissivity of Hydrogen-Assisted Cracking and Fracture of High-Strength Steels

Material/Solution	Summary	Reference/Source
Nitrogen-added 304 stainless steel (SS)	Observed discontinuous AE from the hydrogen embrittlement.	Khatak et al. (1997)
300M ultra-high strength steel	Reported a linear relationship between AE energy and crack length, and AE amplitudes were observed to increase with grain size for studies in NaCl solution.	Padmanabhan et al. (1983)
Mild steel	Studied SCC of mild steel in disodium hydrogen phosphate. AE activity was observed to vary significantly with microstructure, alloys, environments, fracture path, and crack velocity. A broad relationship was developed between AE activity and crack growth rate.	Pollock et al. (1982)
4340 steel	Monitored hydrogen-induced cracking and reported proportional relationship between cumulative AE event rate and number of intergranular microcracks.	Nozue and Kishi (1982)
High-strength 4340 steel	Monitored in 3.5% NaCl solution and reported more intense AE during IGSCC than during TGSCC. Also reported correlation between total AE energy and crack area and correlation between AE energy rate and crack growth rate.	McIntyre and Green (1978)
High-strength martensitic steels	Observed significant AE during failure by hydrogen embrittlement.	Okada et al. (1974, 1976)

4.2.3.2 Emissivity of Anodic Dissolution

In contrast to the emissivity of hydrogen-assisted cracking and fracture of high-strength steels, anodic dissolution has been described as disappointing from the perspective of AE monitoring because it is more of a chemical process versus a mechanical one, and does not result in straining the lattice of the underlying material (Pollock 1986). The release of residual subsurface stress as surface layers are etched away by dissolution is one possible means of AE generation during the dissolution process. Many studies of the emissivity of the anodic dissolution process have been conducted with unclear results. For instance, some of the earliest studies indicated that AE from anodic dissolution was not detectable or could be characterized by low-amplitude signals emitted in an essentially continuous fashion. Several studies have attributed observed AE activity to mechanisms other than anodic dissolution (Sung et al. 1997; Yonezu et al. 2006; Shaikh et al. 2007). Zhang et al. (2008) and Kovac et al. (2010) both report that detectable AE is only generated during the final fracture stages of specimens undergoing SCC. Gerberich et al. (1988) and Jones et al. (1989) identified the rupture of ligaments behind the advancing crack front as a source of AE during SCC and that the intensity of the AE activity was proportional to the fraction of TGSCC. More recently, Alvarez et al. (2008, 2012) and Lapitz et al. (2007) have investigated SCC processes in several materials using AE and have concluded that ligament rupture is a detectable source of AE in all materials studied. These investigators also found that activity from TGSCC was approximately an order of magnitude greater than activity from IGSCC and that the shapes of signals emitted for both processes were similar. Highlights from these works are summarized in Table 4.3.

Table 4.3. Summary of Experimental Studies of the Emissivity of the Anodic Dissolution Process in Steels

Material	Summary	Reference/Source
α-brass 304 SS Silver gold alloys	Studied TGSCC and IGSCC processes and reported that AE activity from TGSCC is approximately an order of magnitude greater than AE activity from IGSCC. Further, it was reported that both processes generate similar AE signals and these are attributed to ligament rupture behind an advancing crack front.	Lapitz et al. (2007) Alvarez et al. (2008) Alvarez et al. (2012)
Sensitized 304 SS	Specimens of sensitized 304 SS exposed to sodium thiosulphate solution to induce IGSCC. Monitored simultaneously with electrochemical noise, AE, and elongation. Electrochemical noise and elongation were sensitive to crack initiation; whereas, AE is associated with final stages of fracture.	Kovac et al. (2010)
304H steel	Monitoring in a dilute sodium tetrathionate solution. It is reported that AE is only sensitive to rapid crack propagation and not sensitive to crack initiation or slow propagation stages. The source of AE activity is attributed to plastic deformation in the rapid propagation stage. It is postulated that SCC initiates via anodic dissolution at depleted grain boundaries but transitions to hydrogen-induced brittle fracture in later stages.	Zhang et al. (2008)
316LN steel	Monitored SCC initiation and propagation in a MgCl solution and observed a decrease in AE energy and event rate with increasing crack growth rate; attributed much of observed AE to plastic deformation at the crack tip.	Shaikh et al. (2007)
304 SS	Study of TGSCC in the heat-affected zone (HAZ) of butt-welded pipes; tests in both concentrated magnesium chloride solution and dilute chloride solution. Tests performed on transgranular cracking in butt-welded type 304 SS pipes. The weld pipe suffered TGSCC in a concentrated magnesium chloride solution (40% mass concentration); suffered IGSCC and falling off of grains in HAZ of a dilute chloride solution (35% mass concentration). AE could sense the propagation of SCC cracks. Secondary AE produced by hydrogen gas evolution and cracking of corrosion products. Primary AE was produced by the falling-off of grains because of the mutual actions of anodic dissolution and the mechanical fracture along a chromium-depleted zone in the grain boundary.	Yonezu et al. (2006)
Inconel 600 alloy	Three phases of SCC crack growth identified: 1) generation of small cracks at the surface, 2) growth of small cracks and formation of dominant cracks, and 3) growth of dominant cracks and fracture. Minimum crack size detectable with AE is 200 to 400 µm in length and below 100 µm in depth.	(Sung et al. 1997)
304 SS	Observed that cracks of 200 µm in length and approximately 100 µm in depth could be detected reliably during studies of IGSCC.	Jones et al. (1991)
304 SS	Postulated that the rupture of ligaments remaining from anodic dissolution was a source of AE during SCC. Observed mixed IGSCC and TGSCC modes of cracking in several steels and reported that AE activity is proportional to the fraction of TGSCC.	Gerberich et al. (1988) Jones et al. (1989)
304 SS and ferritic steels	Unable to observe significant AE activity from anodic dissolution during SCC.	Okada et al. (1974, 1976)

4.2.3.3 Emissivity of Electrochemical Corrosion Processes

Several investigations have noted that electrochemical corrosion processes are clearly emissive. Many studies point to evolution of hydrogen as a significant source of AE during pitting, crevice, and uniform corrosion. Jones and Friesel (1992) and Cakir et al. (1999) have attributed AE during pitting corrosion to rupture of salt caps or oxide films covering gas-filled pits. Others have also attributed observed AE activity to metal deformation (Jirarungsatian and Prateepasen 2010), rupture of passive films (Jirarungsatian and Prateepasen 2010; Xu et al. 2011b), or instantaneous stress changes on the surface (Magaino et al. 1987). Studies by Kovac et al. (2010) and Zhang et al. (2008) indicate that no AE is detected prior to final fracture stages during SCC, indicating that corrosion processes were not present to a significant degree or that these processes did not produce detectable levels of AE. Oxide films can produce detectable AE when they crack or spall as a result of significant stress accumulation from growth or thermal cycling. Detectability of film cracking depends on the thickness of the oxide film. Cracking of oxide films several microns thick is detectable; whereas, passive films on the nanometer order thickness are not detectable through cracking activity (Yuyama 1986). A summary of corrosion studies is provided in Table 4.4.

Table 4.4. Summary of Experimental Studies of the Emissivity of Electrochemical Corrosion Processes

Material	Summary	Corrosion Type/ Emissive Mechanism	Reference
304L	• Study to examine emissivity of transpassive dissolution process and to verify emissivity of hydrogen evolution. • Film rupture identified as main emissive phenomena during transpassive dissolution. • Hydrogen bubble evolution believed to be source of AE during pitting corrosion. • AE activity influenced by H_2SO_4 concentration but not Cl^- concentration. • Observed a current threshold for the generation of AE. • Two types of AE sources detected during pitting corrosion.	Pitting/hydrogen bubbles	Xu et al. (2011a)
304L	• Three AE sources identified during electrochemical corrosion of 304 SS: hydrogen evolution, oxygen evolution, and transpassive dissolution -> each source characterized by AE activity and b-value. • Break down of films believed to be AE sources during transpassive dissolution. • Weak correlation between hydrogen bubble diameter and AE amplitude—small bubbles produce higher frequency signals.	General electrochemical/ gas evolution and film rupture during transpassive dissolution	Xu et al. (2011b)
304	• The AE signal characteristics of pitting corrosion, crack, and bubble break-up are significantly different during the corrosion process. Mode of propagation regarded as TGSCC.	Pitting/crack propagation and gas bubble breakup	Du et al. (2011)

Table 4.4. (contd.)

Material	Summary	Corrosion Type/ Emissive Mechanism	Reference
304, A26	• Three emissive sources associated with pitting corrosion: hydrogen evolution, passive film rupture, and pit propagation. • Two emissive sources associated with uniform corrosion: hydrogen evolution and corrosion propagation. • Hydrogen bubbles verified visually—bubble break-up identified as the emissive phenomenon; analytical solution for minimum frequency of bubble break-up frequency provided. • Duration and average frequency identified as key parameters for distinguishing mechanisms associated with pitting and uniform corrosion.	Pitting and uniform/ hydrogen evolution, passive film rupture, metal deformation	Jirarungsation and Prateepasen (2010) – pitting
AISI 304	• Electrochemical noise and elongation sensitive to crack initiation; whereas, AE is associated with final stages of fracture.	---	Kovac et al. (2010)
316L	• Time delay before significant AE observed – only a few AE events observed during pitting initiation. Delay time and AE event counts related to susceptibility of material for pitting corrosion.	Pitting	Fregonese et al. (2001a)
316L	• Initiation step of pitting corrosion reported as not significantly emissive; propagation step is characterized by the emission of resonant signals. • AE can detect transition from pitting to uniform corrosion. • Attribute emissivity of hydrogen evolution to friction between hydrogen bubbles and walls of pits or impacts with caps of occluded cells.	Pitting/hydrogen evolution	Fregonese et al. (2001b)
316LN	• Aim to separate mechanical and corrosion sources of AE during SCC of 316LN during slow strain rate tests.	Pitting/rupture of salt caps or oxide films	Cakir et al. (1999)
316L	• Significant AE reported during pitting corrosion. Good correlation between pitting corrosion and AE activity.	Pitting/not identified	Mazille et al. (1995)
304L	• AE from pitting corrosion was significant, but AE from dislocation motion or cracking was not significant. • Attributed AE during pitting corrosion to the rupture of salt caps or oxide films covering gas-filled pits.	Pitting/rupture of salt caps or oxide films over pits	Jones and Friesel (1992)
304		Surface relaxation	Magaino et al. (1987)

Table 4.4. (contd.)

Material	Summary	Corrosion Type/ Emissive Mechanism	Reference
304L	• Use AE to monitor corrosion fatigue of 304 SS. The AE energy rate under the corrosive environment is one order of magnitude higher than in-air for positive applied potential for equal macroscopic crack growth rate. • Presence of hydrogen contributes to high AE activity. • Sources that can provide high AE activity include cleavage-like cracking, intergranular cracking, or separations in the plane-strain plastic zone ahead of the growing crack.	Crevice/hydrogen evolution	Yuyama (1984)

4.2.4 Acoustic Emission Transducers

A schematic of a typical AE transducer is shown in Figure 4.20. A review of AE transducers from one vendor (PAC 2005) indicates that typical sensors can range in diameter from 18 to 38 mm (0.7 to 1.5 in.) and can range in height from 15 to 67 mm (0.6 to 2.35 in.). Miniature sensors are also available with diameters as small as 3.6 mm (0.15 in.) and heights as small as 2.4 mm (0.1 in.). Many sensor models are capable of withstanding exposure to temperatures of 177°C and high-temperature models are available to withstand 540°C. Sensors with integral preamps are limited to temperatures of 85°C.

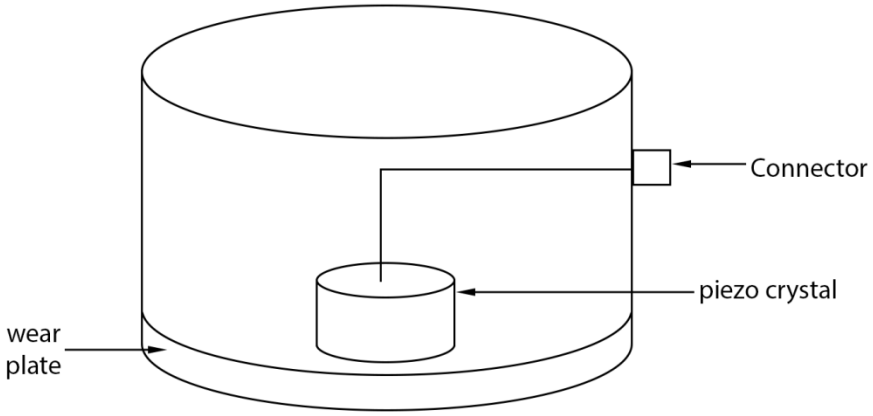

Figure 4.20. Schematic of a Typical Acoustic Emission Transducer

4.3 Visual Techniques

A comprehensive overview of visual testing (VT) can be found in Volume 9 of the ASNT Nondestructive Testing Handbook (ASNT 2010). Visual testing refers to the examination of a component or material using the unaided human eye or with the aid of a variety of tools to enhance the inspection capability. Such aids may include lenses, fiber-optic light guides, cameras, special lighting equipment,

etc. Visual examinations are routinely performed in several industries including the transportation, aircraft, and electrical power generating industries. In the nuclear power industry, VT is one of the NDE methods sanctioned by the ASME Boiler and Pressure Vessel Code for performing surface examinations of nuclear facility structural components (ASME 2007).

The removal of dry cask storage canisters provides an opportunity to perform a visual examination of the canister surface. However, such opportunities should be rare, making it highly desirable to have the ability to perform examinations without removal of the canister from the overpack. This places additional constraints on the examination because of the limited space provided in the annular gap between the canister and the overpack to accommodate VT equipment. Several vendors of visual testing equipment serve the nuclear power industry by providing equipment for specific applications that have unique constraints because of access or environmental factors. Such applications include the examination of fuel, reactor internal components, beltline region welds of the reactor pressure vessel, heat exchanger tubing, etc. Therefore, part of this assessment will consider the potential of applying commercial off-the-shelf (COTS) technology developed primarily for other applications in the nuclear power industry to the visual examination of dry cask storage canisters. In addition to considerations of access and environmental tolerance, the role and effectiveness of VT for managing atmospheric SCC degradation will be evaluated. This evaluation is based primarily on two NUREG documents [NUREG/CR-6860 (Cumblidge et al. 2004) and NUREG/CR-6943 (Cumblidge et al. 2007)] related to evaluating the effectiveness and reliability of visual testing for detecting cracks in nuclear power plant components.

4.3.1 Overview of Commercial Camera Systems

Several vendors provide VT equipment to service the needs of the nuclear power industry. Mostly, this includes special video cameras that are designed to be radiation-tolerant, waterproof, and/or compact in size. Camera products from several commercial vendors were surveyed to understand the types of products on the market with the potential for deployment in the annular space between the canister shell and the overpack. Several camera specifications considered relevant to the application of in-situ welded canister inspection were tabulated for several product families from each vendor (see Table 4.5), including:

- dimensions
- resolution
- optical zoom
- minimum object-to-lens distance
- radiation tolerance
- maximum operating temperature.

Table 4.5. Summary of Specifications for Many Commercial Camera Systems

Vendor	Width/ Diameter (W/D)	Length (L)	Max. Temp.	Rad. Tolerance	Resolution	Optical Zoom	Min. Object to Lens Distance
Ahlberg (rectangular)	75–160 mm	278–374 mm	50–70°C	Total Dose 20 kRad–50 MRad	460–720 lines horizontal	X 3–X 18	≥ 5 mm
Ahlberg (cylindrical)	24–95 mm	105–336 mm	50°C	Total Dose 20 kRad–100 MRad	460–720 lines horizontal	X 3–X 18;	≥ 5 mm
General Electric	70–139 mm	194–468 mm	50°C	Total Dose 22–60 kRad Dose Rate 1 kRad/hr	470 HTV lines NTSC, 460 HTV lines PAL	X 10–X 36	≥ 10 mm
Mirion	29–80 mm	79–370 mm	40–60°C	Total Dose 10 kRad–200 MRad	350–600 lines horizontal	X 3–X 18	≥ 10 mm
Diakont	41–379 mm	246–380 mm	50°C	Total Dose 100 kRad–200 MRad Dose Rate 1 kRad/hr–1 MRad/hr	500–600 lines horizontal	X 2–X 10	≥ 50 mm or unspecified
Thermo Scientific	48.3 mm		30–55°C	Total Dose 1–3 MRad Dose Rate 100–700 kRad/hr			

Most of the commercially available systems surveyed have variable focusing capability, although a few fixed focus systems are marketed as well. Pan/tilt/zoom (PTZ) camera systems that consist of an automatic focusing camera mounted to a robot arm to achieve pan and tilt are frequently marketed. An illustration of a PTZ system is provided in Figure 4.21. The length is the largest dimension of most camera systems; thus, tilting the camera to view the outside surface of a canister shell may not be practical for in-situ viewing. In addition, the attachment arm adds to the overall dimensions of the system.

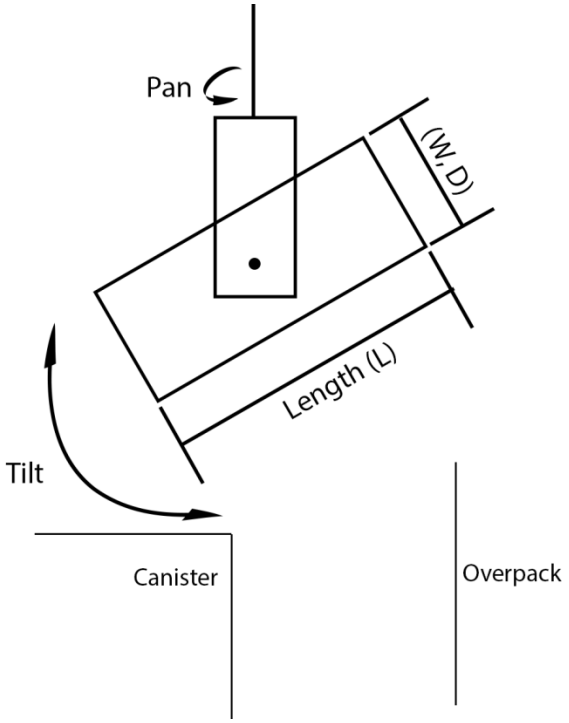

Figure 4.21. Illustration of a Pan/Tilt/Zoom Camera System for Canister Surface Examinations

Alternatively, some camera systems are designed so that they can be suspended from their main signal and/or power cable (see Figure 4.22) for applications with more stringent access constraints. This enables a more compact system for viewing; however, if lowered into the annular space between a canister shell and overpack, the camera lens will not be oriented to view the surface of the canister. In this case, an attachment such as a tilted mirror may be used for perpendicular viewing. The minimum lens-to-object distance of the camera refers to the minimum distance from an object at which a camera can achieve focus. In addition to the physical dimensions of the camera, the annular space between canister wall and overpack must be able to accommodate this minimum distance. Lighting systems also add to camera system dimensions. Most cameras use either light-emitting diodes (LEDs) or halogen bulbs for lighting and the lights may be attached externally to the body of the camera system or may be integral to the camera system body. Most of the camera systems in Table 4.5 are rated to withstand a maximum operating temperature of 50°C and nearly all of the systems are designed to withstand a cumulative radiation dose of greater than 10 kRads.

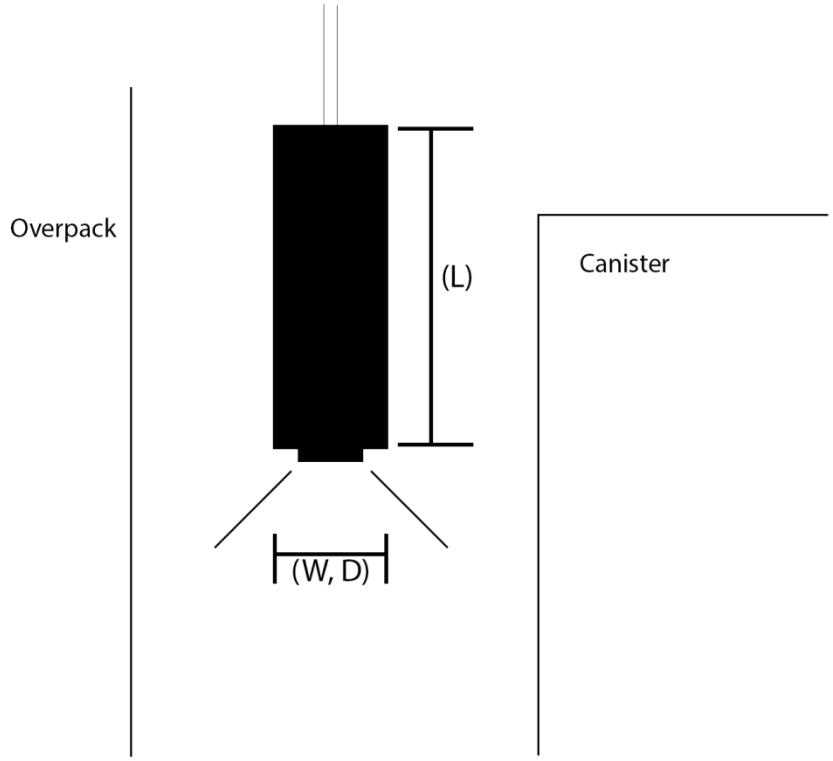

Figure 4.22. Depiction of Camera Suspended from Signal/Power Cable

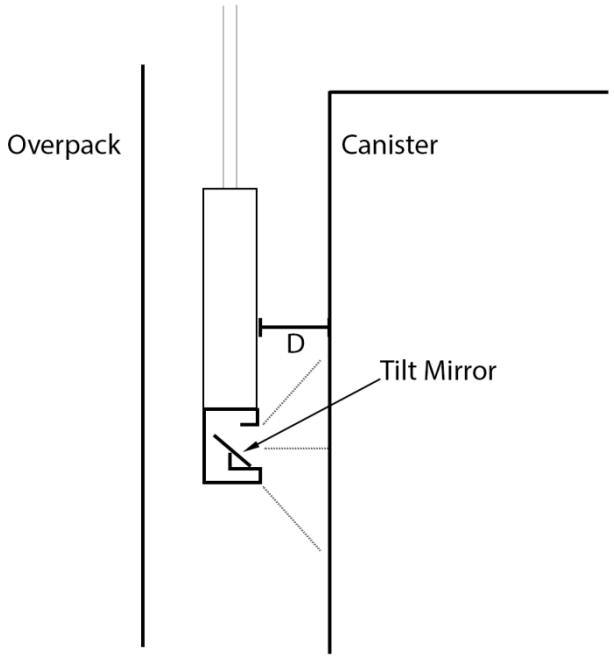

Figure 4.23. Depiction of Camera Suspended in Annular Space between a Dry Cask Storage System Canister and Overpack with Tilted Mirror Extension to Enable Viewing at Right Angles

4.3.2 Overview of Borescopes

Borescopes are an alternative to the use of compact camera systems for accessing the surface of welded canisters for in-situ visual examinations. Both rigid and flexible borescopes are commercially available differing in performance and nature of the light guides that they employ. Rigid borescopes usually consist of a series of relay lenses and other optical components to transfer an image from the objective lens to the eyepiece. Flexible borescopes use coherent fiber-optic bundles to transfer an image from the objective lens to the eyepiece. Typically, a coaxial arrangement of fiber-optic bundles is employed with an outer bundle that transfers a source of light to the object for illumination, while the inner bundle is used to transfer the image back to the eyepiece (ASNT 2010). Rempe et al. (2011) provides a brief overview of commercial borescopes in considering their possible application to fuel studies in material test reactors (MTRs). In a review of products from two commercial vendors and suppliers, it is noted that a typical borescope incorporates thousands of fibers, each representing a pixel of the image. The diameters of the borescopes ranged from 0.35 mm (0.014 in.) to 8 mm (0.315 in.) with lengths up to 15.4 m (50 ft). The presence of a relay to transfer an image from the objective lens to the eyepiece introduces losses that are not present in direct camera viewing.

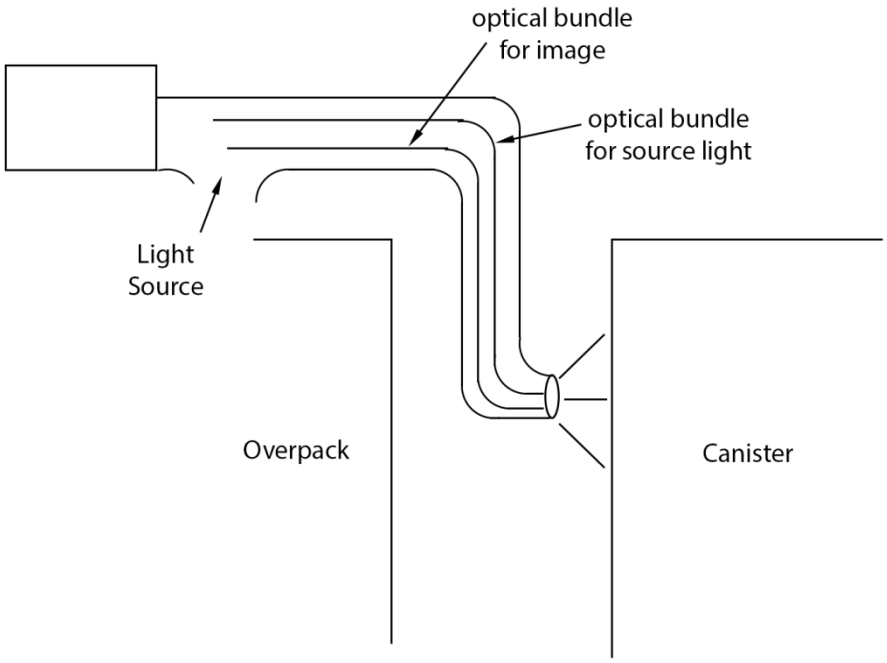

Figure 4.24. Depiction of a Flexible Fiber-Optic Borescope Used for Accessing the Surface of a Welded Canister for an In-Situ Examination

4.3.3 Visual Testing in the Nuclear Power Industry

Section XI of the ASME Code (ASME 2007) describes three types of visual examinations for the inspection of NPP components classified as VT-1, VT-2, or VT-3. Visual testing can range from highly detailed inspections for minute signs of degradation to simply checking that the component is in the correct location. VT-1 testing is a surface examination performed for the detection of degradation such as

cracking or corrosion. VT-2 testing is an examination performed at the outside of a pressure-retaining component to try to detect evidence of leakage, and VT-3 is a general inspection to determine the mechanical or structural condition of the component. Visual examinations are frequently performed on nuclear reactors to determine the condition of critical inner surfaces. Critical surfaces include high stress points at the junctions of nozzles and the vessel or nozzles and the cladding. Visual examinations are also performed to determine the condition of various parts such as studs, bolts, and nuts, as well as vessel bushings and closure washers (ASNT 2010).

The NRC and Electric Power Research Institute (EPRI) have been working in coordination with Pacific Northwest National Laboratory (PNNL) to assess the capability of remote visual inspection techniques as a proposed means for replacing the use of volumetric techniques for the inspection of NPP components. NUREG/CR-6943 (Cumblidge et al. 2007) reviews several previous efforts to relate the probability of detection with the COD parameter. This includes studies by Efsing et al. (2001), Enkvist (2003), and Virkkunen et al. (2004). In addition, a parametric study was conducted to examine the influence of several parameters on the reliability of visual techniques for crack detection. The parameters considered included the COD, lighting conditions, surface conditions, and camera specifications. This work highlights the COD parameter of service-induced flaws as one of the most significant parameters affecting the reliability of a visual examination and that the COD of SCCs have a complex relationship with the environment, material susceptibility, and stress conditions. However, it is generally claimed that more susceptible materials, higher stresses, and more aggressive chemical environments will cause SCCs to have a greater COD.

Some important conclusions from NUREG/CR-6860 (Cumblidge et al. 2004) are that the flaw depth is not correlated to the COD measurements obtained from visual examinations, primarily because of uncertainties in the stress distribution of the component, and that rigorous qualification procedures are necessary to ensure the reliability of a visual examination. NUREG/CR-6943 (Cumblidge et al. 2007) concludes that remote visual inspections conducted with cameras that are typically deployed in the field are most effective at detecting cracks with CODs greater than 100 μm (3.94 mils) and that cracks with CODs smaller than 20 μm (0.79 mils) cannot be effectively detected except under very favorable conditions. Parameters such as the lighting conditions, surface conditions, human factors, and camera specifications can have a dominant impact on detection reliability between these two bounds. Thus, it may be possible to improve the reliability of detecting tighter cracks through careful consideration of lighting and use of higher resolution cameras.

4.4 Electromagnetic Testing

Electromagnetic testing is a very broad and extensive nondestructive testing method. It encompasses various submethods or techniques that are applicable to a multitude of materials and applications. These submethods include eddy current testing, remote field testing, flux leakage testing, alternating current field measurement testing, and microwave testing. Of these submethods, eddy current testing (ET) is by far the most used and in fact may exceed all of the other test methods combined (ASNT 2004). Applications include thickness measurements of coatings and paint; thickness measurements of sheets, plates, and tube walls; defect detection such as cracks; and many others. Examination of spent fuel canisters lends itself to the eddy current method of electromagnetic testing and is therefore discussed in detail in the following sections.

4.4.1 Introduction to Eddy Current Testing

Eddy current testing works on the principal of electromagnetic induction. When an alternating current is applied to a coil of conducting wire, it produces a varying magnetic field. When the coil is placed in proximity of a conducting material, the varying magnetic field induces currents (called eddy currents) in the material. Eddy currents flow in closed loops in a plane perpendicular to the direction of the magnetic field. These eddy currents produce a secondary magnetic field that opposes the coil's (primary) magnetic field according to Lenz's law, producing a change in the impedance of the coil. When a surface anomaly such as a crack is moved into proximity of the coil, a change in the electrical impedance is noted and recorded as shown graphically in Figure 4.25 (Hagemaier 1990).

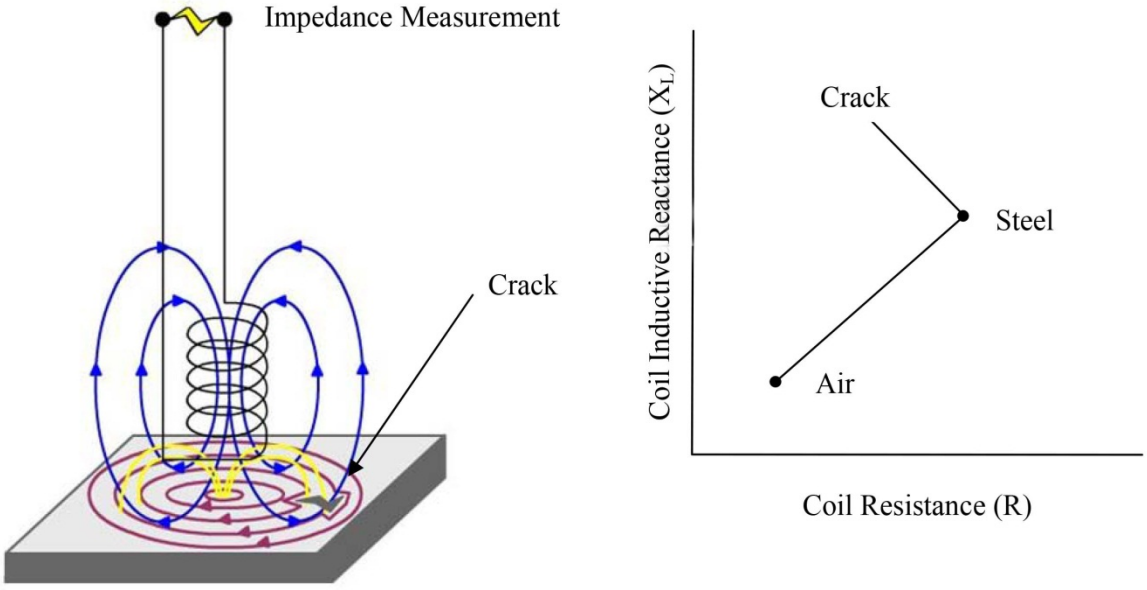

Figure 4.25. Effect of a Crack on the Impedance of an Eddy Current Coil

The electrical impedance of a coil undergoing a time-varying magnetic field will change as the coil is placed into proximity of a conducting material. This can be described as a change in both the resistance R of the coil and the inductive reactance of the coil X_L. Therefore, the impedance of the coil can be described as:

$$Z = R + X_L \tag{4.2}$$

where R is the ohmic resistance of the coil wire, and X_L is a function of the driving frequency and self-inductance of the coil and is described in the equation

$$X_L = 2\,\pi f\,L \tag{4.3}$$

The impedance of this coil can be measured and displayed in an impedance plane plot, which is the fundamental display for most eddy current instrumentation.

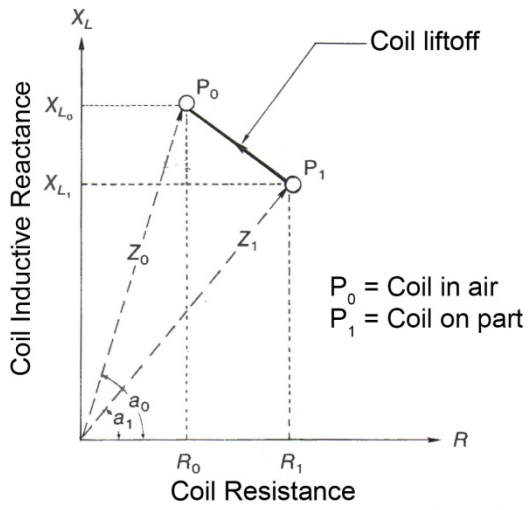

Figure 4.26. Representation of the Test-Coil Characteristics on the Impedance Plane (Hagemaier 1990). Copyright 2002 ©. The American Society for Nondestructive Testing, Inc. Reprinted with permission from The American Society for Nondestructive Testing, Inc.

The magnitude and direction of the displacement shown on the impedance plane plot are functions of the coil parameters and its proximity to a test object. Parameters include frequency of the alternating current in the test coil, size and shape of the test coil, distance from the test object (liftoff), conductivity of the test material, permeability of the test material, and whether there are any flaws such as cracks in the test material.

Eddy current testing is typically thought of as a surface-to-slightly subsurface inspection technique. The governing factor is the depth at which eddy currents can be generated. This is driven by the frequency used and the conductivity and permeability of the test material.

Figure 4.27 shows the relationship between frequency, conductivity, and permeability and how they affect the penetration depth of the eddy current field.

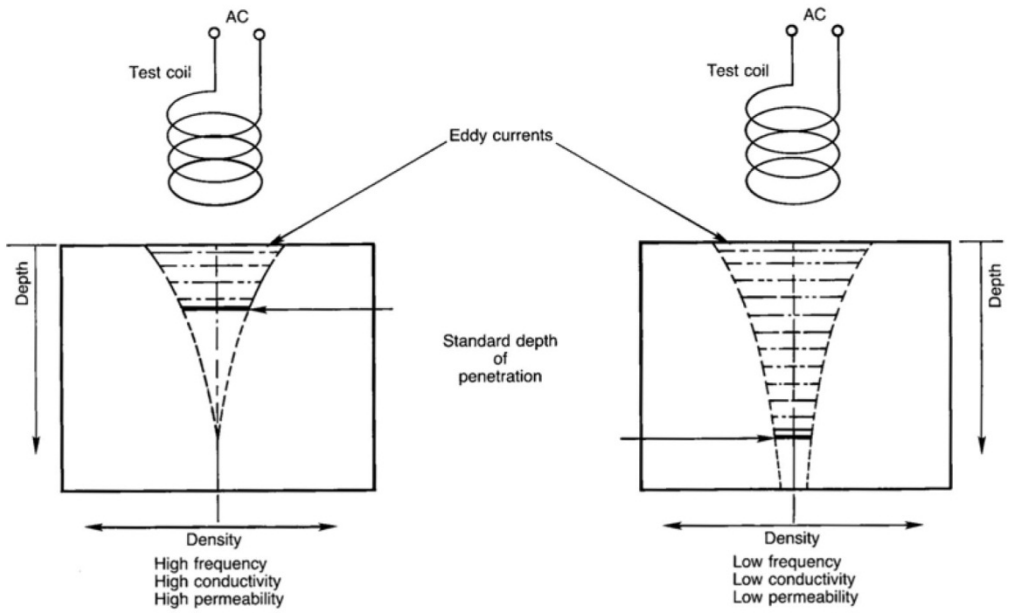

Figure 4.27. Relative Effect of Frequency, Conductivity, and Permeability on Depth of Penetration (Hagemaier 1990). Copyright 2002 ©. The American Society for Nondestructive Testing, Inc. Reprinted with permission from The American Society for Nondestructive Testing, Inc.

A phenomenon known as the skin effect concentrates the eddy currents near the surface of the test object adjacent to the coil and limits the depth of penetration. This can be described as a standard depth of penetration and is given by,

$$\delta = \frac{1}{\sqrt{\pi f \mu \sigma}} \tag{4.4}$$

where π = 3.14159
f = frequency
μ = magnetic permeability
σ = electrical conductivity

Therefore, the standard depth of penetration δ can be defined as the depth at which the current density drops to 37 percent of the current density at the surface. Depending on the material, and the frequency chosen, the penetration depth can be affected greatly and is a crucial variable when establishing test parameters.

4.4.2 Typical Eddy Current Testing Equipment

The typical eddy current testing system consists of a probe that couples the magnetic field to the test object and the driving and imaging electronics that provide applicable voltages and frequencies as well as provide methods to analyze the returned signals. The mechanics of probe design and coupling to the test object are essential in establishing high-quality data. The eddy current probe can be configured in numerous ways, but the most common are absolute and differential. The absolute configuration provides a single-coil arrangement with a direct impedance measurement; whereas, the differential probe consists

of a pair of coils connected in opposition so the net impedance is zero when each of the coils experiences the same test material and configuration. There are many variations to this as well as many variations of coil design.

There are many factors that affect the eddy current measurement process. One of the main factors includes a term known as liftoff, which is essentially the distance the probe is away from the test object. When the probe is residing in air at a great distance from the test object, it is considered to be at infinite impedance. When the probe is moved into proximity with the test object assuming that the test object is conductive, then the impedance begins to change dramatically. When the probe touches the test object surface, it is considered to be at zero impedance. This was shown graphically in Figure 4.26. Most of the time the liftoff of the eddy current probe is considered detrimental and should be minimized; however, this liftoff can be used to provide valuable information and is used frequently for thickness measurement of coatings that are a non-conducting material residing over a conductive material. Another major factor that affects the eddy current measurement process is the depth of penetration. As the eddy current probe is moved into proximity with the test object, eddy currents begin to flow in the object. These eddy currents are not uniformly distributed but vary with depth and tend to concentrate on the surface because of the skin effect as shown previously in Figure 4.27. This effect limits the depth at which anomalies such as voids can be detected and is why eddy current examination is considered a surface or slightly subsurface inspection method.

There are many other factors that can affect the eddy current measurement such as temperature changes near the probe, vibration of the probe, other conducting objects in proximity with the coil, etc. Each of these need to be considered when performing the eddy current test and should be minimized to the extent possible.

4.4.3 Applications of Eddy Current Testing

Applications for eddy current testing vary greatly. It is used extensively on all stages of forming, shaping, and heat treating of metals and alloys. It is used for in-line testing where damage during processing can be detected and removed during high-production speeds. One of the more prevalent uses of the eddy current method is for the inspection of heat exchanger tubing in the petrochemical industry, secondary balance-of-plant (BOP) heat exchangers, and steam generator tubing in nuclear power plants. There are many varied techniques used depending on the application and include single-frequency and multiple-frequency techniques. There are many probe configurations—pancake, differential, cross-axis—all of which can provide valuable information about the condition of a part or component. All of these factors must be considered when providing an acceptable eddy current test on a component in the field or laboratory setting.

4.4.4 Application of Eddy Current Testing to Dry Storage Canisters

The application of eddy current testing to the examination of dry storage canisters appears to be straightforward if it is assumed that the degradation mechanism that is being evaluated is an atmospheric-induced stress corrosion crack condition. This condition results in a surface-connected anomaly that can be readily detected using eddy current technology. Typical dry storage canisters are fabricated from non-ferromagnetic–conducting stainless steel, which is an ideal material for eddy current examination.

Typical eddy current probes that could be used to evaluate stress corrosion cracking would be small in diameter and have a relatively high frequency. The probe would be scanned over the canister surface, and a surface map indicating crack anomalies would be provided. This type of examination using a surface probe (sometimes called a pancake probe) would provide good sensitivity to narrow cracks and would also provide location capability for the weld area. Frequently, the weld areas on stainless steel components are ground flush and sometimes polished, and are not readily seen using visual techniques. Figure 4.28 is a photograph of a stainless steel canister with a weld that has been ground flush. It is essentially impossible to locate the weld visually, even with magnification. This eddy current approach can readily identify the weld location so that other nondestructive methods such as ultrasonics may be used to ascertain the condition of the weld.

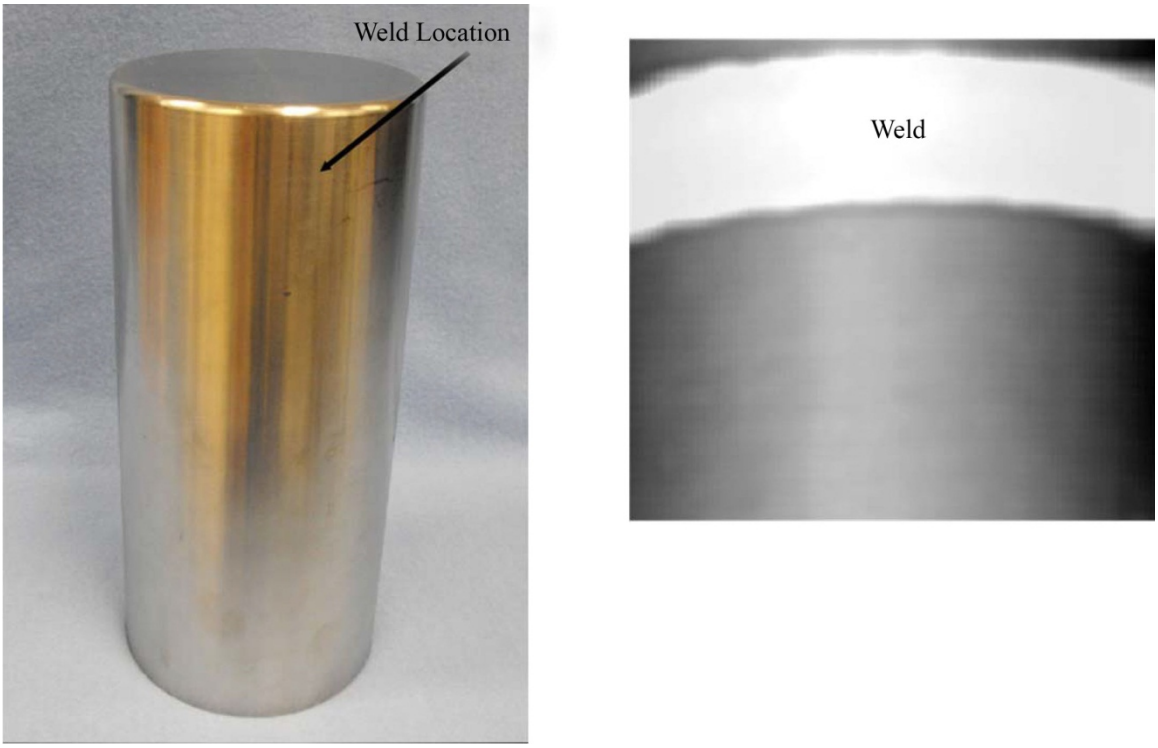

Figure 4.28. Weld in Stainless Steel Canister Imaged Using Eddy Current Examination

Eddy current surface probe methodology works well for mapping crack location and length sizing; however, depth sizing can be difficult for thick components. The small probe can be maneuvered into relatively tight places but does take considerable time to provide surface scans depending on scanner speed and area covered. This method was used during the round-robin studies on bottom-mounted instrumentation (BMI) nozzles at PNNL to provide fingerprinting (location and surface dimensioning) of various samples (Cumblidge et al. 2009). An example of this type of ET surface examination is shown in Figure 4.29. A cut section of a BMI is being examined with a small-diameter pancake probe and the results shown using imaging software. In this case, implanted cracks near the BMI nozzle were imaged.

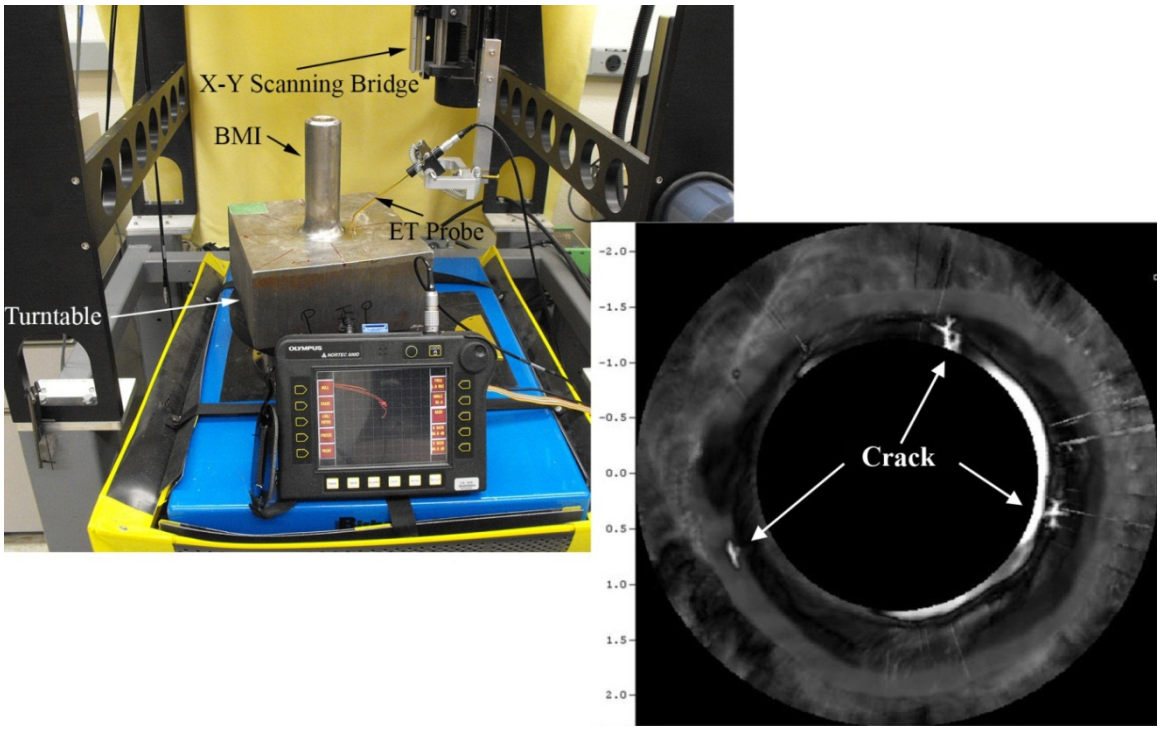

Figure 4.29. Eddy Current Examination of Bottom-Mounted Instrumentation Nozzle Penetration J-groove Weld

For examination of dry storage canisters, a robotic method that deploys an eddy current probe into the annular space between the canister and the overpack would be a possible solution. Because of the large area that would need to be scanned, an array of eddy current probes could be developed to speed up the scanning process. Off-the-shelf eddy current systems can operate up to 32 coils and greater depending on configurations providing decreased scan time for large areas (Figure 4.30).

Figure 4.30. Off-the-Shelf Eddy Current Instrument and Probe Array (courtesy of Olympus NDT)

4.4.5 Environmental Effects

Temperature and radiation not only affect the materials that compose an eddy current sensor system, but also the fundamental physics that surround the actual measurement. Since the fundamental component of an eddy current sensor is an inductive coil and transmission cable, it is anticipated that insulating materials will be the components most vulnerable to failure. An abbreviated search was performed to find specifications of existing COTS eddy current probes, this search uncovered only limited information on operating specifications addressing temperature. This information suggests that commercial probes are available which can withstand temperatures of 250°C-400°C[*]. Specifications for radiation tolerance of commercial eddy current probes that could be used in this application could not be found. The survey does indicate that it is common practice to use coiled wire that is coated with polyurethane. Hanks and Hamman (1971) report that this material shows good stability in both physical and electrical properties when exposed to radiation dose levels up to 10^8 rad. Failure of insulating and jacketing materials in coaxial transmission cables is also a concern when such cables are subject to relatively harsh environments and suitably radiation and temperature tolerant cables should be used for inspections. At this point, only a limited search has been performed to evaluate the temperature and radiation tolerance of eddy current probe systems. A more comprehensive study is needed to identify insulating materials for eddy current probes and cables that will be compatible with the environment near the surface of a dry storage cask canister loaded with used nuclear fuel, and to determine if eddy current systems incorporating such materials are already commercially available or can be fabricated.

4.4.6 Conclusions on Uses of Eddy Current Testing for Canister Inspections

If surface-connected cracks (such as those that might result from atmospheric conditions) are the degradation mechanism, then eddy current examination could provide a consistent reliable detection method. Canisters made from conductive non-ferromagnetic material such as stainless steel are ideal for eddy current examinations. Surface and slightly subsurface anomalies can be imaged and sizing information can be provided. The deployment of an array probe to minimize scan duration can provide extended areas of surface coverage. Using small-diameter surface probes at relatively high frequency can provide accurate surface maps of the canister anomalies such as stress corrosion cracks. The eddy current method can also provide weld area detection so that other nondestructive methods could be directed to the weld and used to address other desired information such as crack depth.

4.5 Guided Ultrasonic Waves

4.5.1 Background

Guided ultrasonic waves (GUW) involve the introduction of ultrasonic energy with wavelengths on the same order as the dimension of the component under inspection and observing the reflection of that energy from flaws or other discontinuities in the component. As a consequence, boundary conditions significantly influence the propagation of GUW energy, and the component under inspection may support the propagation of several modes. Each of these modes experience dispersion that can result in significant variation of phase (Vp) and group velocity (Vg) with respect to frequency. Rigorous derivations for propagating GUW modes in several relevant geometries can be found in standard texts, including the text by Rose (1999). Several articles summarize and review guided wave applications and

[*]Professional Plastics Cut Sheet. Celazole ® PBI Material Data Sheet; http://www.professionalplastics.com

pertinent aspects of the technology (Lowe et al. 1998; Rose 2000; Rose and Soley 2000; Alleyne et al. 2001; Rose 2002; Su et al. 2006; Raghavan and Cesnik 2007). Brief descriptions of GUW propagation in planar and cylindrical components follow.

4.5.1.1 Guided Ultrasonic Waves in Planar Components

GUW propagation in planar components can be described using a Cartesian coordinate system and by defining a planar component of thickness b having infinite extent in the x and y directions and with surface-normal vectors aligned with the z axis. In the setup defined in Figure 4.31, wave propagation is in the positive x-direction. Lamb waves can consist of an infinite number of symmetric, S_n (n = 0,1,2,…), and anti-symmetric, A_n (n = 0,1,2,…), modes. The nomenclature for these two mode classifications refers to the shape of normal displacement profiles. Illustrations of the lowest order symmetric mode, S0, and lowest order anti-symmetric mode, A0, are provided in Figures 4.32 and 4.33, respectively, for frequency × thickness (f·d) ~ 2.5-MHz·mm (0.1 MHz-in.). Dispersion relationships for the group velocity, Vg, and phase velocity, Vp, of Lamb waves in a 25.4 mm (1-in.) thick steel planar component are shown in Figures 4.34 and 4.35, respectively. Figure 4.35 shows that only the fundamental Lamb wave modes, A0 and S0, are supported at very low frequencies. Higher-order modes experience a frequency cutoff, below which they cannot propagate. Lamb waves can propagate long distances and exhibit good sensitivity to defects throughout the entire cross section of a material. However, all Lamb wave modes are dispersive, and the shear vertical component of polarization facilitates leakage to intimately coupled layers.

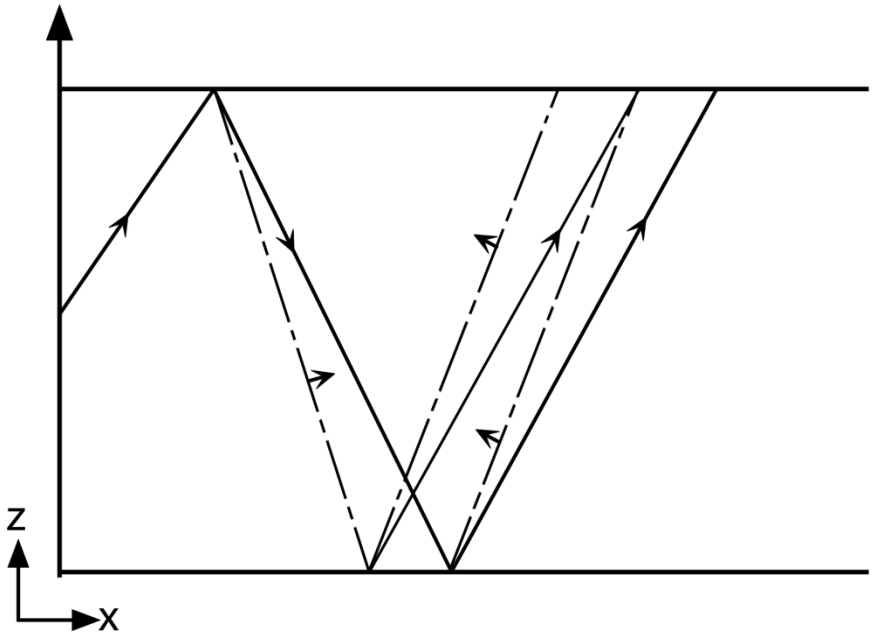

Figure 4.31. Vector Representation of Lamb Wave Propagation Along the x-direction of a Planar Component

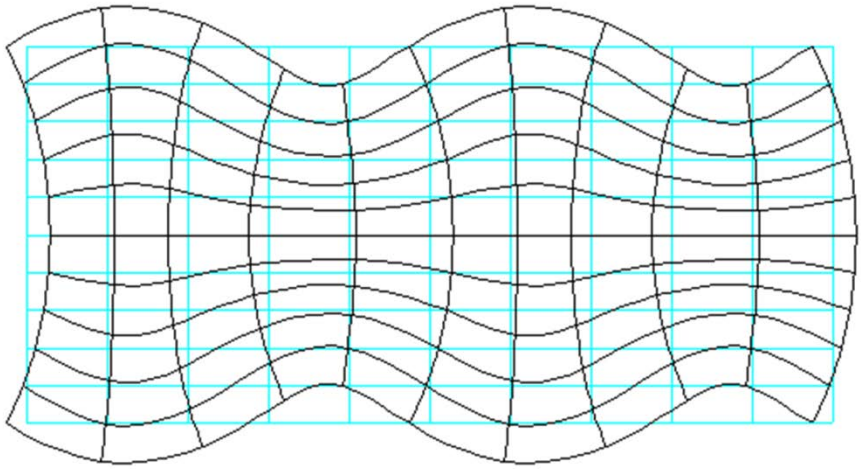

Figure 4.32. Illustration of the Fundamental Symmetric Lamb Wave Mode, S0, Excited in a Planar Component for f·d ~ 2.5-MHz·mm (0.1 MHz-in.)

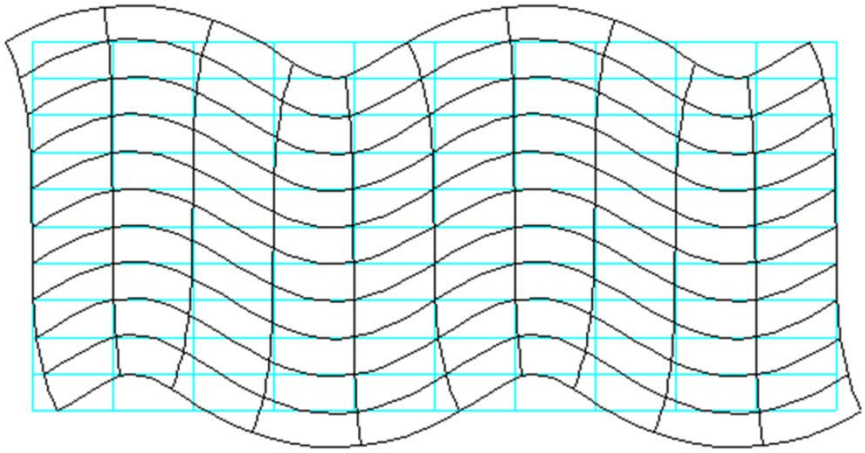

Figure 4.33. Illustration of the Fundamental Anti-Symmetric Lamb Wave Mode, A0, Excited in a Planar Component for f·d ~ 2.5-MHz·mm (0.1 MHz-in.)

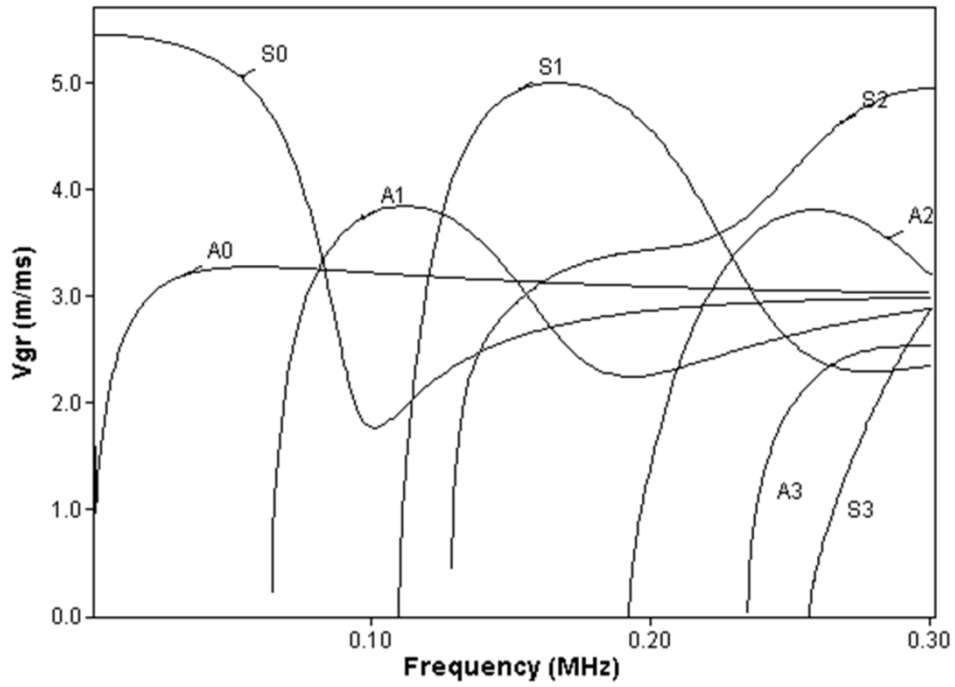

Figure 4.34. Dispersion Relationships for the Group Velocity, Vg, of Lamb Waves Excited in a 25.4 mm (1-in.) Thick Steel Planar Component

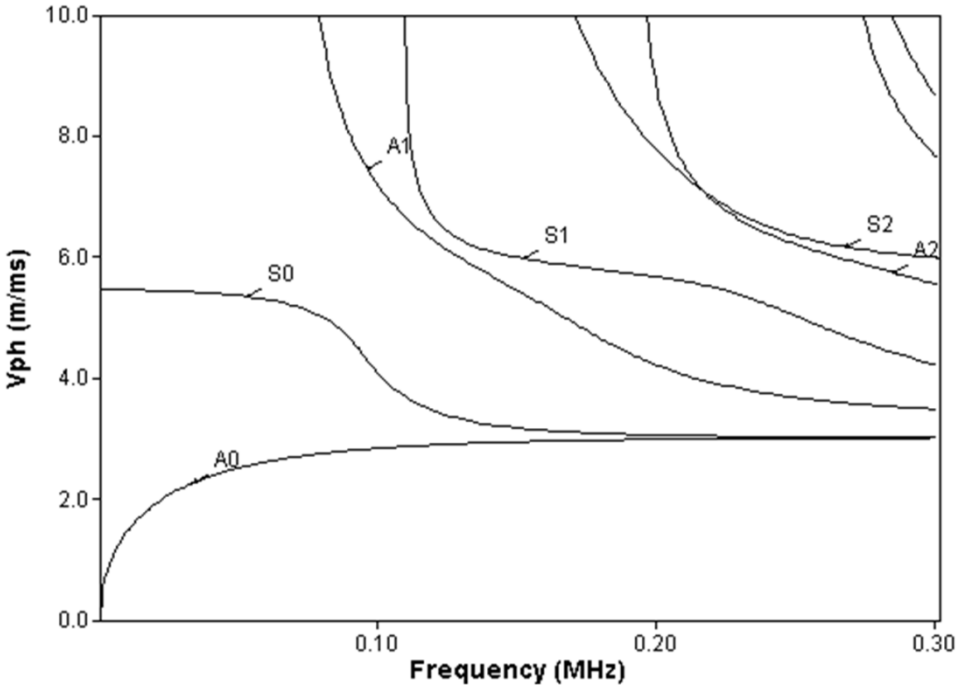

Figure 4.35. Dispersion Relationships for the Phase Velocity, Vp, of Lamb Waves Excited in a 25.4 mm (1-in.) Thick Steel Planar Component

Guided waves polarized such that wave displacement is perpendicular to the surface normal and direction of propagation are referred to as shear-horizontal (SH) waves (see Figure 4.36). Several SH modes may be simultaneously supported in a planar component and the dispersion relationship of Vp for several SH modes in a 25.4 mm (1-in.) thick steel planar component are shown in Figure 4.37. This figure shows that only the fundamental mode (SH0) is supported at very low frequencies and that Vp for SH0 remains constant over the entire frequency range (i.e., it is dispersionless). Higher-order modes experience a cut-off with frequency, below which their propagation is no longer supported. A sharp increase is observed in Vp for higher-order modes as the cut-off frequency is approached from higher frequencies. To isolate the SH0 mode at low frequencies, transducers capable of excitation below 70 kHz are necessary. The polarization of SH modes minimizes coupling (i.e., leaking) of energy to adjacent surfaces.

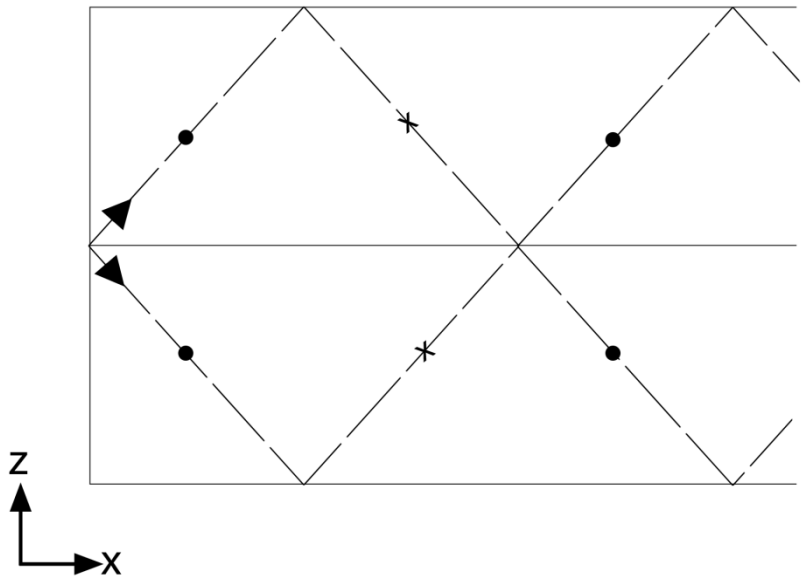

Figure 4.36. Vector Representation of SH Wave Propagation Along the x-direction of a Planar Component in the Sagittal Plane

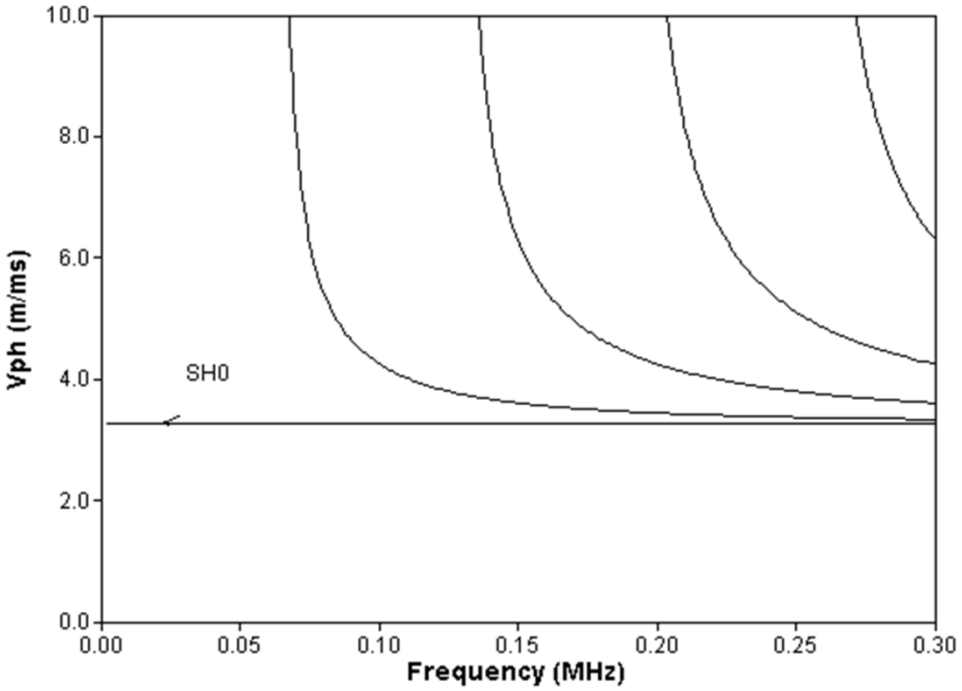

Figure 4.37. Dispersion Curves Calculated for the Phase Velocity of the Several SH Modes in a 25.4 mm (1-in.) Thick Steel Planar Component

4.5.1.2 Guided Ultrasonic Waves in Cylindrical Components

Circumferential guided waves propagate in the circumferential direction of cylindrical components. They can be considered extensions of Lamb waves in planar components (Rose 1999) to curved surfaces as the wavelength approaches and exceeds the radius of curvature of the component. Similar to Lamb waves, circumferential guided waves may consist of an infinite number of symmetric and anti-symmetric modes. It is noted by Rose (1999) that the dispersion relations for circumferential waves are different than for Lamb waves at low frequencies. In addition, for Lamb waves, the value of Vp for the S0 and A0 modes converge at large values of frequency × thickness; whereas, for circumferential wave modes, a significant difference remains between the value of Vp for these two modes at large values of frequency × thickness. Lamb wave approximation may be used for thin-walled piping when the wall thickness of a cylindrical component is much less than its radius of curvature. Ambiguity in the term "circumferential guided wave" exists as it may be used to refer to the use of Lamb waves to inspect thin-walled cylindrical components. The distinction between circumferential guided waves and Lamb waves is indicated in Figure 4.38.

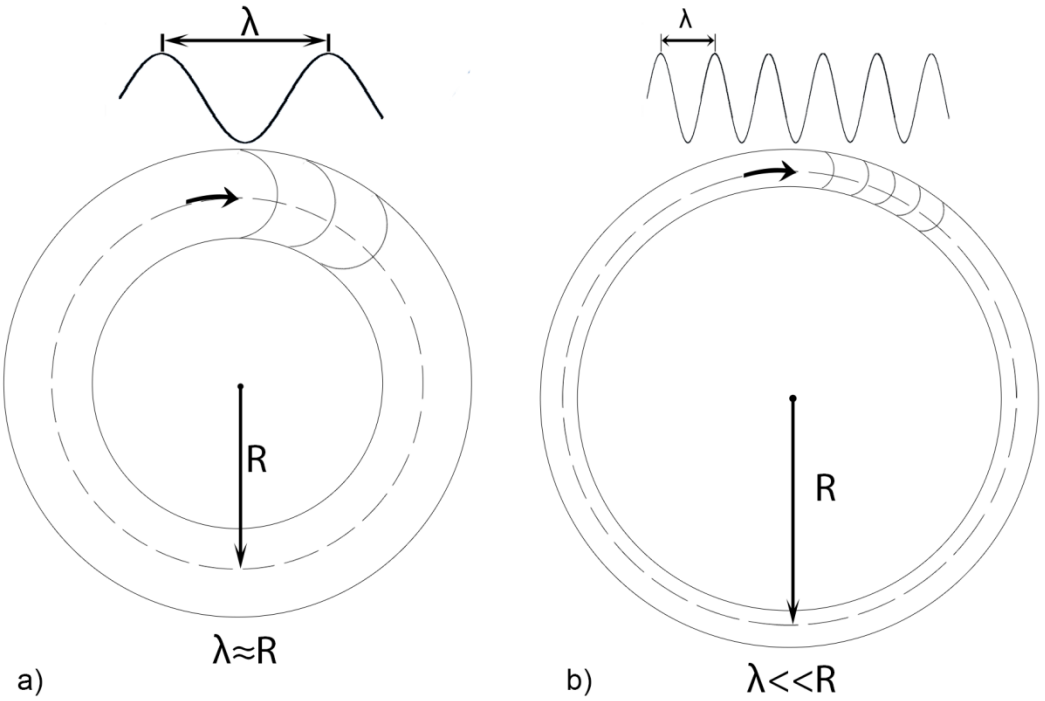

Figure 4.38. Circumferential Guided Waves are Depicted in a) while b) Depicts Lamb Wave Propagation in the Circumferential Direction of a Cylindrical Wall

Axial GUW propagation in tubes is best described in the cylindrical coordinate system with the axis of the cylinder aligned with the z-axis of the coordinate system, which also coincides with the direction of wave propagation. Three mode classes of particular relevance to axial pipe and tube inspection include longitudinal axially symmetric L(0,m) (m = 1,2,3…), torsional axially symmetric T(0,m) (m = 1,2,3…), and non-axially symmetric flexural modes F(n,m) (n = 1,2,3…, m = 1,2,3…). Illustrations of longitudinal, flexural, and torsional mode excitation are provided in Figure 4.39 a)–c), respectively. Analogies can be drawn between L(0,m) modes and Lamb waves with respect to polarization. A similar analogy exists between T(0,m) modes and SH modes in planar components. Similar to the SH0 mode in planar components, the T(0,1) mode is dispersionless for all frequencies. L(0,m) and T(0,m) modes are typical selections for long-range pipe and tube inspections (Demma et al. 2004), while F(n,m) modes receive less consideration because of their relative complexity. However, the reflection from non-axially symmetric features makes knowledge and understanding of F(n,m) modes relevant to practical implementation (Demma et al. 2004). F(n,m) modes are also applicable to non-axially symmetric loading of components in cases of limited circumferential access (Rose 2002).

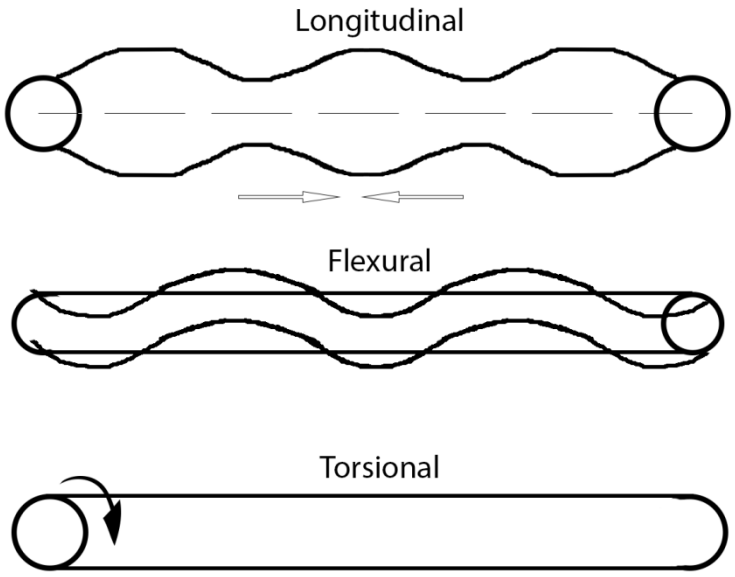

Figure 4.39. Illustration of a) Longitudinal Mode Excitation, b) Flexural Mode Excitation, and c) Torsional Mode Excitation in Cylindrical Components

4.5.2 Relevant State of the Art

Guided wave technology for long-range inspection of piping has been developed by Imperial College. An important criterion in the selection of guided ultrasonic wave modes for inspection includes the dispersion relationship for Vg as a function of frequency to ensure minimal distortion of the signal as it propagates through a component. Guided wave sensors for long-range axial screening inspections of pipes are primarily based on excitation in the dispersionless region of the L(0,2) mode at low frequency (see Figures 4.40 and 4.41) and excitation of the dispersionless T(0,1) mode (see Figure 4.42). The T(0,1) has some advantages over the L(0,2) mode for long-range inspection devices because it experiences less attenuation from fluid loading or visco-elastic coatings and the T(0,1) is dispersionless for all frequencies (Lowe and Cawley 2006).

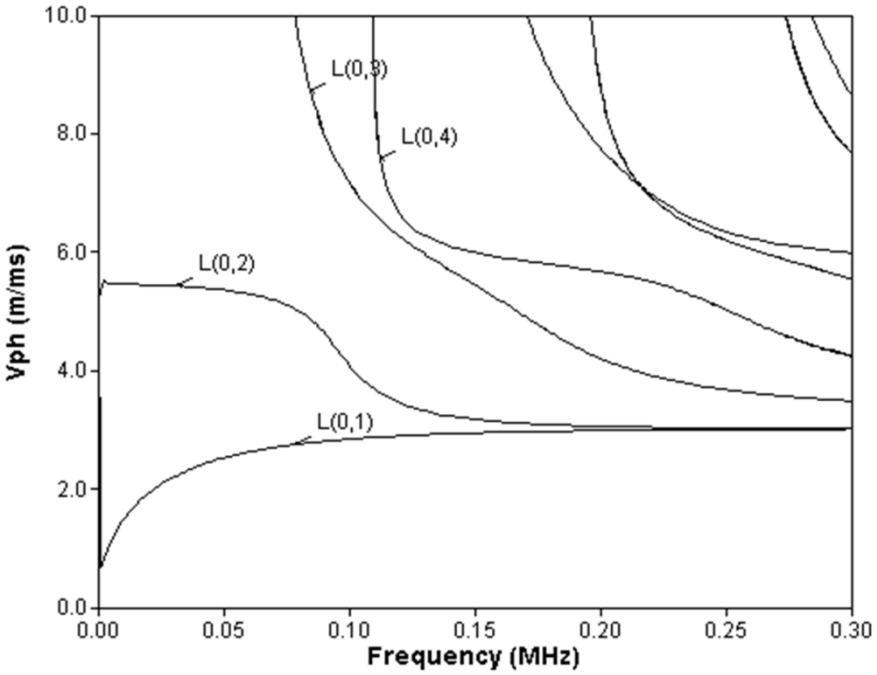

Figure 4.40. Dispersion Curves Calculated for the Phase Velocity of the Several L(0, n) Modes in a Steel Cylinder with a 1.7 m Diameter (67 in.) and 25.4 mm (1-in.) Wall Thickness

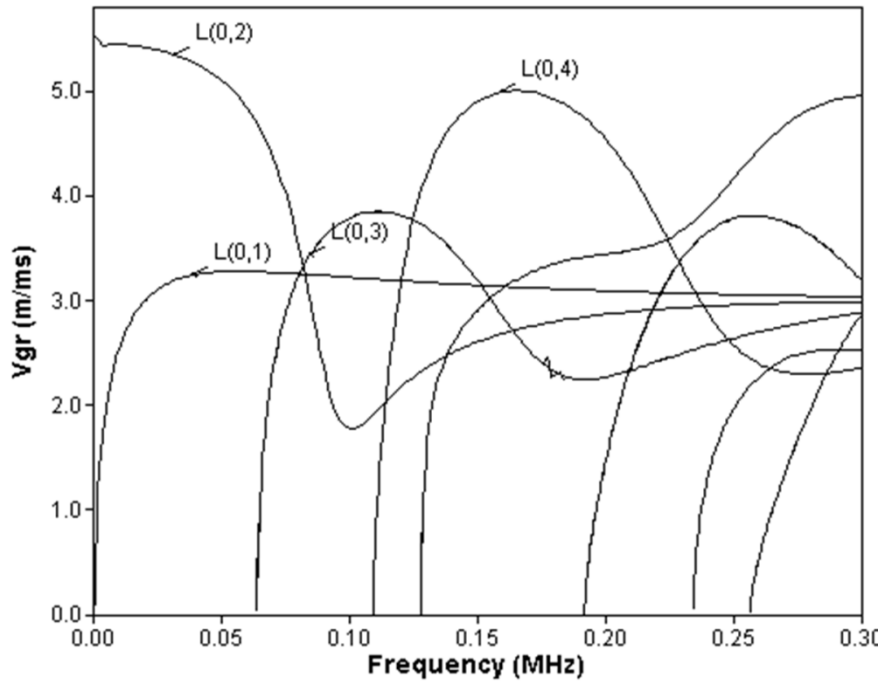

Figure 4.41. Dispersion Curves Calculated for the Group Velocity of the Several L(0, n) Modes in a Steel Cylinder with a 1.7 m (67 in.) Diameter and 25.4 mm (1-in.) Wall Thickness

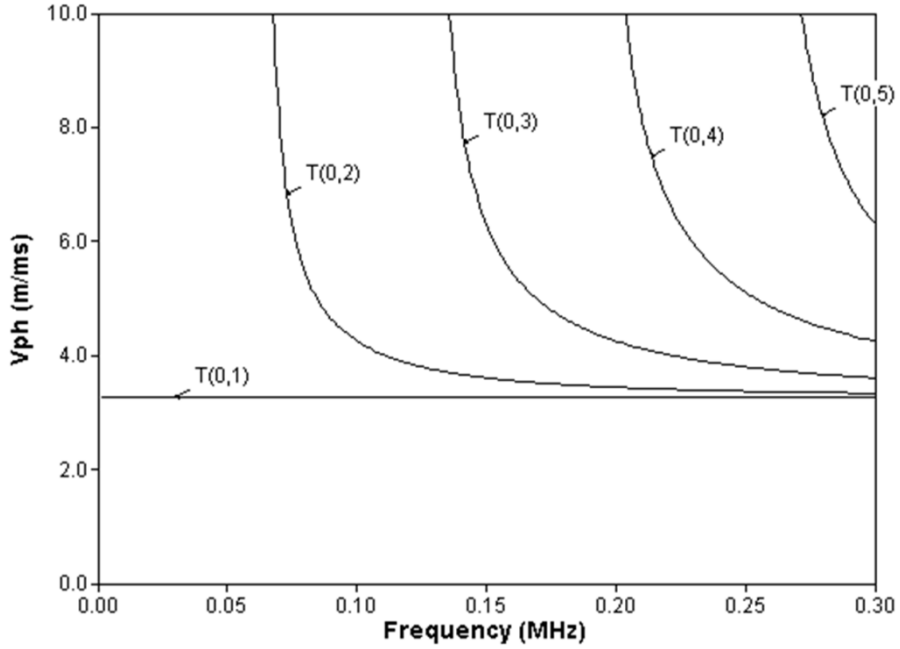

Figure 4.42. Dispersion Curves Calculated for the Phase Velocity of T(0, n) Modes in a Steel Cylinder with a 1.7 m (67 in.) Diameter and 25.4 mm (1-in.) Wall Thickness

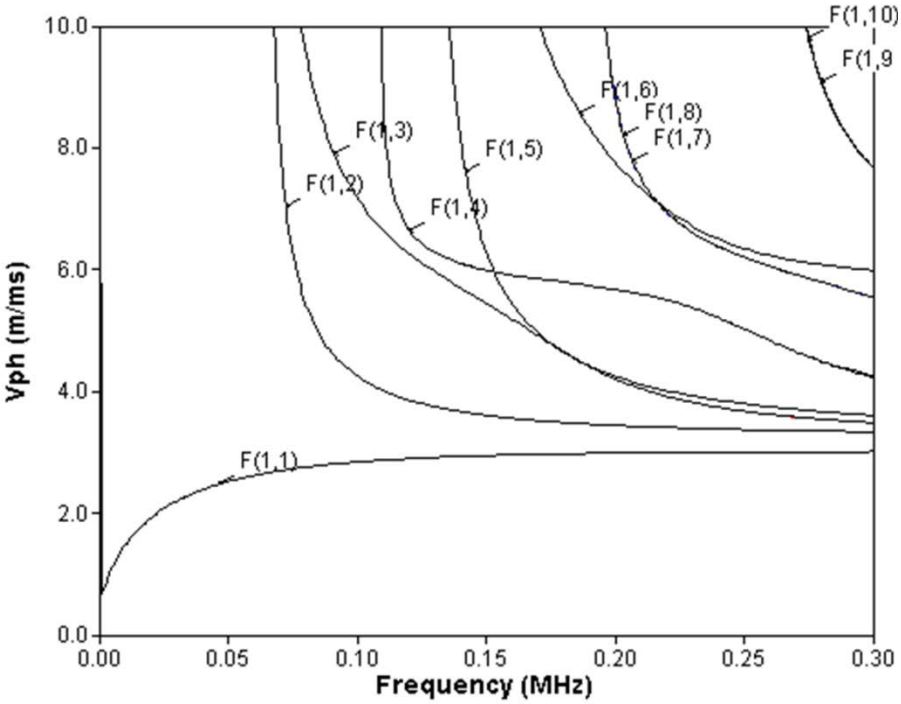

Figure 4.43. Dispersion Curves Calculated for the Phase Velocity of F(1, n) Modes in a Steel Cylinder with a 1.7 m (67 in.) Diameter and 25.4 mm (1-in.) Wall Thickness

Long-range pipe inspection devices were initially developed for inspection of piping for corrosion defects (Lowe et al. 1998). Axisymmetric guided wave modes can be generated using a ring-shaped array of shear polarized piezoelectric elements to suppress flexural modes and are wrapped around the circumference of the pipe for inspection. Elements are dry coupled to test components, and multiple rings of elements are often required to isolate the desired mode of operation and control the direction of the beam. Characterization studies have been conducted on pipes using circumferential notches to simulate flaws (Demma et al. 2004). These studies have parametrically examined the response of L(0,2) and T(0,1) systems to changes in notch dimensions. It has been observed that the reflection coefficient for L(0,2) and T(0,1) modes exhibit a linear relationship with the circumferential dimension of notches and increases monotonically with defect depth. Reflection from a non-axisymmetric reflector will result in mode conversion to flexural modes. The circumferential dimension of a reflector can be determined from the ratio of the reflection coefficient for the L(0,2)/T(0,1) mode to the reflection coefficient for the flexural mode [F(1,3) mode for L(0,2); F(1,2) for T(0,1)]. The T(0,1) mode exhibits significantly greater sensitivity to axial cracks than the L(0,2) mode. The distinction between axisymmetric reflectors (i.e., welds) and non-axisymmetric reflectors (i.e., cracks) is facilitated by detection of flexural modes generated from a reflection.

The sensitivity of long-range inspection systems is often expressed in terms of percent cross-sectional wall loss. The minimum detectable flaw size is reported to be approximately 5 percent wall loss (Lowe and Cawley 2006) with claims as low as 1 percent reported commercially (GUL 2012). For a 50 percent through-wall outer diameter (OD) circumferential crack in a 1.7 m (67 in.) diameter dry storage canister (DSC), this would correspond to crack length of approximately 10–50 cm (4–20 in.). Inspections on both sides of the transducer can be performed simultaneously or the signal can be focused in a single direction. The range of these systems depends on specific conditions of the applications such as the presence of internal fluid, visco-elastic coatings, pipe bends, etc. Typical ranges are on the order of tens of meters (Lowe and Cawley 2006).

The use of long-range guided wave inspection systems as a screening tool for pipelines implies that follow-up examinations are required using alternative technologies to more accurately characterize the degradation. Advancements in signal analysis may improve the ability of these systems to more precisely characterize degradation (Lowe and Cawley 2006). Other concepts consider the integration of phased-array scanning with the long-range screening operation to improve the characterization of defects.

Photos of two commercial transducers based on the piezoelectric ring technology developed by Imperial College are shown in Figures 4.44 and 4.45. Figure 4.44 is a photograph of an inflatable ring transducer for the Teletest Focus system from Plant Integrity Ltd., which is a wholly owned subsidiary of TWI (http://www.twi.co.uk). Figure 4.45 is a photograph of an inflatable ring transducer from Guided Ultrasonics Ltd. (GUL) (http://www.guided-ultrasonics.com/). Inflatable rings are available for GUL transducers up to 914 mm (36 in.) in diameter, and it is claimed that structures up to 2.79 m (110 in.) in diameter may be accommodated by combining multiple rings. GUL also claims that the transducer can operate from −40°C to +180°C and that a minimum of 51 mm (2 in.) of clearance around the component is required to accommodate the transducer ring.

Figure 4.44. Photograph of the Teletest Focus Plus Inflatable Ring Transducer. Reproduced courtesy of Plant Integrity Ltd. (a TWI subsidiary company)

Figure 4.45. Photograph of Inflatable Ring Transducer. Image used with permission of Guided Ultrasonics Ltd.

4.5.2.1 Circumferentially Guided Ultrasonic Wave Systems

Alleyne and Cawley (1992) investigated the interaction of individual Lamb waves with a variety of notch defects using finite-element analysis bench-scale tests. A two-dimensional (2-D) Fourier transform method was developed to quantify Lamb-wave interactions with defects in these studies. The sensitivity is shown to be dependent on a number of factors including the frequency-thickness product, the mode type, the mode order, and defect geometries. The sensitivity of the fundamental extensional modes, A0 and S0, and the higher-order A1 mode, were examined as a function of frequency-thickness product and as a function of the defect depth-to-component thickness ratio. Analysis of the characteristics of frequency sweep profiles was identified as a potentially useful means of defect sizing.

The interaction of the fundamental symmetrical Lamb mode (S0) with cracks in aluminum plates was examined by LeClezio et al. (2002). A model decomposition method is used to analyze diffraction of energy near the crack and the variation of far-field reflection and transmission coefficients with crack depth were determined. Numerical and experimental studies were also carried out to benchmark results on a set of flaws ranging from 0 to 100 percent through-thickness depth in 25 percent increments. The reflection coefficient is considered more suitable than the transmission coefficient for sizing purposes.

Model decomposition and finite element method (FEM) have been used to study the interaction of fundamental shear horizontal (SH0) modes from defects in plates (Demma et al. 2003). This work examined the impact of notch depth and frequency on reflection from notches and considered the use of thin notches to simulate cracks. It is noted that the interaction of nonpropagating modes between crack faces could significantly affect the scattering behavior of cracks versus approximating notches.

Shear horizontal modes have been investigated for performing circumferential examinations of tar-coated piping (Luo et al. 2006). It is noted that the axial extent of the inspection is limited by the axial footprint of the piezoelectric transducers used for inspection. A linear transducer array is implemented to achieve greater axial coverage for inspection. The attenuation of "wrap-around" signals (the periodic input signals that travel the full circumference of the pipe) and pulse-echo signals between periodic wrap-around signals served as the basis for identification of defects. The system was tested on fabricated through-wall holes and simulated delamination and gouging defects. The time of arrival for a pulse reflected from a defect located 180° from the transducer array is equal to the travel time for wrap-around signals. Thus, a blind spot exists in this particular arrangement for defects located at 180°.

Shivaraj et al. (2008) investigated a circumferentially guided wave system for detection and imaging of pitting corrosion of piping at pipe supports regions. The system employed a dual-transducer, pitch-catch arrangement using the A1 extensional plate mode. The transducers were separated circumferentially such that no flaw could simultaneously be in the 180° blind spot observed in the studies by Luo et al. (2006). This technique was explored to address inspection of pipelines for several process industries and, more specifically, pipelines in or near marine environments that are subject to crevice corrosion where the piping is in contact with support brackets. Consideration of the A1 mode is based on the expected increased sensitivity to corrosion defects on the surface when compared to lower-order modes whose energy would be more uniformly distributed through the wall of the pipe. The specific technique considered used angle beam piezoelectric transducers coupled through acrylic wedges. The detection of pinholes as small as 1.5 mm (0.06 in.) in diameter and 20 percent through-wall depth is reported. Shivaraj et al. (2008) also discussed the implementation of a robotic crawler system to scan in the axial direction. Satyarnarayan et al. (2008) also investigated the circumferential propagation of guided waves to detect and image pitting corrosion and cracking in the support bracket regions of piping. Specifically, they investigated the propagation of higher-order mode clusters, which experience little dispersion. In addition, these guided wave modes at high frequency (frequency × thickness product of 20 MHz-mm) are more sensitive to small defects than fundamental Lamb modes, A0 and S0.

Circumferentially guided waves have also been investigated as a means to inspect fatigue cracking in helicopter rotor hubs. Dispersion relationships for the first few modes of a layered annular structure have been computed numerically (Valle et al. 1999) and Auld's model for representing scattering has been investigated in efforts to develop a systematic algorithm for crack sizing (Valle et al. 2001).

Cheong et al. (2004) explored the use of circumferentially guided waves in conjunction with axially guided waves for the examination of feedwater pipes in pressurized heavy water reactors (PHWRs). Axially guided waves are discussed as a means to screen piping sections that may be inaccessible because of thermal insulation. Circumferentially guided waves could then be used to characterize flaws in greater detail after they have been located by the axial inspection. A potentially effective means for detecting and sizing axially oriented flaws in feedwater piping is described using torsional mode inspections for locating flaws and circumferentially guided waves to perform a follow-up characterization.

4.5.2.2 Magnetostrictive Sensors and Electromagnetic Acoustic Transducers

In addition to piezoelectric-based transducers, guided waves may be excited in a component using magnetostrictive sensors (MsSs) or electromagnetic acoustic transducers (EMATs). The MsS sensing mechanism is based on the force in ferromagnetic materials generated by strains associated with the motion of magnetic domains (Kittel 1949). The technique may be contactless for the inspection of ferromagnetic materials and can be applied to the inspection of other materials with the aid of an intermediate strip of ferromagnetic material in direct contact with the test component to convert magnetic domain motion to elastic wave motion. Magnetostrictive sensors based on technology developed at the Southwest Research Institute have been licensed to several commercial vendors. Several transducer forms are possible depending on the application to planar or cylindrical components. MsS transducers are generally considered rugged, simple, and inexpensive relative to piezoelectric transducers. A ribbon cable-based MsS transducer from M.K.C. Korea (http://www.mkckorea.com/english.htm) for performing long-range axial screening inspections of pipelines is shown in Figure 4.46. This system is reported to require a clearance of only 25.4 mm (1 in.) or greater between pipes for installation.

Figure 4.46. Photograph of Ribbon Cable MsS Transducer for Axial Pipe Inspections (photo courtesy of Guided Wave Analysis LLC)

In EMATs, guided wave detection and generation is facilitated by the Lorentz force mechanism. The EMAT transducer and receiver both consist of a permanent magnet or electromagnet and a coil. The transmitter induces eddy currents in the test component through radio-frequency excitation. The induced eddy currents interact with the magnetic field from the coil to produce a Lorentz force and generate guided waves. Detection is achieved through the reverse process. EMATs are contactless transducers,

making them relatively insensitive to surface conditions, and can be applied through thin coatings of insulating material. EMATs are often considered for the generation SH modes.

4.5.3 Application to Dry Storage Canisters

Two potential implementations of guided ultrasonic wave systems for examination of dry cask storage canisters include axially and circumferentially guided wave inspections. A depiction of an installation of a piezoelectric ring transducer for performing axially guided wave inspections on a dry cask storage canister is shown in Figure 4.47. This figure illustrates installation of a ring transducer in the middle of the canister and at the top. Installation at the middle of the canister would enable simultaneous screening of the circumferential welds for the top plate and bottom plate. A torsional mode may be excited to detect axially oriented flaws particularly near the longitudinal seam weld of the canister. However, a dead zone will exist at the site of the transducer and in the immediate vicinity on either side of the transducer. To ensure this dead zone is sampled, a second examination may be performed with the ring transducer installed at the top of the canister. Torsional mode excitation may also be employed to mitigate potential attenuation or interference caused by internal components of the canister. The utility of this type of examination is uncertain because of relatively poor sensitivity to flaws. Assuming a sensitivity of 1–5 percent wall loss, these systems would be limited to detecting 50 percent through-wall flaws that are greater than approximately 10-50 cm (4-20 in.) in length. Improved sensitivity may be achieved by exploring advanced signal processing techniques.

The annular gap between the dry storage canister and overpack may present a challenge to installation of piezoelectric ring transducers. Commercially available inflatable ring transducers from GUL require approximately 50 mm (2 in.) of clearance or greater for installation. MsS transducers have a lower profile than the inflatable piezoelectric ring transducers and would be more easily accommodated by the restricted annular space between the canister wall and the overpack.

Circumferentially guided waves could be implemented for the examination of the dry storage canister with improved sensitivity and the potential to more accurately characterize flaws than can be achieved with axially guided modes. An illustration of a circumferentially guided wave setup is shown in Figure 4.48. Axial coverage could be achieved through the use of a linear transducer array spanning the height of the canister or implementation of a robot crawler system to scan the canister length. The ultimate implementation will depend on several factors such as cost and physical space to accommodate the sensor package. A dual transducer pair could be implemented to avoid the “blind spot” at 180°.

Generally, the effectiveness of a GUW examination will depend significantly on the mode used to perform the examination and this offers the potential to tailor an exam for specific inspection scenario through controlled excitation of modes. For the most part, is an established tool for some screening applications but the ability to characterize complex such degradation is a subject of ongoing research.

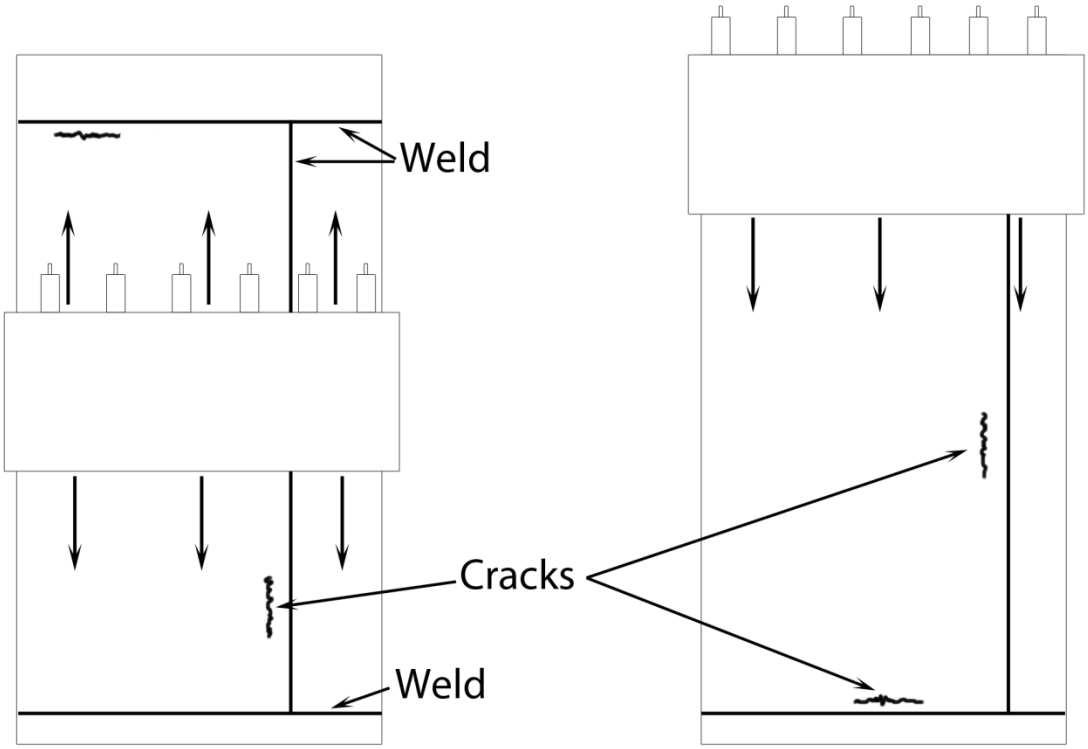

Figure 4.47. Illustration of a Piezoelectric Ring Transducer Installed on a Dry Cask Storage Canister for Used Nuclear Fuel

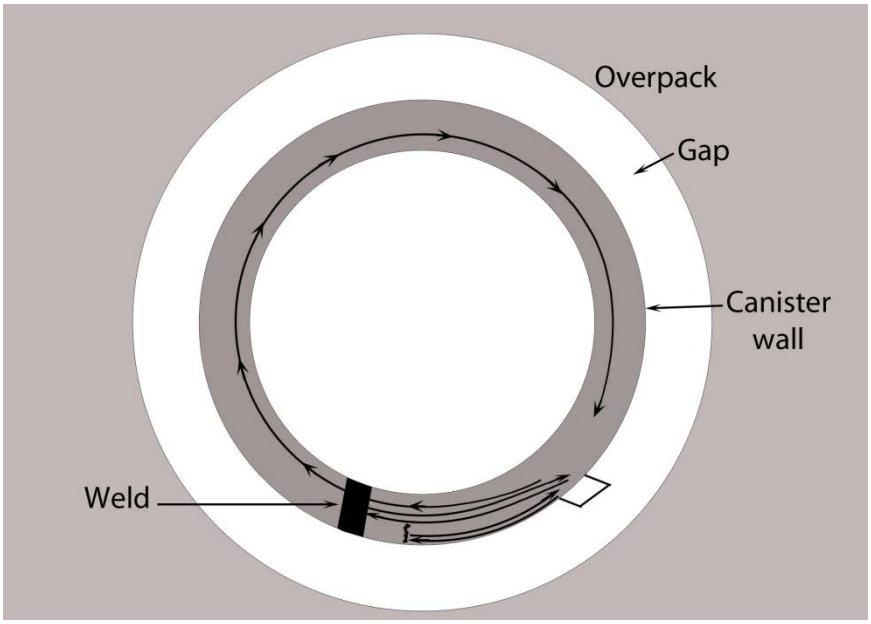

Figure 4.48. A Depiction of a Circumferentially Guided Ultrasonic Wave Inspection of a Dry Storage Canister Wall

5.0 Discussions

5.1 Cross-cutting Needs

A few cross-cutting needs that are applicable to improving examinations via several of the methods discussed include:

- Development of a robotic crawler or scanner is needed to encode the location of NDE data on a canister surface, maintain consistent scan rate, maintain consistent probe-to-canister surface distance, and minimize the impact of human factors. This need is associated with bulk ultrasonic, visual, and eddy current methods. Robotic mechanisms are also needed for the placement of AE and GUW transducers even though the sensors are not scanned over the surface.
- A compilation of atmospheric SCC flaw morphology parameters (width, orientation, etc.) that affect NDE performance would enable a more complete assessment of the capability of most NDE methods to detect atmospheric SCC.
- Detailed and specific design information related to welded canisters for DCSSs is needed to understand specific access constraints and examination geometries. In turn, this information is relevant to choosing the most appropriate strategy for examination. It is anticipated that the bottom plate-to-shell welds will be the most difficult to access and will pose the most significant examination challenge. The difficulty of the examination will depend on the specific weld configuration.
- Environmental factors such as temperature and radiation in general can affect both the physics of an examination and the performance of equipment exposed to the environmental conditions. Future efforts should seek to enumerate these effects and identify any gaps in knowledge with regards to the behavior of certain types of sensors in anticipated environments.

5.2 Summary

A brief summary of each NDE method discussed in Section 4.0 is provided in Table 5.1. An expanded summary of each NDE method evaluation follows in Sections 5.2.1 to 5.2.6.

Table 5.1. Summary NDE Method Evaluation for Detection and Monitoring of Atmospheric SCC in Welded Canisters

Method	Pros	Cons	Recommended Usage	Suggestions for Future Work
Bulk ultrasonics	• Can provide quantitative characterization of through-wall crack dimensions • Significant experience from use in nuclear power plants • Can potentially be performed in situ (i.e., no removal from overpack)	• Requires use of couplant or use of contactless transducer (EMAT, air-coupled, etc.) with associated loss of sensitivity • Features on inner canister surface may affect inspections • Scanning will be required to inspect regions of significant size	• Use primarily as a follow-up technique to characterize and depth size flaws detected by other means	• Study basic capability of non-contact and coupled transducers for atmospheric SCC detection • Study the influence of internal canister features on examination results • Perform detailed analysis of specific weld and examination geometries to identify most appropriate bulk UT technique • Consider implementation with mechanical scanner or robotic crawler
Acoustic emission	• Sensitive to dynamic processes of crack growth • Sensitive to electrochemical corrosion processes • Potential for global monitoring of welded canisters • Well suited for in situ “monitoring” of welded canister (i.e., no removal from overpack) • Capability for monitoring the growth of IGSCC flaws in the field in nuclear power plants has been demonstrated (Hutton et al. 1993).	• Sensitivity to atmospheric SCC crack growth is unclear – requires brittle fracture contribution to crack growth • Capability to quantify significance of detected flaws is unlikely • May be exposed to large cumulative radiation doses during continuous monitoring	• Potential use as a global screening technique to detect atmospheric SCC at early stages • Potential application as localized monitoring tool to monitor growth of existing cracks • Potential application to monitoring regions difficult to access by conventional NDE equipment (e.g., monitoring the bottom plate)	• Laboratory investigations to understand sensitivity to atmospheric SCC • Characterization of background AE for typical canisters under field conditions

Table 5.1. (contd.)

Method	Pros	Cons	Recommended Usage	Suggestions for Future Work
Visual	• Significant experience from use in nuclear power plants • Intuitive data output • Can reliably detect cracks with COD > 100 µm • Can potentially be performed in situ (i.e., no removal from overpack)	• Studies by SSM indicate mean COD of SCC flaws is 16–30 µm • Performance depends significantly on human factors, lighting conditions, surface conditions, and camera specs., and scanning parameters • Cannot determine through-wall depth of cracks • Follow-up characterization exams using another NDE method required • Reliability and effectiveness for detecting atmospheric SCC requires further knowledge regarding COD characteristics of atmospheric SCC flaws	• Potential use as a screening tool for crack detection • Recommended use of automated scanner or robotic crawler to encode position and maintain consistent lens-canister distance	• Perform comparison study on cracked samples to evaluate impact of tilted mirror or other attachments and borescope optical relay systems on effectiveness of visual testing • Consider use of automated scanner or robotic crawler to encode position and maintain consistent lens-canister distance
Eddy current	• Significant experience from use in nuclear power plants • Potential small probe geometries make it well suited for in situ "monitoring" of welded canister (i.e., no removal from overpack) • Does not require use of couplant or direct contact • Consistent lift-off is desired • Can detect weld locations to direct other NDE efforts	• Scanning will be required to inspect regions of significant size	• Good potential for use as a screening tool for detection of atmospheric SCC • May be able to depth size shallow flaws	• Determine optimal probe configuration for atmospheric SCC inspection (e.g., single versus multi-frequency, frequency) • Determine conditions for which ET can accurately depth size SCC flaws • Consider use of automated scanner or robotic crawler to encode position and maintain consistent liftoff

Table 5.1. (contd.)

Method	Pros	Cons	Recommended Usage	Suggestions for Future Work
Guided ultrasonic waves (axial)	• Developed mostly as a screening tool for corrosion in pipelines • Can potentially be performed in situ (i.e., no removal from overpack) if annular gap accommodates space for transducer	• Commercially available systems require full circumferential clearance for transducer installation • Sensitivity claims from 1 to 5%; cross-section loss are relatively poor	• Poor sensitivity (1–5%) limits usefulness as a screening technology for atmospheric SCC detection (in 1-in.-thick shell, would correspond to a 50% through-wall crack 4–20 in. in length)	• Work required on advanced signal analysis to improve sensitivity
Guided ultrasonic waves (circumferential)	• Developed to detect pitting corrosion at pipe supports in pipelines • Good sensitivity reported in laboratory (down to 1.5-mm-diameter pin holes) • SH mode may be necessary to minimize influence of features on the inner surface of canister • Can potentially be performed in situ (i.e., no removal from overpack) • Potential to improve effectiveness by tailoring mode excitation for target inspection scenario • Full surface scan is not required; full coverage achieved through implementation of linear array or robotic crawler to scan sensor along length of canister	• Not usually applied to structures as large as welded canister— attenuation of signal as it travels full circumference may be an issue • Significant development is required	• Potential use as a screening technology for atmospheric SCC detection • Potential use as characterization technology • Multiple transducers may be necessary to manage signal attenuation and 180° “blind spot” • Significant development work required	• Significant system development required • Consider use of robotic crawler to encode position and translate probe along full length of canister

5.2.1 Bulk Ultrasonic Techniques

Of all the techniques evaluated, bulk ultrasonic techniques are the most suited for immediate deployment to characterize or depth size atmospheric SCC flaws. Several bulk ultrasonic techniques may be evaluated for inspection including full V-path, large angle beam, surface waves, TOFD, or phased-array techniques. Full V-path and TOFD techniques may be influenced by contact of the fuel basket with the inner surface of the canister shell. Common UT sensors require a couplant to transmit ultrasound from the transmitter to the test component. The couplant may be liquid, gel, or solid. The use of couplant for inspection of welded canister surfaces may be undesirable because the use of couplant may contaminate the surface or introduce a source of moisture that may contribute to eventual degradation. To minimize the potential effects of couplant, bulk ultrasonic examinations can be limited to characterizing flaws that are already known to exist or bulk UT exams may be conducting using air coupled or contactless transducers such as EMATs (with a trade-off in potential sensitivity). Use of a robotic crawler or mechanical scanner to encode data with location information can help ensure the quality of the examination.

5.2.2 Acoustic Emission

The application of acoustic emission to monitoring welded DCSS canisters is attractive because the lack of coolant flow and relatively small size make global monitoring achievable with a reasonable number of transducers. Future efforts may seek to characterize the background AE produced by typical welded canisters in the field. Further, sensitivity to SCC phenomena and electrochemical corrosion has been reportedly observed in several laboratory studies. Sensitivity to corrosion can be a benefit in that it potentially enables early detection of SCC or the identification of regions susceptible to SCC.

The efficacy of AE monitoring of atmospheric SCC depends mostly on its sensitivity to atmospheric SCC. Phenomena that result in significant release of elastic energy are detectable by AE. The main driving stress for atmospheric SCC growth is anticipated to be residual stress in welds. Stresses from external loads are anticipated to be relatively low as the cask is only slightly over-pressurized during normal storage conditions. This suggests that chemistry may have a dominant role in the growth of atmospheric SCC. In this case, AE may not be very sensitive to the growth of atmospheric SCC.

The maximum stresses may be anticipated to occur at the bottom plate-to-shell welds as these welds are subject to stresses caused by the weight of the canister in addition to residual stresses. The bottom plate and associated welds are anticipated to be the most difficult to access for inspection. Therefore, greater reliance on AE to monitor this portion of the canister may be necessary.

5.2.3 Visual

Like bulk ultrasonic and eddy current inspections, visual inspections are frequently performed in nuclear power plants and several vendors cater to the nuclear industry to provide products for unique inspection challenges. Some of this technology may be directly applied to the inspection of welded canisters. In-situ examinations are conceivable using a suitably small camera with an angled mirror attachment. The annular gap separating the canister wall and overpack must be large enough to accommodate the camera and the minimum lens-to-object distance. Studies that have been performed to characterize the reliability and effectiveness of visual inspections for crack detection in the nuclear power

industry found that crack opening displacement is the parameter that has the most significant impact on the inspection performance. Further, using technologies typical of field deployment, visual techniques are considered reliable for detecting cracks with COD greater than 100 μm. Otherwise, the reliability and effectiveness of a visual examination is significantly affected by several variables including human factors, surface conditions, lighting conditions, camera specifications, and scanning parameters.

Visual techniques may potentially be used as a screening technology to detect atmospheric SCC, but they cannot be used to depth size flaws and determine their structural significance because crack depth is not correlated to measurements of COD. To understand the effectiveness and reliability of visual techniques for detecting atmospheric SCC, an effort is needed to determine the characteristics of atmospheric SCC flaws (especially the COD parameter). An extensive compilation of the characteristics of SCC observed in LWR components reveals that many SCC cracks have mean CODs of 16–30 μm (Wåle 2006). This raises concerns regarding the ability of remote visual techniques for detecting atmospheric SCC flaws in welded canisters.

5.2.4 Eddy Current

Eddy current has several advantages over other techniques. ET coils can be compact and should be accommodated by the space between the canister shell and overpack in most designs. Compared to UT, ET does not require the use of a couplant and the probe can remain contactless (although maintaining consistent liftoff is important). Compared to VT techniques, ET probes are generally smaller, less expensive, and more rugged than cameras and are not dependent on lighting conditions. However, ET is a surface inspection technique; thus, a follow-up examination will be necessary to characterize flaws detected using the ET method.

5.2.5 Guided Ultrasonic Waves (Axial)

Axially guided ultrasonic waves can be considered an emerging technology for the nuclear power industry although commercial systems have been developed for long-range screening inspections of pipelines. The usefulness of this technique for performing screening examinations of canisters is probably limited because of poor sensitivity (claimed sensitivities of 1 to 5 percent; in a 1-in.-thick shell—this would correspond to a 50 percent through-wall crack 4 to 20 inches in length). Potentially better sensitivity can be achieved using advanced signal analysis techniques. Excitation of axial GUW is often achieved using transducers requiring full circumferential access to the component under inspection.

5.2.6 Guided Ultrasonic Waves (Circumferential)

Circumferential GUW systems have been developed for inspecting hard-to-access pipe support regions of pipelines. Laboratory efforts indicate that this method is sensitive to 1.5-mm-diameter holes. Shear horizontal mode excitation may be most appropriate to minimize interaction of GUW with the internal fuel basket. Attenuation is another significant concern as welded canisters are very large in diameter. It may be possible to mitigate the consequence of attenuation by dividing the canister shell into smaller inspection regions. Full coverage may be achieved by implementing an array of transducers that span the length of the canister or employing a scanner or robotic crawler to translate the probe along the full length of the canister. Circumferential GUW systems would have potential application as a screening method for detecting SCC flaws. The potential also exists to perform characterization functions with circumferential GUW systems.

5.3 Potential Strategies

The technologies evaluated in Section 4.0 have been classified according to their potential application for screening (crack detection), characterizing (sizing), or both as indicated in Table 5.2. Potential strategies for inspecting and monitoring atmospheric SCC in welded canisters are identified below:

- Eddy current techniques have good potential for detection of atmospheric SCC flaws and may be used for screening, followed by a bulk ultrasonic examination for characterization of detected flaws. Eddy current techniques may be suitable for follow-up characterization examinations if conditions permit.
- Visual methods may be used for screening, followed by a bulk ultrasonic examination for characterization of detected flaws. The reliability of remote visual techniques for detection of atmospheric SCC is a concern. These concerns could potentially be alleviated with the use of equipment with improved performance specifications.
- Acoustic emission may be used for global canister monitoring, followed by a bulk ultrasonic examination for characterization of detected flaws. Presently, the sensitivity of AE to atmospheric SCC degradation is unclear and laboratory testing would be needed to establish its capability. Further, an understanding of background noise sources and their potential to interfere with atmospheric SCC detection and monitoring is needed to facilitate AE monitoring.
- Acoustic emission may be used for localized monitoring of existing flaws to monitor their growth and serve as the basis for scheduling follow-up examinations in lieu of periodic, regularly scheduled examinations. Limiting the zone of AE monitoring limits the interference by background noise sources. AE monitoring may be especially desirable for locations of the canister that are difficult or impossible to access by other methods.
- Circumferential guided wave systems could potentially be implemented to perform both screening and characterization functions, although significant work is needed to develop a system for application to welded canisters for DSCCs.

Table 5.2. Classification of NDE Technologies According to Their Function for Screening (crack detection), Characterizing (sizing), or Both

Screening Only	Characterization Only	Screening and Characterization
• Acoustic Emission • Visual • Guided Ultrasonic Waves (axial)	• Bulk Ultrasonics	• Guided Ultrasonic Waves (circumferential) • Eddy Current (conditions for which flaw characterization is possible should be enumerated)

5.4 Other Considerations

This report has focused on DCSSs that have welded metal canisters that act as the primary confinement barrier for UNF, which represent 88 percent of the DCSSs in use. The other 12 percent of DCSSs implement thick, bolted containers that integrate the functions of the confinement barrier and the overpack of welded canister-based systems. A similar assessment could be performed for these systems—the primary differences being the thickness of the containers and accessibility. Metal

containers such as the Castor V/21, which incorporate metal fins on the outer diameter to facilitate cooling, may pose a challenge to examination. The troughs of the metal fins may collect or trap debris and may be regions of significant residual stress. These factors may contribute to the likelihood of atmospheric SCC or corrosion. The fin geometry also poses restrictions on physical access for NDE technologies, potentially making examinations difficult. The identification of suitable methods to inspect the troughs of cooling fins will be needed, especially if casks are located in coastal environments.

In addition to atmospheric SCC, aqueous corrosion is referred to as a degradation mechanism of concern for DCSSs. The damage from aqueous corrosion may manifest as a staining, wall thinning, or small pits. Visual techniques may be better suited for the detection of corrosion than cracking because significant corrosion defects can be expected to have a more prominent surface profile than narrow cracks. Acoustic emission may also be useful for the detection of corrosion in welded canisters.

6.0 Conclusions/Recommendations

Most of the NDE methods considered in this assessment may be classified as screening technologies that are suitable for detecting cracks, but not sizing their depth dimension. Eddy current methods have good potential for screening applications because of the potential for compact probe designs to enable in-situ examination of the canister. The conditions for which eddy current techniques can accurately characterize flaws should be enumerated. In addition, eddy current probes are rugged and do not require the use of couplant or contact with the component under examination. Bulk ultrasonic techniques are most suitable for performing accurate follow-up sizing examinations. Other potential strategies for monitoring atmospheric SCC in welded canisters include:

- Visual methods may be used for screening, followed by a bulk ultrasonic examination for characterization of detected flaws. The reliability of remote visual techniques for detection of atmospheric SCC is a concern. These concerns could potentially be alleviated with the use of equipment with improved performance specifications.
- Acoustic emission may be used for global canister monitoring, followed by a bulk ultrasonic examination for characterization of detected flaws. Presently, the sensitivity of AE to atmospheric SCC degradation is unclear and laboratory testing would be needed to establish its capability. Further, an understanding of background noise sources and their potential to interfere with atmospheric SCC detection and monitoring is needed to facilitate AE monitoring.
- Acoustic emission may be used for localized monitoring of existing flaws to monitor their growth and serve as the basis for scheduling follow-up examinations in lieu of periodic, regularly scheduled examinations. Limiting the zone of AE monitoring limits the interference by background noise sources. AE monitoring may be especially desirable for locations of the canister that are difficult or impossible to access by other methods.
- Circumferential guided wave systems could potentially be implemented to perform both screening and characterization functions, although significant work is needed to develop a system for application to welded canisters for DSCCs.

Cross-cutting needs to enable effective examination of canisters include the following:

- Development of a robotic crawler or scanner is needed to encode location of NDE data on canister surface, maintain consistent scan rate, maintain consistent probe-to-canister surface distance, and minimize the impact of human factors. This need is associated with bulk ultrasonic, visual, and eddy current methods. Robotic mechanisms are also needed for the placement of AE and GUW transducers even though the sensors are not scanned over the surface.
- A compilation of atmospheric SCC flaw morphology parameters (width, orientation, etc.) that affect NDE performance would enable a more complete assessment of the capability of most NDE methods to detect atmospheric SCC.
- Detailed and specific design information related to welded canisters for DCSSs is needed to understand specific access constraints and examination geometries. In turn, this information is relevant to choosing the most appropriate strategy for examination. It is anticipated that the bottom plate-to-shell welds will be most difficult to access and will pose the most significant examination challenge. The difficulty of the examination will depend on the specific weld configuration.

- Environmental factors such as temperature and radiation in general can affect both the physics of an examination and the performance of equipment exposed to the environmental conditions. Future efforts should seek to enumerate these effects and identify any gaps in knowledge with regards to the behavior of certain types of sensors in anticipated environments.

7.0 References

10 CFR 72.122. 2012. "Overall Requirements." Code of Federal Regulations, Washington, D.C.

Alexander D, P Doubell, and C Wicker. 2010. "Degradation of Safety Injection System and Containment Spray Piping and Tank Fracture Toughness Analysis." In *FONTEVRAUD 7, Contribution of Materials Investigations to Improve the Safety and Performance of LWRs*. September 26-30, 2010, Avignon, France. French Nuclear Energy Society.

Alleyne DN and P Cawley. 1992. "The Interaction of Lamb Waves with Defects." *IEEE Transactions on Ultrasonics, Ferroelectrics and Frequency Control* 39(3):381-397.

Alleyne DN, B Pavlakovic, MJS Lowe, and P Cawley. 2001. "Rapid long-range inspection of chemical plant pipework using guided waves." *Insight* 43(2):93-+. <Go to ISI>://WOS:000167101300013. ISI Document Delivery No.: 404MC.

Alvarez MG, P Lapitz, and J Ruzzante. 2008. "AE Response of Type 304 Stainless Steel During Stress Corrosion Crack Propagation." *Corrosion Science* 50(12):3382-3388.

Alvarez MG, P Lapitz, and J Ruzzante. 2012. "Analysis of acoustic emission signals generated from SCC propagation." *Corrosion Science* 55(0):5-9. http://www.sciencedirect.com/science/article/pii/S0010938X11004276.

ASME. 2007. *2007 ASME Boiler and Pressure Vessel Code, Section XI: Rules for Inservice Inspection of Nuclear Power Plant Components*. American Society of Mechanical Engineers, New York.

ASNT. 1991. *Nondestructive Testing Handbook, Second Edition: Volume 7, Ultrasonic Testing*. AS Birks, RE Green Jr. and P McIntire, American Society for Nondestructive Testing, Columbus, Ohio.

ASNT. 2004. *Nondestructive Testing Handbook, Third Edition: Volume 5, Electromagnetic Testing*. SS Udpa and PO Moore, American Society for Nondestructive Testing, Columbus, Ohio.

ASNT. 2007. *Nondestructive Testing Handbook, 3rd Edition: Volume 7, Ultrasonic Testing*. PO Moore, D Kishoni and GL Workman, American Society for Nondestructive Testing, Columbus, Ohio.

ASNT. 2010. *Nondestructive Testing Handbook, 3rd Edition: Volume 9, Visual Testing*. MW Allgaier, RE Cameron and PO Moore, American Society for Nondestructive Testing, Columbus, Ohio.

Bentley PG. 1981. "A Review of Acoustic Emission for Pressurised Water Reactor Applications." *NDT International* 14(6):329-335.

Benz AEG. 1998. "Use of acoustic emission techniques for detection of discontinuities." *Materials Evaluation* 56(10):1215-1222. Compilation and indexing terms, Copyright 2009 Elsevier Inc.

Borst JF. 1977. "Acoustic emission-is it a promise or mirage?" *Nuclear Engineering International* 22(254):54-6.

Cakir A, S Tuncell, and A Aydin. 1999. "AE Response of 316L SS During SSR Test Under Potentiostatic Control." *Corrosion Science* 41:1175-1183.

Caseres L and TS Mintz. 2010. *Atmospheric Stress Corrosion Cracking Susceptibility of Welded and Unwelded 304, 304L, and 316L Austenitic Stainless Steels Commonly Used for Dry Cask Storage Containers Exposed to Marine Environments*. NUREG/CR-7030, U.S. Nuclear Regulatory Commission, Washington, D.C.

Cheeke JDN. 2002. *Fundamentals and Applications of Ultrasonic Waves*. CRC Press, Boca Raton. ISBN 0849301300.

Cheong Y-M, D-H Lee, and H-K Jung. 2004. "Ultrasonic Guided Wave Parameters for Detection of Axial Cracks in Feeder Pipes of PHWR Nuclear Power Plants." *Ultrasonics* 42(1–9):883-888. http://www.sciencedirect.com/science/article/pii/S0041624X04000812.

Cumblidge SE, MT Anderson, and SR Doctor. 2004. *An Assessment of Visual Testing*. NUREG/CR-6860, U.S. Nuclear Regulatory Commission, Washington, D.C.

Cumblidge SE, MT Anderson, SR Doctor, FA Simonen, and AJ Elliot. 2007. *A Study of Remote Visual Methods to Detect Cracking in Reactor Components*. NUREG/CR-6943, PNNL-16472, U.S. Nuclear Regulatory Commission, Washington, D.C.

Cumblidge SE, PG Heasler, SR Doctor, and TT Taylor. 2009. *Program for the Inspection of Nickel Alloy Components Report from the Program's Steering Committee: Inspection of Bottom-Mounted Instrumentation Nozzles Round Robin*. PNNL-18985, Pacific Northwest National Laboratory, Richland, Washington.

Davis JM. 1998. "Advanced Ultrasonic Flaw Sizing Handbook." *NDT.net* 3(11). http://www.ndt.net/article/1198/davis/davis.htm.

Demma A, P Cawley, and M Lowe. 2003. "Scattering of the Fundamental Shear Horizontal Mode from Steps and Notches in Plates." *Journal of Acoustical Society of America* 113(4):1880-1891.

Demma A, P Cawley, M Lowe, AG Roosenbrand, and B Pavlakovic. 2004. "The Reflection of Guided Waves from Notches in Pipes: A Guide for Interpreting Corrosion Measurements." *NDT & E International* 37(3):167-180. <Go to ISI>://WOS:000220447400001.

DePaula S and G Oberson. 2012. "Regulatory Issue Resolution Protocol (RIRP) Pilot: Marine Atmosphere Stress Corrosion Cracking (SCC)." U.S. Nuclear Regulatory Commission, Washington, D.C.

Doctor SR. 2008. "The History and Future of NDE in the Management of Nuclear Power Plant Materials Degradation." In *Proceedings of the ASME 2008 Pressure Vessels and Piping Division Conference*, pp. 197-207. July 27-31, 2008, Chicago, Illinois. American Society of Mechanical Engineers, New York.

Du G, J Li, WK Wang, C Jiang, and SZ Song. 2011. "Detection and Characterization of Stress-Corrosion Cracking on 304 Stainless Steel by Electrochemical Noise and Acoustic Emission Techniques." *Corrosion Science* 53:2918-2926.

Efsing P, J Berglund, C Sandelin, and A Werner. 2001. "Visual Inspection of Brackets for Emergency Core Spray System in Barsebäck Unit 2." In *3rd International Conference of NDE in Relation to Structural Integrity for Nuclear and Pressurized Components*, pp. C25-C32. November 14-16, 2001, Seville, Spain.

Ekstrom P and J Wåle. 1995. *Crack Characterization for In-service Inspection Planning*. SKI Report 95:70, Swedish Nuclear Power Inspectorate, Stockholm, Sweden.

Enkvist J. 2003. "A Study of Operator Performance in a Visual NDT Inspection Task by Remote Video Camera." *Insight* 45(4):252-257.

Ensminger D and LJ Bond. 2011. *Ultrasonics: Fundamentals, Technology and Applications, Third Edition (Revised and Expanded)*. CRC Press, Boca Raton, Florida.

EPRI. 2010. *Industry Spent Fuel Storage Handbook*. Report No. 1021048, Electric Power Research Institute, Palo Alto, California.

Fregonese M, H Idrissi, H Mazille, G Renaud, and LR Cetre. 2001a. "Monitoring Pitting Corrosion of AISA 316L Austenitic Stainless Steel by Acoustic Emission Technique: Choice of Representative Acoustic Parameters." *Journal of Materials Science* 36:557-563.

Fregonese M, H Idrissi, H Mazille, L Renaud, and Y Cetre. 2001b. "Initiation and Propagation Steps in Pitting Corrosion of Austenitic Stainless Steels: Monitoring by Acoustic Emission." *Corrosion Science* 43:627-641.

Gerberich WW, RH Jones, MA Friesel and A Nozue. 1988. "Acoustic Emission Monitoring of Stress Corrosion Cracking." *Materials Science and Engineering A* 103(1):185-191. http://www.sciencedirect.com/science/article/pii/0025541688905654.

Hagemaier DJ. 1990. *Fundamentals of Eddy Current Testing*. American Society for Nondestructive Testing, Columbus, Ohio.

Hanson BD, H Alsaed, C Stockman, D Enos, RM Meyer, and K Sorenson. 2012. *Used Fuel Disposition Campaign - Gap Analysis to Support Extended Storage of Used Nuclear Fuel, Rev. 0*. FCRD-USED-2011-000136 Rev. 0, PNNL-20509, U.S. Department of Energy, Washington, D.C.

Heasler PG and SR Doctor. 2003. *A Comparison of Three Round Robin Studies on ISI Reliability of Wrought Stainless Steel Piping*. NUREG/CR-6795, PNNL-13873, U.S. Nuclear Regulatory Commission, Washington, D.C.

Heasler PG, TT Taylor, and SR Doctor. 1993. *Statistically Based Reevalutaion of PISC-II Round Robin Test Data*. NUREG/CR-5410, PNL-8577, U.S. Nuclear Regulatory Commission, Washington, D.C.

Hutton PH. 1989. "An Overview of Development and Application of Acoustic Emission Methods in the United States." *Nuclear Engineering and Design* 113(1):59-69.

Hutton PH, MA Friesel, and JF Dawson. 1993. *Continuous AE Crack Monitoring of a Dissimilar Metal Weldment at Limerick Unit 1*. NUREG/CR-5963, PNL-8844, U.S. Nuclear Regulatory Commission, Washington, D.C.

IAEA. 2011. *Stress Corrosion Cracking in Light Water Reactors: Good Practices and Lessons Learned*. NP-T-3.13, International Atomic Energy Agency, Vienna, Austria.

Iida K, K Takumi, and A Naruse. 1988. "Influence of Stress Condition on Flaw Detectability and Sizing Accuracy by Ultrasonic Inspection." In *The Ninth International Conference on Nondestructive Evaluation in the Nuclear Industry*, pp. 563-567. April 25-28, 1988, Tokyo, Japan.

Jax P and K Ruthrof. 1989. "Acoustic Emission Inspections of Nuclear Components Considering Recent Research Programmes." *Nuclear Engineering and Design* 113(1):71-79. http://dx.doi.org/10.1016/0029-5493(89)90297-5.

Jirarungsatian C and A Prateepasen. 2010. "Pitting and Uniform Corrosion Source Recognition Using Acoustic Emission Parameters." *Corrosion Science* 52(1):187-197. http://www.sciencedirect.com/science/article/pii/S0010938X0900434X.

Jones RH and MA Friesel. 1992. "Acoustic Emission During Pitting and Transgranular Crack Initiation in Type 304 Stainless Steel." *Corrosion* 48(9):751-758.

Jones RH, MA Friesel, and WW Gerberich. 1989. "Acoustic Emission from Integranular Subcritical Crack Growth." *Metallurgical and Materials Transactions A* 20(4):637-648.

Jones RH, MA Friesel, and R Pathania. 1991. "Evaluation of Stress Corrosion Crack Initiation Using Acoustic Emission." *Corrosion* 47(2):105-115.

Kemppainen M and I Virkkunen. 2011. "Crack Characteristics and Their Importance to NDE." *Journal of Nondestructive Evaluation* 30(3):143-157.

Khatak HS, H Shaikh, and JB Gnanamoorthy. 1997. "Assessment of Acoustic Emission Generated During Stress Corrosion Crack Growth in AISI Type 304 Austenitic Stainless Steel." In *14th World Conference on Nondestructive Testing (14 WCNDT)*. December 8-13, 1996, New Delhi.

Kim HM, IK Park, US Park, YW Park, SC Kang, and JH Lee. 2004. "Statistical Reliability Assessment of UT Round-Robin Test Data for Piping Welds." *Key Engineering Materials* 270-273, Part 3:1743-1748.

Kittel C. 1949. "Physical Theory of Ferromagnetic Domains." *Review of Modern Physics* 21(4):541-583.

Kovac J, C Alaux, TJ Marrow, E Govekar, and A Legat. 2010. "Correlations of Electrochemical Noise, Acoustic Emission and Complementary Monitoring Techniques During Intergranular Stress-Corrosion Cracking of Austenitic Stainless Steel." *Corrosion Science* 52:2015-2025.

Kunerth DC, T McJunkin, M McKay, and S Bakhtiari. 2012. *Inspection of Used Fuel Dry Storage Casks*. INL/EXT-12-27119, FCRD-UFD-2012-000273, Idaho National Laboratory, Idaho Falls, Idaho.

Kupperman DS, SH Sheen, WJ Shack, DR Diercks, P Krishnaswamy, D Rudland, and GM Wilkowski. 2004. *Barrier Integrity Research Program: Final Report*. NUREG/CR-6861, U.S. Nuclear Regulatory, Washington, D.C.

Lapitz P, J Ruzzante, and MG Alvarez. 2007. "AE Response of α-brass During Stress Corrosion Crack Propagation." *Corrosion Science* 49:3812-3825.

Le Clézio E, M Castaings, and B Hosten. 2002. "The Interaction of the S_0 Lamb Mode with Vertical Cracks in an Aluminum Plate." *Ultrasonics* 40:187-192.

Lowe MJS, DN Alleyne, and P Cawley. 1998. "Defect detection in pipes using guided waves." *Ultrasonics* 36(1–5):147-154. http://www.sciencedirect.com/science/article/pii/S0041624X97000383.

Lowe MJS and P Cawley. 2006. *Long Range Guided Wave Inspection Usage - Current Commercial Capabilities and Research Directions.* Imperial College, London.

Lucia AC and F Tonolini. 1989. "General Review of Recent Activities in Acoustic Emission Technology in Italy." *Nuclear Engineering and Design* 113(1):81-86. http://dx.doi.org/10.1016/0029-5493(89)90298-7.

Luo W, JL Rose, JK Van Velsor, MJ Avioli, and J Spanner. 2006. "Circumferential Guided Waves for Defect Detection in Coated Pipe." In *Review of Quantitative Nondestructive Evaluation, Volume 25*, pp. 165-172. July 31-August 5, 2005, Brunswick, Maine. American Institute of Physics, Melville, New York.

Macleod ID, R Rowley, MJ Beesley, and P Olley. 1991. "Acoustic Monitoring Techniques for Structural Integrity." *Nuclear Engineering and Design* 129:191-200.

Magaino S-i, A Kawaguchi, A Hirata, and T Osaka. 1987. "Spectrum Analysis of Corrosion Potential Fluctuations for Localized Corrosion of Type 304 Stainless Steel." *Journal of the Electrochemical Society* 134(12):2993-2997.

Mazille H, R Rothea, and C Tronel. 1995. "An Acoustic Emission Technique for Monitoring Pitting Corrosion of Austenitic Stainless Steels." *Corrosion Science* 37(9):1365-1375.

McIntyre P and G Green. 1978. "Acoustic Emission During Stress Corrosion Cracking in High Strength Steels." *British Journal of Non-destructive Testing* 20(3):135-140.

Mintz T, L Caseres, X He, J Dante, G Oberson, D Dunn, and T Ahn. 2012. "Atmospheric Salt Fog Testing to Evaluate Chloride-Induced Stress Corrosion Cracking of Type 304 Stainless Steel." San Antonio, Texas, Southwest Research Institute.

Moran TL, P Ramuhalli, AF Pardini, MT Anderson, and SR Doctor. 2010. *Replacement of Radiography with Ultrasonics for the Nondestructive Inspection of Welds - Evaluation of Technical Gaps - An Interim Report.* PNNL-19086, Pacific Northwest National Laboratory, Richland, Washington.

Nozue A and T Kishi. 1982. "An Acoustic Emission Study of the Intergranular Cracking of AISI 4340 Steel." *Journal of Acoustic Emission* 1(1):1-6.

Ogilvy JA. 1989. "Model for the Ultrasonic Inspection of Rough Defects." *Ultrasonics* 27(2):69-79.

Okada H, Y Yukawa, and H Tamura. 1974. "Application of Acoustic Emission Technique to the Study of Stress Corrosion Cracking in Distinguishing Between Active Path Corrosion and Hydrogen Embrittlement." *Corrosion* 30(7):253-255.

Okada H, Y Yukawa, and H Tamura. 1976. "Transition of Cracking Mechanisms from Active Path Corrosion to Hydrogen Embrittlement in High Strength Steels in a Boiling Nitrate Solution." *Corrosion* 32:201-213.

PAC. 2005. *DiSP with AEwin, User's Manual, Rev. 3*. PAC Part #: 6320-1001, Physical Acoustics Corporation (PAC), Princeton Junction, New Jersey.

Padmanabhan R, N Suriyayothin, and WE Wood. 1983. "Grain Size-Acoustic Emission Relationships in Hydrogen Induced Delayed Cracking." *Metallurgical and Materials Transactions A* 14(11):2357-236.

Pollock AA. 1986. "Acoustic Emission Capabilities and Applications in Monitoring Corrosion." In *Corrosion Monitoring in Industrial Plants Using Nondestructive Testing and Electrochemical Methods*, pp. 30-42 eds: GC Moran and P Labine. ASTM, Philadelphia, Pennsylvania.

Pollock AA, JM Carlyle, and SJ Ternowchek. 1988. "Acoustic Emission Proves Its Worth in Nuclear Plants." *Nuclear Engineering International* 33(405):52-53.

Pollock AA, D Hardie, and NJH Holroyd. 1982. "Monitoring Sub-Critical Crack Growth due to Stress Corrosion or Hydrogen Embrittlement by Acoustic Emission." *British Corrosion Journal* 17(3):103-111.

Raghavan A and CES Cesnik. 2007. "Review of guided-wave structural health monitoring." *Shock and Vibration Digest* 39(2):91-114. http://dx.doi.org/10.1177/0583102407075428. 9532280.

Rebello JMA, AA Carvalho, LVS Sagrilo, and SD Soares. 2006. "Reliability of the Ultrasonic Technique Applied to Detection of Pipe Weld Defects." In *33rd Annual Review of Quantitative Nondestructive Evaluation, Volume 26*, pp. 1839-1846. July 30-August 4, 2006, Portland, Oregon. American Institute of Physics, Melville, New York.

Rempe JL, H MacLean, R Schley, D Hurley, J Daw, S Taylor, J Smith, J Svoboda, D Kotter, D Knudson, M Guers, SC Wilkins, and LJ Bond. 2011. *Strategy for Developing New In-pile Instrumentation to Support Fuel Cycle Research and Development*. INL/EXT-10-19149, Idaho National Laboratory, Idaho Falls, Idaho.

Rose JL. 1999. *Ultrasonic Waves in Solid Media*. Cambridge University Press, Cambridge, United Kingdom.

Rose JL. 2000. "Guided Wave Nuances for Ultrasonic Nondestructive Evaluation." *IEEE Transactions on Ultrasonics, Ferroelectrics and Frequency Control* 47(3):575-583.

Rose JL. 2002. "A Baseline and Vision of Ultrasonic Guided Wave Inspection Potential." *Transactions of the ASME, Journal of Pressure Vessel Technology* 124(3):273-282. http://dx.doi.org/10.1115/1.1491272.

Rose JL and LE Soley. 2000. "Ultrasonic guided waves for anomaly detection in aircraft components." *Materials Evaluation* 58(9):1080-1086. <Go to ISI>://WOS:000089248800007. ISI Document Delivery No.: 352ZG.

Rudlin JR, CRA Schneider, and GR Razmjoo. 2004. "Reliability of Inspection for Root Flaws in Riser Girth Welds." In *Proceedings of the 23rd International Conference on Offshore Mechanics and Arctic Engineering - OMAE*, pp. 255-263. June 20-25, 2004, Vancouver, BC, Canada. American Society of Mechanical Engineers, New York.

Runow P. 1985. "Use of Acoustic Emission Methods as Aids to the Structural Integrity Assessment of Nuclear Power Plants." *International Journal of Pressure Vessels and Piping* 21(3):157-207. http://dx.doi.org/10.1016/0308-0161(85)90001-8.

Satyarnarayan L, J Chandrasekaran, B Maxfield, and K Balasubramaniam. 2008. "Circumferential Higher Order Guided Wave Modes for the Detection and Sizing of Cracks and Pinholes in Pipe Support Regions." *NDT&E International* 41:32-43.

Scruby CB. 1987. "An introduction to acoustic emission." *Journal of Physics E: Scientific Instruments* 20(8):946. http://stacks.iop.org/0022-3735/20/i=8/a=001.

Shaikh H, R Amirthalingam, T Anita, N Sivaibharasi, T Jaykumar, P Manohar, and HS Khatak. 2007. "Evaluation of Stress Corrosion Cracking Phenomenon in an AISI Type 316LN Stainless Steel Using Acoustic Emission Technique." *Corrosion Science* 49(2):740-765.

Shivaraj K, K Balasubramaniam, CV Krishnamurthy, and R Wadhwan. 2008. "Ultrasonic Circumferential Guided Wave for Pitting-Type Corrosion Imaging at Inaccessible Pipe-Support Locations." *Journal of Pressure Vessel Technology* 130:021501-1 to 021502-11.

Su Z, L Ye, and Y Lu. 2006. "Guided Lamb Waves for Identification of Damage in Composite Structures: A Review." *Journal of Sound and Vibration* 295(3–5):753-780. http://www.sciencedirect.com/science/article/pii/S0022460X0600109X.

Sung KY, IS Kim, and YK Yoon. 1997. "Characteristics of Acoustic Emission During Stress Corrosion Cracking of Inconel 600 Alloy." *Scripta Materialia* 37(8):1255-1262.

TenCate JA, TJ Ulrich, and NR Brown. 2012. *Corrosion and Stress Corrosion Cracking: Recommendations for Mitigation and Advanced Detection*. LA-UR-12-26380, FCRD-FUEL-2012-000483, Los Alamos National Laboratory, Los Alamos, New Mexico.

Transnuclear. 2004. "Appendix K, NUHOMS® 61BT DSC." In *Final Safety Analysis Report, Volume 2 of 4, Appendices K & L: Standardized NUHOMS® Horizontal Modular Storage System for Irradiated Nuclear Fuel*. Transnuclear, Inc., Columbia, Maryland.

Valle C, M Niethammer, J Qu, and LJ Jacobs. 2001. "Crack Characterization Using Guided Circumferential Waves." *Journal of Acoustical Society of America* 110(3):1282-1290.

Valle C, J Qu, and LJ Jacobs. 1999. "Guided Circumferential Waves in Layered Cylinders." *International Journal of Engineering Science* 37:1369-1387.

Virkkunen I, M Kemppainen, R Paussu, P Seppala, DS Dybal and AA Nikitin. 2004. *Cracked Samples for Visual Testing*. Technical Report 286AER002, Trueflaw Ltd., Espoo, Finland. Available at http://www.trueflaw.com/Publications/SamplesForVisual.pdf.

Wåle J. 2006. *Crack Characterisation for In-service Inspection Planning - An Update*. SKI Report 2006:24, Swedish Nuclear Power Inspectorate, Stockholm, Sweden.

Xu J, X Wu, and E-H Han. 2011a. "Acoustic emission during pitting corrosion of 304 stainless steel." *Corrosion Science* 53(4):1537-1546. http://www.sciencedirect.com/science/article/pii/S0010938X11000527.

Xu J, X Wu, and E-H Han. 2011b. "Acoustic emission during the electrochemical corrosion of 304 stainless steel in H2SO4 solutions." *Corrosion Science* 53(1):448-457. http://www.sciencedirect.com/science/article/pii/S0010938X10004877.

Yonezu A, H Cho, and M Takemoto. 2006. "Monitoring of Stress Corrosion Cracking in Stainless Steel Weldments by Acoustic and Electrochemical Measurements." *Measurement Science & Technology* 17:2447-2454.

Yuyama S. 1986. "Fundamental Aspects of Acoustic Emission Applications to the Problems Caused by Corrosion." In *Corrosion Monitoring in Industrial Plants Using Nondestructive Testing and Electrochemical Methods*, pp. 43-74 eds: GC Moran and P Labine. ASTM, Philadelphia, Pennsylvania.

Yuyama S, T Kishi, and Y Hisamatsu. 1984. "Fundamental Aspects of AE Monitoring of Corrosion Fatigue Processes in Austenitic Stainless Steel." *Journal of Materials for Energy Systems* 5(4):212-221.

Zhang W, L Dunbar, and D Tice. 2008. "Monitoring of Stress Corrosion Cracking of Sensitised 304H Stainless Steel in Nuclear Applications by Electrochemical Methods and Acoustic Emission." *Energy Materials* 3(2):59-71.

Pacific Northwest
NATIONAL LABORATORY

Proudly Operated by **Battelle** *Since 1965*

U.S. DEPARTMENT OF
ENERGY

902 Battelle Boulevard
P.O. Box 999
Richland, WA 99352
1-888-375-PNNL (7665)
www.pnnl.gov